# THE FUNCTIONALIZATION OF SINGLE-WALLED CARBON NANOTUBES WITH BIOMOLECULES TO TARGET PROFESSIONAL PHAGOCYTES AND PROMOTE BIODEGRADATION

by

Nagarjun Venkata Konduru

B.V.Sc & A.H., College of Veterinary Sciences, Tirupathi, Acharya N.G.Ranga Agricultural University, India, 2001

Submitted to the Graduate Faculty of
the Graduate School of Public Health in partial fulfillment
of the requirements for the degree of
Doctor of Philosophy

University of Pittsburgh

2010

UNIVERSITY OF PITTSBURGH

GRADUATE SCHOOL OF PUBLIC HEALTH

This dissertation was presented

by

Nagarjun Venkata Konduru

It was defended on July 2nd, 2010

and approved by

Chairperson and dissertation advisor: Valerian E. Kagan, Ph.D., D.Sc., Professor, Department of Environmental and Occupational Health, Graduate School of Public Health, University of Pittsburgh

James Fabisiak, Ph.D., Associate Professor, Department of Environmental and Occupational Health, Graduate School of Public Health, University of Pittsburgh

Hulya Bayir, M.D., Associate Professor, Department of Environmental and Occupational Health, Graduate School of Public Health, University of Pittsburgh

Alexander Star, Ph.D., Assistant Professor, Department of Chemistry, School of Arts and Sciences, University of Pittsburgh

Copyright © by Nagarjun Venkata Konduru

2010

**THE FUNCTIONALIZATION OF SINGLE-WALLED CARBON NANOTUBES WITH BIOMOLECULES TO TARGET PROFESSIONAL PHAGOCYTES AND PROMOTE BIODEGRADATION**

Nagarjun Venkata Konduru, Ph.D.

University of Pittsburgh, 2010

Aggressive penetration of nanomaterials in different spheres of our life – from novel technologies to a plethora of consumer products, raises concerns about their possible adverse effects on public health. Several studies report that nanotubes cause lung toxicity. With increase in day-to-day applications of carbon nanotubes, particulate exposure either under occupational or environmental settings is inevitable. In the classic inflammatory response to nanotubes, emigration of neutrophils (PMNs) followed by macrophages into sites of particle deposition has been observed. The major role of the cells is to phagocytoze and promotes particulate clearance and the clearance might be essentially dependent on effective recognition. Carbon nanotubes are not effectively recognized by professional phagocytes and delayed clearance of particles within the lung parenchyma can thus be majorly attributed to impaired phagocytosis or deficiency in components involving their effective degradation. We in our research coated nanotubes with biomolecules to promote recognition, uptake and biodegradation by professional phagocytes. Coating nanotubes with "eat-me"-phospholipid signal, phosphatidylserine proved to be an effective strategy for targeting particles to professional phagocytes, specifically macrophages both in vitro and in vivo. However, opsonization of nanotubes made them competent for both macrophages and neutrophils. This targeting also enhanced the biodegradation in neutrophils and to a lesser extent in macrophages via action of myeloperoxidase and its potent oxidants whose critical role in biodegradation was delineated in cell free based in vitro studies. Further, in vivo

experiments using wild type and myeloperoxidase null mice showed a significantly lower degree of biodegradation and particle elimination in latter animal type, underscoring the role of neutrophil peroxidase in biodegrading carbon nanotubes. Using contemporary techniques-confocal, transmission and scanning electron microscopy, Vis-NIR and Raman spectroscopy, we evaluated the hypothesis. Taken together, the results from the doctoral work suggest that targeting of nanotubes to professional phagocytes can be achieved by coating with certain biomolecules and this targeting can reduce the biopersistence and inflammation associated due to the presence of otherwise relatively biodurable nanotubes in biological ambience. The dissertation also foresees functionalization of nanotubes as a strategy to combat potential toxic effects of nanotubes which pose potential risk to the public health.

# TABLE OF CONTENTS

# LIST OF FIGURES

## PREFACE

This dissertation would not have been possible without the help and understanding of many people over the past 5 years. My mentor and advisor Dr. Valerian Kagan was primarily responsible for guiding my progress. He tirelessly supported my scientific progress and intellectual development and was always accessible for advice, professional and personal. His ability to manage a successful laboratory and gain a reputation as an expert in the field of Nanotechnology and Nanotoxicology has made him an excellent role model for me. I profoundly thank him from core of my heart for taking me under his wings and guiding me.

I was also benefited by the expertise of many members of the Kagan laboratory and Center for Free Radical Research. Yulia manages to keep the lab running smoothly and introduced me to the complexities of Biochemistry. My animal studies would not have been possible without the assistance and expertise of Drs. Anna Shvedova and Elena Kisin at NIOSH. My research was also benefited by the cell culture expertise of Dr. Wei Hong Feng and molecular modeling and structural biology expertise of Drs. Judith-Klien Seetharaman and Naveena Yanamala and also expertise of Drs. Olexander Kapralov and Irina Vlasova.

I also would not have been able to perform these studies without assistance and expertise from other laboratories including Dr. Alexander Star at University of Pittsburgh, Department of Chemistry and Dr. Yuri Volkov lab at Trinity College, Dublin. Dr. Donna Beer Stolz provided invaluable technical advice on electron microscopic studies. My special note of thanks to Brett Allen from Dr. Star's group who helped me with spectroscopic studies.

I am also indebted to my thesis committee of Drs. James Fabisiak, Hulya Bayir, and Alexander Star for their advice and support. I would especially like to thank Dr. Adilaxmamma and Dr Venkateshwarlu for their support of the infancy of my scientific career while I was at the Vet school.

Lastly, my progress would not be possible without the love and support of my family. My parents Sri Sivaram Prasad and Smt. Rajarani went above the call of duty to support my personal and professional development for the 30 odd years of my life. My wife Smt. Shangeetha Rajagopal has been unbelievably supportive and understanding through these years and eagerly waiting for my arrival in India.

The portion of chapter 3 (Section 3.3) was originally published in Journal of Biological Chemistry. Tyurina, Y. Y., L. V. Basova, et al. (2007). "Nitrosative stress inhibits the aminophospholipid translocase resulting in phosphatidylserine externalization and macrophage engulfment- Implications for the resolution of inflammation." J Biol Chem 282(11):8498-509. The portion of chapter 4 (Section 4.3) was originally published in PLoS One. Konduru, N. V., Y. Y. Tyurina, et al. (2009). "Phosphatidylserine targets single-walled carbon nanotubes to professional phagocytes in vitro and in vivo." PLoS One 4(2):e4398.The portions of chapter 5 and 6 (Sections 5.3 and 6.3.1) were originally published in Nature Nanotechnology. Kagan, V. E., N. V. Konduru, et al. (2010). "Carbon nanotubes degraded by neutrophil myeloperoxidase induce less pulmonary inflammation." Nat Nanotechnol 5(5):354-9

# 1 CHAPTER 1 – INTRODUCTION

## 1.1 DISSERTATION GOALS AND OBJECTIVES

Single-walled carbon nanotubes (SWCNT) are allotropes of carbon with a cylindrical structure formed primarily by coaxial graphite layer. Often, the manufactured (as synthesized) nanotubes contain significant amounts of transition metals such as Iron/Nickel etc which are required catalysts in the process of synthesis and the amounts usually vary depending on the synthesis method employed (Muradyan, Tarasov et al. 2008). Their diameters range between 0.8-1.5 nm and reach several nanometers to micrometers in length. Due to their unique physical and electrical properties, these particles are at the leading edge of the rapidly developing field of nanotechnology (Shvedova, Kisin et al. 2009). With increasing applications owing to their inherent properties, future foresees an exponential increase in the production. However, many toxicological studies have demonstrated that the particles pose potential adverse effects to both the humans and environment (Shvedova, Kagan et al.). Reports have raised concerns regarding health risks in particular for industrial workers that may be inhaling carbon nanotubes during the manufacture of certain products. Also, the studies raise alarm towards exploring particle benefits for the various human biomedical applications including drug delivery. Although many in vitro studies have shown that carbon nanotubes can be toxic to macrophages (Kagan, Tyurina et al. 2006) and other immune cells (Dumortier, Lacotte et al. 2006), human keratinocytes (Shvedova, Castranova et al. 2003), epithelial cells (Sharma, Sarkar et al. 2007) etc but diminishing catalyst content and a well dispersion strategy have conferred lesser cytotoxicity (Kagan, Tyurina et al. 2006). In vivo, immune cells, in particular macrophages are in prolonged contact with the particulates when clearing them from the lung and other tissues and can initiate and sustain inflammatory responses. These cells play a critical role as

orchestrators of inflammation as they regulate the production and release of pro- and anti-inflammatory mediators, reactive oxygen (ROS) and nitrogen species (RNS), particularly after exposure to particles (Gonzalez-Flecha 2004), and are significant contributors to the distribution of SWCNT in the body thus determining their potential toxic effects (Oberdorster, Sharp et al. 2004; Elder and Oberdorster 2006). Importantly, non-functionalized nanotubes are poorly recognized by macrophages both in vitro and in vivo resulting in the avoidance of SWCNT from macrophage mediated "surveillance" (Shvedova, Kisin et al. 2005; Kagan, Tyurina et al. 2006) and could be the factor responsible for nanoparticle biopersistence. In contrast, functionalization of nanotubes induces their recognition by professional and non-professional macrophages and other cells (Kam and Dai 2005; Klumpp, Kostarelos et al. 2006; Nimmagadda, Thurston et al. 2006; Sayes, Liang et al. 2006).

In vivo toxicological data reported the potential for carbon nanotubes to induce inflammation (Shvedova, Kisin et al. 2008), pulmonary fibrosis (Lam, James et al. 2004) and malignant mesothelioma (Poland, Duffin et al. 2008) similar to asbestos fibers. The process of functionalization with carboxylic groups has been demonstrated to decrease toxicity to human dermal fibroblasts (Sayes, Liang et al. 2006). Similarly, $NH_3$-functionalization on SWCNT has been shown to reduce cytotoxicity to immune cells such as mouse B and T lymphocytes (Dumortier, Lacotte et al. 2006). Most of the in vitro studies though provided some mechanistic insights into the toxicity, but did not evaluate particulate uptake, phagocytosis, fate up on ingestion and resultant effects due to the uptake by the phagocytic cells which could be very important to determine when considering the particles for drug delivery and other pharmaceutical applications. Bio-persistence of carbon nanotubes in tissue is defined as the amount of carbon nanotubes retained in the tissue following deposition and clearance by

macrophages/other phagocytic cells and chemical degradation (Oberdorster, Oberdorster et al. 2005). Therefore, the role that macrophages and other professional phagocytic cells play in the clearance and biodegradation of carbon nanotubes could be the major determinant of carbon nanotube mediated in vivo toxicity. Because of the role that macrophages and other professional phagocytes may play in the process of effective SWCNT clearance and degradation, we have undertaken the required studies to test the hypothesis that; **Targeting of single-walled nanotubes to professional phagocytes is an essential step to effective biodegradation** (Figure 1). In macrophages, degradation is minimal; yet targeting into macrophages stimulates clearance.

A major goal of this dissertation was to functionalize carbon nanotubes with bio-molecules that would promote effective recognition, uptake and biodegradation by professional phagocytic cells. Professional phagocytes such as neutrophils, monocytes, and macrophages have numerous important functions in immunity, particularly the ingestion of microorganisms, foreign particles and cells. As suggested by Vandivier R.W and Gardai S.J (Gardai, Bratton et al. 2006; Vandivier, Henson et al. 2006), macrophage recognition and uptake of apoptotic cells (also termed "efferocytosis") is an important type of cell/cell communications regulating inflammation. This interaction triggers not only effective clearance of apoptotic cells but also suppression of the inflammatory response (Fadok, Bratton et al. 1998; Huynh, Fadok et al. 2002) or of adaptive immunity (Hoffmann, Kench et al. 2005), thus limiting local tissue responses and normally leading to a quiet cell removal (Gardai, Bratton et al. 2006). In contrast, inefficient apoptotic cell clearance is pro-inflammatory and pro-immunogenic. The recognition of apoptotic cells by macrophages is largely dependent on the appearance on the cell surface of an anionic phospholipid, phosphatidylserine (PS), which is normally confined to

the cytosolic leaflet of plasma membrane (Daleke 2003; Devaux, Lopez-Montero et al. 2006). Thus, externalization of PS during apoptosis generates an "eat-me" signal for macrophages. Notably, non-apoptotic cells with externalized PS can also be taken up by macrophages and suppress reactive oxygen (ROS) and nitrogen species (RNS) production (Serinkan, Gambelli et al. 2005) .

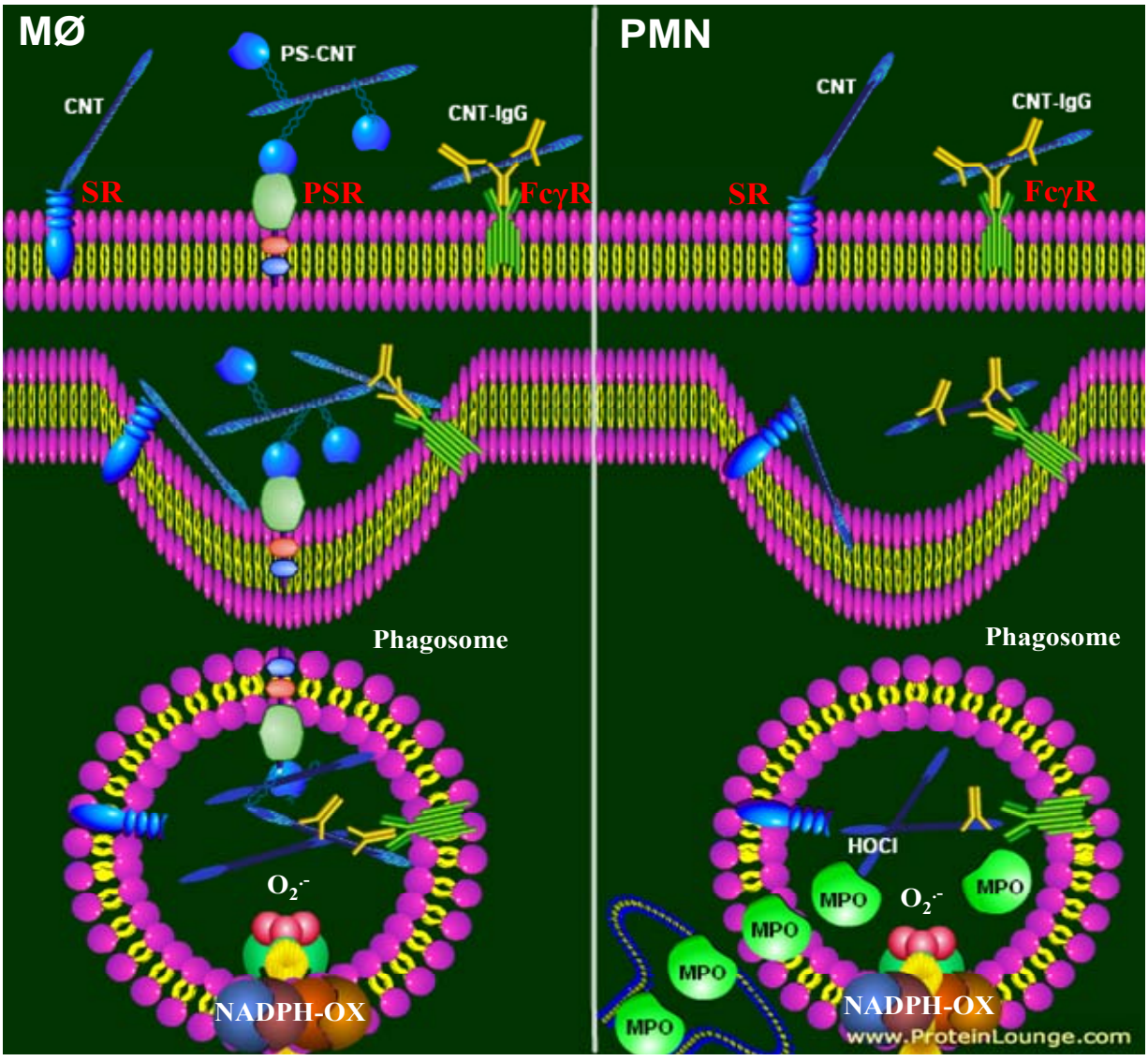


**Figure 1. Targeting of SWCNT to macrophages and neutrophils.**

Phosphatidylserine is also shown to occur on the nuclei expelled from erythroid precursor cells (Yoshida, Kawane et al. 2005) and exosomes excreted from maturing mammalian reticulocytes (Thery, Zitvogel et al. 2002). Several receptors have been identified to play role in the recognition of PS, including lectin-like oxidized low-density lipoprotein receptor–1 (LOX-1), $ß_2$-glycoprotein I ($ß_2$GPI) receptor, $\alpha_v ß_3$ vitronectin receptor, Mer receptor tyrosine kinase, and phosphatidylserine receptor (PSR) (Napirei and Mannherz 2009). Recently, Miyashi et al identified Tim4 as phosphatidylserine receptor and reported that the receptor bound apoptotic cells by recognizing phosphatidylserine via its immunoglobulin domain. They also showed that by expressing Tim4 in fibroblasts, enhanced their ability to engulf apoptotic cells. Interestingly, administration of the anti-Tim4 monoclonal antibody resulted in significant blockade of apoptotic cell engulfment by thymic macrophages, and the mice developed auto-antibodies (Miyanishi, Tada et al. 2007). Even though many surface signaling molecules have been identified (Arur, Uche et al. 2003; Obeid, Tesniere et al. 2007), PS remains a universal component of the recognition pattern on the surface of apoptotic cells (Martin, Reutelingsperger et al. 1995). Recently, a definitive role for PS, P-selectin and β2 integrin–dependent cell clearance of activated platelets by neutrophils has been shown in vivo (Maugeri, Rovere-Querini et al. 2009). In addition, knockout-mouse studies have shown that PS-dependent clearance of apoptotic cells is crucial for the maintenance of tissue homeostasis (Hanayama, Tanaka et al. 2004). To model such a mechanism in vitro, we conducted experiments testing the externalization of PS on cells induced by nitrosylation of aminophospholipid translocase (APLT) in target cells and testing the capacity of macrophages to efficiently engulf such target cells with externalized PS. Literature supporting the role of the enzyme APTL in PS externalization has been discussed elaborately in section 3.1.3 of chapter 3. Mimicking this phenomenon of macrophage recognition, we hypothesized that coating of

SWCNT with PS will interface them with macrophages and other professional phagocytes and stimulate the recognition, tethering and engulfment of nanotubes. To model both in vitro and in vivo recognition of carbon nanotubes coated with PS, we used different phagocytic cell types to evaluate the degree of particle uptake and also assessed the same in mice aspirated with PS coated nanotubes.

Opsonization is another process by which foreign particles and micro-organisms becomes surface coated with opsonin proteins, thereby bringing them under phagocytic cell surveillance. Opsonization leads to phagocytosis of particles for eventual destruction or removal of foreign materials from the circulation. In the case of non-biodegradable nanoparticles, which cannot normally be destroyed by the phagocytes, sequestration in the mononuclear phagocyte system (MPS) or organs, most commonly the liver and spleen can occur leading to toxicity and other negative side effects (Moghimi, Muir et al. 1993; Moore, Weissleder et al. 1997; Ezekowitz 2002). Opsosnization commonly occurs when particles reach or when deliberately delivered into blood circulation and the most common opsonins include immunoglobulins and components of the complement system such as C3, C4, and C5. Other blood serum proteins included into the list include laminin, fibronectin, C-reactive protein, type I collagen and many others (A.S. Hoffman, Hoffman et al. 2004). Alternatively, recognition of carbon nanotubes opsonized with Immunoglobulin-G (IgG), a well known mediator of Fcγ-receptor dependent internalization of microorganisms in phagocytic cells and activator of antimicrobial responses (McKenzie and Schreiber 1998), was also tested. Few studies have also reported endocytosis of polystyrene and other nanoparticles via scavenger receptors (Raynal, Prigent et al. 2004; Kanno, Furuyama et al. 2007) (Figure 2).

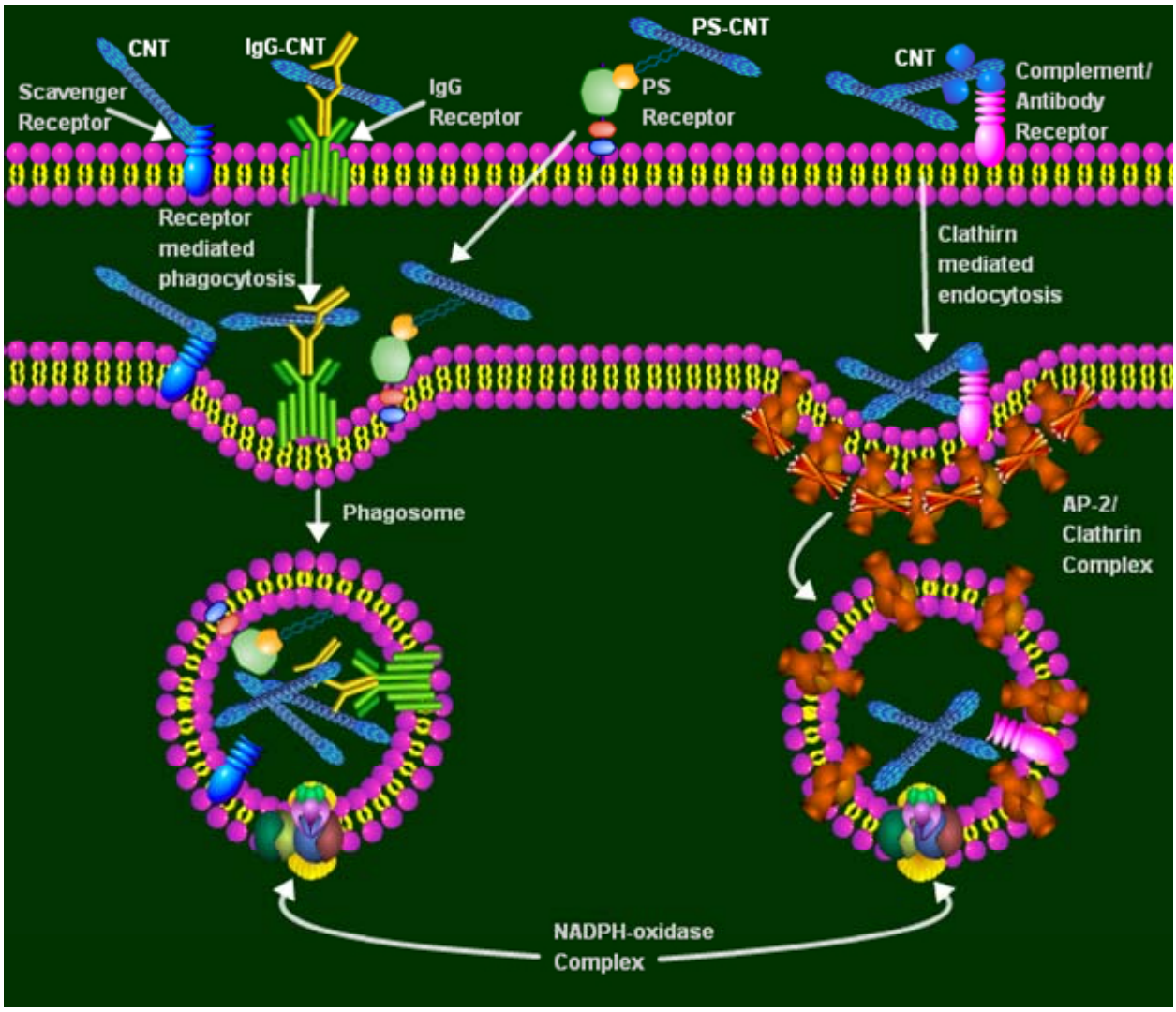


**Figure 2. Different routes of SWCNT uptake in macrophages.**

# 2 CHAPTER 2 - BACKGROUND

## 2.1 BROAD FUNCTIONS OF PROFESSIONAL PHAGOCYTES

### 2.1.1 Macrophages

Elie Metchnikoff was the first to observe ingestion of bacteria and reported the importance of phagocytosis as a defense mechanism in organisms (Jones and Rous 1917). The word “macrophage” derives its origin from the Greek for ‘big eaters’, from “makros” meaning “large” and “phagein” "eat". Amongst the professional phagocytes, macrophages represent the key cellular elements that function as the sensors of pathogenic organisms and are important in the initiation of inflammatory responses, elimination of pathogens, regulation of the adaptive immune responses and also in the process of tissue remodeling following inflammation (Dale, Boxer et al. 2008). The other major role is the removal of necrotic cellular debris in the tissues. Removing necrotic and apoptotic cell debris is an important step in resolution of inflammation, as the pro-inflammatory (early stages of inflammation) are dominated by polymorphonuclear neutrophils, which are ingested by macrophages. Macrophages can either be derived from promonocytes under the influence of Granulocyte Macrophage Colony Stimulating Factor (GM-CSF) or from bone marrow regulated by macrophage-colony stimulating factor (M-CSF) and lodge themselves in various tissues. Monocyte-derived macrophages are relatively short-lived and non-proliferating when in inflammatory sites. Contrastingly, tissue macrophages survive longer and exhibit considerable proliferation while maintaining homeostasis (Plowden, Renshaw-Hoelscher et al. 2004).

### 2.1.2 Biology of apoptotic cell clearance by macrophages

Dying cells are recognized by professional phagocytes such as macrophages. Macrophage mediated ingestion or phagocytosis of pathogenic organisms triggers secretion of molecular mediators capable of initiating protective but potentially deleterious inflammatory responses. Interestingly, macrophage mediated phagocytosis of apoptotic cells averts this release of pro-inflammatory mediators and shifts the release paradigm to anti-inflammatory mediators, and also in macrophage generation and release of reactive oxygen and nitrogen species (Meagher, Savill et al. 1992; Huynh, Fadok et al. 2002). However, deliberate change in experimental conditions by coating apoptotic cells with IgG can lead to release of pro-inflammatory mediators (Meagher, Savill et al. 1992). Dysregulation and ineffective clearance of apoptotic cells result in postapoptotic cytolysis (Gardai, Bratton et al. 2006) and cause pro-inflammatory conditions that are associated with a number of autoimmune and chronic inflammatory diseases such as systemic lupus erythematosus (Gaipl, Kuhn et al. 2006), chronic obstructive pulmonary disease (Demedts, Demoor et al. 2006), chronic granulomatous disease (Fadeel, Ahlin et al. 1998), and asthma (Huynh, Fadok et al. 2002).

### 2.1.3 Role of phosphatidylserine in recognition of apoptotic cells

Phagocytic recognition of apoptotic cells requires a remarkable rearrangement of their membrane surface. Most notably, collapse of plasma membrane phospholipid asymmetry, appearance of phosphatidylserine (PS), an essential “eat-me” signal, on the cell surface (Savill and Fadok 2000), and its interactions with specialized binding proteins (Bottcher, Gaipl et al. 2006; Hanayama, Miyasaka et al. 2006)) are involved in recognition, tethering, and engulfment of apoptotic cells by phagocytes. Moreover, externalized PS is essential for triggering of anti-

inflammatory responses in macrophages (Huynh, Fadok et al. 2002; Gaipl, Kuhn et al. 2006; Henson and Hume 2006). Therefore, failure to externalize PS may disrupt the clearance of apoptotic cells in vivo and contribute to perpetuating a calamitous proinflammatory environment (Fadeel 2003). Notably, non-apoptotic cells with externalized PS can also be taken up by macrophages and suppress reactive oxygen species (ROS) and reactive nitrogen species production (RNS) (Serinkan, Gambelli et al. 2005).

Normally PS is confined exclusively to the cytoplasmic surface of the plasma membrane (Devaux, Lopez-Montero et al. 2006); maintenance of this asymmetric PS distribution is because of energy (ATP)-dependent aminophospholipid translocase (APLT) responsible for the inward translocation of amino phospholipids (Daleke and Lyles 2000; Devaux, Lopez-Montero et al. 2006). During apoptosis, APLT is inactivated causing egress of PS from the inner to the outer leaflet of the plasma membrane (Fabisiak, Tyurin et al. 2000; Gleiss, Gogvadze et al. 2002; Tyurina, Serinkan et al. 2004). The mechanisms of apoptotic APLT inactivation remain to be elucidated. Reportedly, APLT is not a substrate for apoptosis-activated caspases suggesting that alternative mechanisms may be involved (Verhoven, Krahling et al. 1999). In line with this, PS externalization can be divorced from the common caspase-initiated pathway of apoptosis (Zhuang, Ren et al. 1998; Uthaisang, Nutt et al. 2003). PS externalization is one of several features contributing to recognition of apoptotic cells. Chemotactic factors such as lyso-phosphatidylcholine , and bridging molecules such as MFG-E8 (Hanayama, Tanaka et al. 2002) are some examples of other important participants in the process of apoptotic cell clearance. Moreover, additional recognition signals on the surface of apoptotic cells have also been shown to be involved in this process, including proteins such as annexin I and calreticulin (Arur, Uche et al. 2003; Obeid, Tesniere et al. 2007). However, PS

remains a universal component of the recognition pattern on the surface of apoptotic cells (Martin, Reutelingsperger et al. 1995), and recent studies have implicated several different macrophage receptors in the process of PS-dependent clearance of cell corpses (Miyanishi, Tada et al. 2007; Park, Tosello-Trampont et al. 2007).

### 2.1.4 Neutrophils and the phagosome components

Neutrophils or polymorphonuclear cells (Neutrophils) as they are referred- are also members of the innate immune system and play critical role in host defense and inflammation (Dale, Boxer et al. 2008). This cell types have a relatively short life span and undergo apoptosis. Apoptozed neutrophils are then phagocytozed by macrophages in an anti-inflammatory setting. Neutrophils usually engage pseudopodia like extensions around particles or microorganisms for entrapment and to engulf them. These highly phagocytic cells have been regarded as first line of defense. The cells have the capacity to generate toxic oxygen radicals, lytic enzymes and cationic proteins to destroy the invading microorganisms they phagocytoze. The generation of superoxide anions ($0_2^{\cdot-}$) occurs as a sequel to NADPH oxidase reaction. The superoxide radical thus produced is then dismutated into hydrogen peroxide ($H_2O_2$) either spontaneously or by a reaction catalyzed by superoxide dismutase (Hampton, Kettle et al. 1998). The reactive oxygen species are believed to be produced at the plasma membrane and released both extracellularly and into phagosomes. The cytoplasmic azurophilic granules of neutrophils are packed with Myeloperoxidase (MPO), a heme peroxidase, which consumes most of the hydrogen peroxide generated by neutrophils (Klebanoff 1999). MPO, apart from generating potent reactive radical intermediates, also produces hypochlorous acid (HOCl), a potent oxidant, in presence of chloride ions (Winterbourn and Kettle 2000). Components of

neutrophils have been shown to contribute in degrading implantable polymeric materials such as poly(ester-urea-urethane) (Sutherland, Mahoney et al. 1993).

### 2.1.5 General mechanisms underlying particulate phagocytosis

Phagocytosis is a fundamental cellular function of most of the professional phagocytes and involves the internalization of exogenous foreign particles or pathogens into the cytoplasmic vesicles called phagosomes (Rosales and Brown 1991). The factors that influence the in vivo bio-distribution, internalization, and metabolism of nanoparticles factors include the physicochemical properties such as particle size, surface charge, solubility, and surface functionality. These factors play role in influencing the uptake of particles and subsequent clearance by macrophages. (Panyam and Labhasetwar 2003; Alexis, Pridgen et al. 2008). Nanoparticles when present in bloodstream are rapidly cleared by the reticulo-endothelial system (RES) (Hans and Lowman 2002). Surface functionalization of nanoparticles with molecules such as polyethylene glycol (PEG) significantly reduces the RES uptake and also prevents surface opsonization. The pegylation procedure enhances the systemic half life of nanoparticles which proved the strategic use of nanoparticles for intravenous drug delivery platform (Park, Fong et al. 2009). Particles in systemic circulation encounter a plethora of plasma proteins and immune cells. In circulation some of the blood cells that can encounter nanoparticles include monocytes, platelets, leukocytes, and dendritic cells (DC) and in tissues by resident phagocytes (e.g., Kupffer cells in liver, DC in lymph nodes, macrophages and B cells in spleen). It has been shown that surface functionalization of nanoparticles with positive or negatively charged molecules targets them to phagocytes and contrastingly functionalization with neutrally charged molecules such as PEG avoids macrophage surveillance (Villanueva, Canete et al. 2009). Surface adhesion of proteins mainly depends on the inherent chemical

nature, surface chemistry and the method of preparation of nanoparticles. Many pathways have been proposed to be involved in the uptake of nanoparticles and can be facilitated by the adsorption of opsonins (plasma proteins) on the particle's surface. Mammalian cells have five ways to internalize macromolecules and/or nanoparticles which includes: phagocytosis (via mannose receptor-, complement receptor, Fcγ receptor, and scavenger receptor mediated pathways), macropinocytosis, clathrin-mediated, caveolin mediated,and clathrin/caveolin-independent endocytosis (Dobrovolskaia and McNeil 2007). The internalization of foreign material and pathogens then follows attempted destruction by phagocytic cells and may involve several sequential steps including phagosome acidification (Blanchette, Woo et al. 2009), phagosome-lysosome fusion with subsequent exposure of the pathogens or foreign material to degradative enzymes (Hart and Young 1975; Knapp and Swanson 1990), and generation of diffusive potent oxidants/microbicidal substances such as reactive oxygen and or nitrogen species. The phagocytosis is a three step process and involves particle recognition, tethering followed by ingestion. Professional phagocytes are known to internalize both unmodified and modified particles such as naked or opsonized (IgG) particles and microbes. Phagocytosis of opsonized nanoparticles involves receptor-mediated interaction of specific proteins absorbed on the surface of the nanoparticles with phagocytes. Opsonization with IgG triggers signaling cascades, through clustering of cell surface Fcγ receptors, thus accelerating the engulfment process and activating the generation of microbicidal oxygen and nitrogen species (Trivedi, Zhang et al. 2006). Dissolution of particulate matter inside the intracellular vacuoles depends on the crystallinity, chemical composition and surface area of particles. Studies have demonstrated significant inhibition of polymeric nanoparticles at 4 °C by macrophages, and suggested that an energy-dependent endocytic process might be majorly responsible for nanoparticle uptake while a lesser degree of uptake could be attributed to

physical adhesion or diffusion. He. C et al, 2010 (Biomaterials) showed that non-phagocytic cells favored the uptake of smaller particles compared to phagocytic cells (He, Hu et al.).

## 2.2 SINGLE-WALLED CARBON NANOTUBES

### 2.2.1 Nanoparticle features and biomedical applications

Single-walled carbon nanotubes are typically allotropes of carbon resembling sheets of graphite (a hexagonal lattice of carbon) rolled into cylinders. The particles were first discovered in 1991 by S. Iijima (Iijima, Ajayan et al. 1992). These nanotubes are unique for their size, shape, and remarkable physical properties. The electronic, mechanical, thermal, and structural properties of nanotubes change with the diameter, length, and chirality. These unique features make particles the potential nanomaterials suitable for plethora of biomedical and other applications. The particles are suitable as bio-sensors (Wang, Wang et al. 2004), drug/vaccine delivery (Bianco, Kostarelos et al. 2005), and variety of diagnostic and therapeutic agents (Bianco 2004; Bianco, Kostarelos et al. 2005) including cancer therapy (Kam, O'Connell et al. 2005) and as new generation biomaterials. Many studies so far have offered the advantage of carbon nanotubes to act as protein, peptides, nucleic acids, drug and other specified cargo carriers (Bianco, Kostarelos et al. 2005). Thermal conductivity property of SWCNT in terms of heat generation due to irradiation has been explored in areas of cancer cell destruction as possible cellular nanobombs (Kam, O'Connell et al. 2005). However, the toxicity and biocompatibility of carbon nanotubes is still under scrutiny.

### 2.2.2 Tools for characterizing single-walled carbon nanotubes

Based on the orientation of graphite plane relative to the axis of the nanotube, the nanotubes can become insulating, semiconducting or metallic in their electrical conductance. Various spectroscopic calculations predict the electronic and vibrational properties of carbon nanotubes. Many techniques have been applied till date to characterize SWNT which include

techniques such as infra red (IR), Raman, and UV/visible spectroscopies, atomic force microscopy (AFM), transmission electron microscopy (TEM), Sacnning electron microscopy (SEM) etc (Belin and Epron 2005).

Raman spectroscopy technique provides information about tangential G mode (ca. 1550 – 1600 $cm^{-1}$) which is characteristic of $sp^2$ carbons on the hexagonal graphene network. The D-band, so-called disorder mode (found at ca.1320 $cm^{-1}$ for ext = 633 nm) appears due to disruption of the hexagonal $sp^2$ network of SWCNT. The D-band is also referred as disorder band is related to presence of defects such as vacancies or due to presence of dopants. Additionally, D-band is also used to characterize functionalized SWCNT to ensure functionalization is covalent and that it occurred at the sidewalls. The increase of D/G-band ratio and the decrease of the intensity of the tangential G mode are attributed to oxidation of nanotubes and to the larger content of amorphous carbon as an impurity in the material (COSTA, BOROWIAK-PALEN et al. 2009).

As described above, carbon nanotubes are mixtures of different diameters and helicities; the resultant spectrum includes electronic transitions for both metallic and semiconducting nanotubes. For this reason, Visible-Near infrared spectroscopy is a most accessible technique that provides information about the electronic states of SWCNT. The absorption spectrum typically depicts bands between 1000 and 1100 nm representing the broad S2 semiconducting band of the carbon nanotubes, as well as the M1 metallic band between 650 and 750 nm. A complete loss of such structures is observed after chemical alteration of SWCNT. AFM, TEM and SEM are useful imaging microscopic techniques to characterize SWCNT. These techniques are used to visualize individual nanoparticles, and provide details

on the morphology. AFM is often used to characterize the length and height profiles of nanotubes and also the presence of either covalently attached functional groups or physically adsorbed molecules on sidewall of SWCNT. TEM and SEM commonly used for imaging nanotubes and can also provide information on intactness or exfoliation of nanotubes.

### 2.2.3 Chemical oxidation of nanotubes

Oxidation of carbon nanotubes is a vital step towards chemical functionalization and for nanotubes processing to remove catalyst impurities (Bahr, Yang et al. 2001). The chemical processing of pristine single-walled carbon nanotubes uses strong acids and oxidants (such as mixtures of sulphuric acid, nitric acid and hydrogen peroxide) to modify the surfaces of the nanotubes and to cut them into shorter carboxylated nanotubes (Liu, Rinzler et al. 1998; Wei, Kondratenko et al. 2006). Smalley group reported the first use of concentrated sulfuric acid and nitric acid mixture (3:1) to cut long nanoropes into short, open ended nanotubes. Similarly, 4:1 mixture of sulfuric acid and hydrogen peroxide induce cutting of SWCNT. The resultant cut nanotubes thus formed due to chemical oxidation are conferred with oxygen containing groups. Hypochlorite is also known to generate carboxyl and hydroxyl groups on nanotube surfaces (Wu 2007; Yoon, Kim et al. 2008). Ozone has been predicted to chemisorb via a [2+3] cycloaddition (Criegee's mechanism) creating a short-lived ozonide species that spontaneously decomposes into an epoxide or carbonyl (Simmons, Nichols et al. 2006). In the case of nanotubes, Criegee's mechanism has been predicted to occur even in the absence of a pre-existing defect site (Lu, Tian et al. 2002)

## 2.3 TOXICITY OF NANOTUBES

### 2.3.1 General concepts underlying carbon nanotubes toxicity

Carbon nanotubes have a very high aspect ratio thus making difficult to extrapolate toxicological comparisons with other carbon forms and this also makes toxicological investigation difficult as they possess the qualities of both nanoparticles and fibers (Donaldson, Stone et al. 2004). The three generally accepted factors determining the potential of a particle to cause toxicity irrespective of methods of exposure (Smart, Cassady et al. 2006) are as following:

1) The surface area/mass ratio of the particle-a large surface area gives the particle(s) a greater area of contact with the cellular membrane.

2) The particle retention time-the longer the particle stays in contact with the cellular membrane the greater the chance for cellular damage.

3) The chemical reactivity or inherent toxicity of the chemical(s) contained within the particle.

### 2.3.2 In vitro toxicity studies

The first cytotoxicity report on carbon nanotubes was published by Shvedova et al (Shvedova, Castranova et al. 2003). The study reported that exposure of human dermal keratinocytes to non-purified carbon nanotubes (30 wt % Iron) accelerated oxidative stress in terms of increased free radical and peroxide generation and depletion of total antioxidant reserves, loss in cell viability and morphological alterations to cellular structure. The study attributed the effects observed to the Iron catalyst contaminant. Controversies relating to evaluation of cytotoxicity using dye-base viability assays have surfaced recently and the studies have cautioned that SWCNT can interfere with the dye based vialibity assays (Shvedova, Kisin et al. 2009). This is

evident from studies reporting that in vitro exposure to SWCNT caused asbestos-like cytotoxicity in RAW 264.7 cells as determined using the MTT assay. Similar results using the MTT viability assay were reported for RAW 264.7 cells (Worle-Knirsch, Pulskamp et al. 2006), for human alveolar basal epithelial A549 cells, and THB-1 human macrophages (Davoren, Herzog et al. 2007; Soto, Garza et al. 2007) Contrastingly, Davoren et al reported a substantially lower level of cytotoxicity for SWCNT in A549 cells using alamar blue, neutral red and MTT viability assays (Davoren, Herzog et al. 2007). In contrast, two other studies reported low cytotoxicity for raw SWCNT (high iron contamination), purified SWCNT (low iron), and purified MWCNT (low iron) in A549 cells and NR8383 rat alveolar macrophages (Worle-Knirsch, Pulskamp et al. 2006; Pulskamp, Diabate et al. 2007). In vitro exposure of RAW 264.7 cells to purified SWCNT with negligible metal content did not cause cytotoxicity or cellular apoptosis (Kagan, Tyurina et al. 2006). Increase in the agglomeration state of SWCNT and/or acid oxidation of the SWCNT surface appears to be correlated to cytotoxicity as shown by Wick et al, 2007 and Porter et al, 2008 (Wick, Manser et al. 2007; Porter, Sriram et al. 2008). Presence of iron catalyst as contaminant in as synthesized SWCNT has been shown to be the major toxicant in evoking cytotoxicity. However, SWCNT samples with low iron contamination were found to be significantly less toxic as demonstrated in A549 or BEAS-2B cells by Herog et al., 2007 (Herzog, Casey et al. 2007) and RAW 264.7 cells (Kagan et al., 2006) (Kagan, Tyurina et al. 2006). In conclusion, taken together the cytotoxicity evaluation strategies, the data reported till date favor the conclusion that well-dispersed, purified SWCNT exhibit relatively low cytotoxicity in vitro.

### 2.3.3 Cellular uptake studies on SWCNT

There has been substantial research in area of SWCNT recognition and their uptake by different cells. Most of the studies conclude that the presence or absence of specialized signals is necessary for the targeting and recognition of SWCNT depending on the cell type. Overall, the studies report that naïve non-functionalized SWCNT carrying no recognizable signals are poorly taken-up whereas SWCNT chemically modified (e.g., oxidatively modified during purification and storage) or functionalized by bio-molecules such as proteins (Kam and Dai 2005) or phospholipids are more readily recognized and engulfed by cells (Kam and Dai 2006). Several in vitro studies support the concept that non-functionalized and unmodified SWCNT are not readily taken up by lung cells. Davoren et al. (2007) (Davoren, Herzog et al. 2007) reported no significant uptake of SWCNT in lung epithelial cells. Similarly, Herzog et al.(2007) (Herzog, Casey et al. 2007) reported no uptake of SWCNT in either A549 cells or BEAS-2B cells (a human bronchial epithelial cell line). Lastly, no evidence of uptake of SWCNT was reported after electron microscopic evaluation of exposed RAW 264.7 cells (a mouse peritoneal macrophage cell line) (Shvedova et al.,2005) (Shvedova, Kisin et al. 2005) . In a study by Mercer et al. (2008) (Mercer, Scabilloni et al. 2008) investigating the deposition and fate of gold-labeled SWCNT after aspiration in a mouse model, it was reported that disperse SWCNT structures were not efficiently recognized and engulfed by alveolar macrophages. The report interestingly showed that the vast majority of SWCNT escaped phagocytosis and rapidly migrated into the interstitium of the alveolar septa. Contrasting to the above studies, Dutt et al., 2007 (Dutta, Sundaram et al. 2007) and Pulskamp et 2007 (Pulskamp, Diabate et al. 2007) showed a significant uptake of SWCNT in RAW 264.7 cells and NR8383 cells (a rat alveolar macrophage cell line). Jia et al. (2005) (Jia, Wang et al. 2005) reported uptake of SWCNT by primary guinea pig alveolar macrophages after in vitro

exposure. Interestingly, in studies which reported cellular uptake, SWCNT were suspended in media containing high serum concentrations (10–15% fetal bovine or calf serum) throwing light on role of adsorption of serum factors in mediating the cellular uptake process. Taken together, these studies infer that recognition signals on surface of SWCNT are important for cellular recognition and uptake and functionalization could become the determining factor for biopersistence of SWCNT in extracellular environments.

### 2.3.4 Lung as the primary target

Respiratory system represents a prime target for aerosolized particles. Initially, the particles deposit on the airway or alveolar epithelium and encounter lung surfactants lining the epithelium. This subsequently follows interaction with phagocytic cells which may result in their clearance or translocation to the interstitium where they may make contact with fibroblasts, endothelial cells or other immunogenic cells. Several studies have demonstrated that particulate physical properties such as particle size and size distribution, high surface area, and reactivity determine the fate and distribution of inhaled particles within the lung compartments (Araujo and Nel 2009; van Ravenzwaay, Landsiedel et al. 2009). Evocation of inflammatory response in the lung may also be determined based on these physical features of particles and is intertwined with concomitantly evolving oxidative stress (Li, Xia et al. 2008). Inefficient particle recognition, clearance and biopersistence of particles may all play predominant role in governing the duration or resolution of inflammation from particle mediated lung oxidative injury. SWCNT inhalation has been shown to cause robust inflammatory responses in mice and exhibit a very early termination of the acute phase and onset of chronic fibrosis (Shvedova, Kisin et al. 2005). The process of resolution of inflammation integrates with a phase of apoptosis of infiltrated neutrophils and subsequently

followed macrophage mediated apoptotic clearance. In this process, NADPH oxidase system contributes to the control of apoptotic cell death and in the clearance of neutrophils (Fadeel 2003). It was reported that in NADPH oxidase-deficient mice which lack the $gp91^{phox}$ sub-unit of the enzymatic complex, the responses to SWCNT exposure were characterized with a marked accumulation of neutrophils and elevated levels of apoptotic cells in the lungs, production of pro-inflammatory cytokines as well as decreased production of the anti-inflammatory and pro-fibrotic cytokine, TGF-β, and significantly lower levels of collagen deposition (Shvedova, Kisin et al. 2008). The study emphasized on the significant role donned by NADPH oxidase-derived reactive oxygen species in determining the susceptibility to SWCNT-induced pulmonary damage.

### 2.3.5 Pulmonary toxicity

Till date a few published reports have demonstrated the pulmonary toxicity of SWCNT (Lam, James et al. 2004; Shvedova, Kisin et al. 2008). Warheit et al.2004 (Warheit, Laurence et al. 2004) investigated the lung toxicity of unrefined SWCNT (synthesized via laser ablation with a composition of approximately 55–65% SWCNT, 30–40% amorphous carbon and 5 wt % Ni and Co) in rats via intra-tracheal instillation. This instillation study showed that exposure to SWCNT produced only transient inflammation, as assessed by cell proliferation and cytotoxicity indices. A much detailed histological examination of exposed animals identified multifocal granulomas. The granulomas were non-uniform in distribution and not progressive after 1 month. The presence of the granulomas was considered inconsistent with the lack of lung toxicity as determined by other parameters and the authors concluded that more research was needed. A series of toxicity studies then following, reporting the histological evaluation on lung tissues derived from animals either exposed to carbon nanotubes via the intra-tracheal

instillation or aspiration of SWCNT revealed formation of granulomatous lesions encased by epithelioid macrophages produced by large agglomerates (Mercer, Scabilloni et al. 2008; Shvedova, Kisin et al. 2008). Studies by Shvedova et al, 2005, 2008) have reported an unusual inflammatory response to SWCNT delivered to the lung via pharyngeal aspiration which was characterized by a robust phase of inflammatory response followed by an early onset of lung fibrosis. Another interesting study by Shvedova et al compared the toxicity of nanotubes administered via two methods i.e, inhalation vs. aspiration. The inhalation of non-purified SWCNT (iron content of 17.7 wt %) at 5 $mg/m^3$, a lung burden of 5 μg/mouse, which is a predictive estimate of lung burden that would be achieved by workers under occupational setting in less than a year time frame reported by Maynard et al, 2004 (Maynard, Baron et al. 2004).

The inhalation exposure was 5 h/day for 4 days and was compared with pharyngeal aspiration of varying doses (5–20 μg/mouse) of the same SWCNT. The study demonstrated that the SWCNT inhalation was more effective than aspiration in causing inflammatory response, oxidative stress, collagen deposition and fibrosis as well as mutations of K-ras gene locus in the lung of C57BL/6 mice. Lam et al (Tox Sci 2004) reported that even purified carbon nanotubes with <2 wt % iron suspended in mouse serum, produced prominent granulomas in mice when instilled with a relatively high dose of carbon nanotubes per mice (100 μg/animal) (Lam, James et al. 2004). The study however lacked details on pathological events due to lower dose of above material. A recent study by Poland et al reported that abdominal injection of long but not short MWCNT caused an inflammatory reaction of the abdominal lining, which was similar to that seen after exposure of mice to asbestos (Poland, Duffin et al. 2008). Conclusively, outcomes from animal studies till date indicate that SWCNT

are potentially toxic to the lung and could pose a definitive threat to the workers involved in their manufacture and handling.

### 2.3.6 Bio-distribution and fate of intravenously administered SWCNT

The most appropriate route of drug delivery for biomedical applications would be the systemic route. A recent study by Schipper M.L et al, 2008 showed that functionalized SWCNT (pegylated-SWCNT) injected intravenously into nude mice did not cause any significant toxicity during an observation period of four months following injection (Schipper, Nakayama-Ratchford et al. 2008) . However, the study entertains ambiguity with respect to choosing immune compromised nude mice as the in vivo test model. Kupffer cells of liver seemed to be target cells lodging the nanotubes. In a similar study by Wang et al, toxicity due to intravenously administered short cut SWCNT functionalized with polymer chitosan, was assessed and was investigated by using the Raman spectroscopy and fluorescent labeling (Wang, Shen et al. 2005). It was shown that SWCNT exhibited a rapid blood clearance with a half-life time of 3–4 h. However, rapid uptake and high levels of SWCNT was observed in liver of mice. The study showed that most of SWCNT accumulated in liver and were hard to excrete. The SWCNT in liver led to pathological changes of liver, including injury of macrophages, cellular swelling, unspecific inflammation and blood coagulation. The study also reported that similar SWCNT uptake behavior was found in spleen and kidney, whereas, no obvious pathological changes were observed in these organs. Both the studies reported absence of any acute toxicity due to intravenous administration of SWCNT. A study conducted in rabbits by Cherukuri et al, 2006 (PNAS) utilized pristine nanotubes for understanding the fate of systemically administered SWCNT (Cherukuri, Gannon et al. 2006). The study concluded that the nanotube concentration in the blood serum decreased exponentially with a half-life of

1.0 ± 0.1 h. No adverse effects from low-level nanotube exposure could be detected from behavior or pathological examination. At 24 h after systemic administration, significant concentrations of nanotubes were found only in the liver. In line with other two studies, the study by Cherukuri et al also emphasized that systemically administered SWCNT did not pose any toxicity to the organ systems. However, the studies are still scarce to infer positively about the toxicity associated with administration of SWCNT for pharmaceutical and biomedical applications.

# 3 CHAPTER 3 - PHOSPHATIDYLSERINE TARGETS SINGLE-WALLED CARBON NANOTUBES TO PROFESSIONAL PHAGOCYTES IN VITRO AND IN VIVO

## 3.1 INTRODUCTION

One of the major biomedical applications of single-walled carbon nanotubes is their use as nanovectors in drug delivery paradigms. Professional phagocytes, particularly macrophages, are very attractive targets during the process of drug delivery because these cells are significant contributors to the distribution and clearance of SWCNT and eventually their fate in terms of bio-persistence in the body thus determining their potential toxic effects. Importantly, non-functionalized nanotubes are poorly recognized by macrophages in vitro and in vivo resulting in the avoidance of SWCNT from macrophages-mediated "surveillance" (Shvedova, Kisin et al. 2005; Kagan, Tyurina et al. 2006). In contrast, functionalization of nanotubes induces their recognition by professional and non-professional macrophages and other cells (Kam and Dai 2005; Klumpp, Kostarelos et al. 2006; Nimmagadda, Thurston et al. 2006; Kostarelos, Lacerda et al. 2007). However, the universal nature of the engulfment of covalently functionalized SWCNT by different types of cells precludes the possibility of their targeted specific delivery to professional phagocytic cells (Kostarelos, Lacerda et al. 2007). This stimulated new lines of research on targeted interfacing of SWCNT with living cells through specific coatings mimicking the cell surface (Chen, Tam et al. 2006). In particular, glycopolymers - that mimic cell surface mucin glycoproteins and facilitate carbohydrate receptor interactions - have been developed to stimulate targeted engulfment of SWCNT by specific types of cells (Chen, Lee et al. 2004; Chen, Tam et al. 2006).

Macrophage recognition and uptake of apoptotic cells (also termed "efferocytosis") is an important type of cell/cell communications regulating inflammation (Vandivier, Henson et al. 2006). This interaction triggers not only effective clearance of apoptotic cells but also suppression of the inflammatory response (Fadok, Bratton et al. 1998; Huynh, Fadok et al. 2002) or of adaptive immunity (Hoffmann, Kench et al. 2005), thus limiting local tissue responses and normally leading to a quiet cell removal (Gardai, Bratton et al. 2006). In contrast, inefficient apoptotic cell clearance is pro-inflammatory and pro-immunogenic. The recognition of apoptotic cells by macrophages is largely dependent on the appearance on the cell surface of an anionic phospholipid, phosphatidylserine (PS), which is normally confined to the cytosolic leaflet of plasma membrane (Daleke 2003; Devaux, Lopez-Montero et al. 2006). Thus, externalization of PS during apoptosis generates an "eat-me" signal for macrophages. Notably, non-apoptotic cells with externalized PS can also be taken up by macrophages and suppress ROS and RNS production (Serinkan, Gambelli et al. 2005). PS externalization is one of several features contributing to recognition of apoptotic cells. Chemotactic factors such as lyso-PC (Lauber, Bohn et al. 2003) and bridging molecules such as MFG-E8 (Hanayama, Miyasaka et al. 2006) are some examples of other important participants in the process of apoptotic cell clearance. Moreover, additional recognition signals on the surface of apoptotic cells have also been shown to be involved in this process, including proteins such as annexin I and calreticulin (Arur, Uche et al. 2003; Obeid, Tesniere et al. 2007). However, PS remains a universal component of the recognition pattern on the surface of apoptotic cells (Martin, Reutelingsperger et al. 1995) and recent studies have implicated several different macrophage receptors in the process of PS-dependent clearance of cell corpses (Miyanishi, Tada et al. 2007; Park, Tosello-Trampont et al. 2007). In addition, knockout-mouse studies have shown that PS-dependent clearance of apoptotic cells is crucial for the maintenance of tissue homeostasis

(Hanayama, Tanaka et al. 2004). Therefore, we hypothesized that coating of SWCNT with PS will interface them with macrophages and stimulate the recognition, tethering and engulfment of nanotubes. Thus, PS-coated SWCNT can be utilized for specifically targeting macrophages and also for targeted delivery of specialized cargos - regulators, inhibitors - into macrophages to control their functions including inflammatory responses to SWCNT themselves.

### 3.1.1 Inactivation of enzyme APLT and PS externalization

Connor and Schroit demonstrated that reversible PS externalization can be induced by -SH reagents in non-apoptotic cells (Connor and Schroit 1990). Conversely, certain cell types can under go apoptosis without PS externalization (Fadeel, Gleiss et al. 1999; Forsberg, Kagan et al. 2004), but the resistance to PS externalization in these cells can be completely reversed by treatment with thiol reagents (Connor and Schroit 1990; Forsberg, Kagan et al. 2004). Apparently, the sensitivity of catalytically competent cysteines of APLT to oxidation/alkylation may be important in the regulation of the enzyme activity during apoptosis (de Jong, Geldwerth et al. 1997; Serinkan, Gambelli et al. 2005). S-Nitrosylation is another redox-related mechanism participating in the modification of protein cysteines (Foster, McMahon et al. 2003). A variety of enzymes contain essential cysteines whose S-nitrosylation results in changed catalytic activity (Hess, Matsumoto et al. 2005). The two major pathways for protein S-nitrosylation are as follows: 1) trans-nitrosylation resulting from the transfer of the nitrosyl functionality from a donor S-nitrosothiol (commonly S-nitrosoglutathione or other low molecular weight thiol) to a recipient cysteine, and 2) direct nitrosylation by peroxynitrite ($ONOO^-$) (formed as a product of the reaction between radical species, nitric oxide ($NO^\cdot$) and superoxide ($O_2^\cdot$)) (Crow and Beckman 1995). Importantly, during inflammation, NADPH oxidase and inducible nitric-oxide synthase in activated macrophages massively produce $O_2^\cdot$.

and $NO^{\cdot}$, respectively, to yield $ONOO^{-}$ (Rubbo, Batthyany et al. 2000; Forman and Torres 2001). The latter can readily S-nitrosylate low molecular thiols (van der Vliet, Hoen et al. 1998) and hence generate pools of trans-nitrosylating species ready to attack protein cysteines (Foster, McMahon et al. 2003). As the enzyme APLT is sensitive to redox modifications of its -SH groups. Because activated macrophages produce reactive oxygen and nitrogen species, we hypothesized that macrophages can directly participate in apoptotic cell clearance by S-nitrosylation/oxidation and inhibition of APLT causing PS externalization.

## 3.2 METHODS

**Cell Culture:** HL-60 human promyelocytic leukemia cells (American Type Culture Collection) were grown in RPMI 1640 with phenol red supplemented with 12.5 % heat-inactivated fetal bovine serum at 37°C in a humidified atmosphere (5 % $CO_2$ plus 95 % air). Cells from passages 45–50 were used for the experiments. The density of the cells at collection time was $0.5x10^6$ cell/ml. RAW 264.7 macrophages (American Type Culture Collection) were grown in Dulbecco's modified Eagle's medium supplemented with 10 % heat-inactivated fetal bovine serum (Invitrogen), 100 units/ml penicillin, and 100 μg/ml streptomycin in a humidified atmosphere (5 % $CO_2$ plus 95 % air) at 37°C.

**Measurement of Thiol Contents:** Low molecular weight thiols and protein thiol contents in the cells were determined fluorometrically using ThioGlo$^{TM}$-1 as described previously (Tyurina, Serinkan et al. 2004). Briefly, cells treated with either SNCEE (50–300 μM) or GSNO (50–300 μM) for 30 min at 37°C were collected by centrifugation, washed, and resuspended in PBS. GSH was measured in cell lysates prepared by freezing and thawing cells. Immediately after addition of ThioGlo$^{TM}$-1 to the cell lysates, fluorescence was measured in a Packard Fusion$^{TM}$ Multifunctional Plate Reader (PerkinElmer Life Sciences) using excitation 390 ± 15 nm and emission 515 ± 30 nm. Protein sulfhydryls were determined as an additional increase in fluorescence response after addition of SDS (4 mM) to cell lysates.

**Measurement of S-Nitrosothiols:** The content of S-nitrosothiols was determined by fluorescence HPLC using DAF-2 that specifically reacts with $NO^{\cdot}$ (but not with other $NO_x$, $ONOO^-$, $NO_2^-$, or $NO_3^-$), yielding fluorescent DAF-2 triazole (Kojima, Nakatsubo et al. 1998). Briefly, samples (50 μl) were mixed with DAF-2 (5 μM) in 2.5 ml of PBS and exposed to UV irradiation (15 min at room temperature) using an Oriel UV light source (model 66002) (Oriel

Instruments, Stratford, CT) and cut-off filter (Balzers, >330 nm) (Tyurin, Tyurina et al. 2002). After UV irradiation, chloroform (200 µl) was added to precipitate proteins, and samples were centrifuged at 14,000 x g for 5 min. Supernatant was used for the measurements. Fluorescence HPLC (Eclipse XDB-C18 column, 5 µm, 150 x 4.6 mm; mobile phase was composed of 25 mM disodium phosphate buffer, pH 7.0, acetonitrile (94:6 v/v), Ex = 495 nm, Em = 515 nm) was performed on a Shimadzu LC-100AT HPLC system equipped with fluorescence detector (RF-10Axl) and autosampler (SIL-10AD). The data obtained were exported and processed using Shimadzu RF-5301 PC personal software. A standard curve was established using GSNO as the standard.

**PS Exposure on Cell Surface:** PS exposure on the surface of cells was determined by flow cytometric detection of annexin V staining using a protocol outlined in the annexin V-fluorescein isothiocyanate apoptosis detection kit (BioVision Research Products, Mountain View, CA). Briefly, HL-60 cells ($0.5 \times 10^6$) exposed to either S-Nitroso-L-Cysteine-ethyl ester SNCEE (50-300 µM) or S-nitrosoglutathione GSNO (50-300 µM) for 30 min at 37 °C in serum-free RPMI 1640 medium without phenol red, washed once with PBS, and resuspended in binding buffer were stained with annexin V (0.5 µg/ml) and propidium iodide (0.6 µg/ml) for 5 min at room temperature. After staining, cells were immediately analyzed using a FACScan flow cytometer (BD Biosciences) with simultaneous monitoring of green fluorescence (530 nm, 30 nm bandpass filter) for annexin V-fluorescein isothiocyanate and red fluorescence (long pass emission filter that transmits light >650 nm) associated with propidium iodide. Ten thousand events were collected and analyzed using the LYSIS™ II software (BD Biosciences).

**Caspase-3/7 Activity Assay:** Caspase-3/7 activity was measured using a luminescence Caspase-Glo® 3/7 assay kit (Promega, Madison, WI). HL-60 cells ($4 \times 10^5$) were incubated in

serum-free RPMI 1640 medium without phenol red in the presence of SNCEE (300 μM) or GSNO (300 μM) for 30 min at 37 °C. At the end of the incubation, cells were washed twice, and caspase-3/7 activity was measured. Luminescence was measured using a plate reading chemiluminometer ML1000 (Dynatech Laboratories). Activity of caspase-3/7 was expressed as luminescence arbitrary units per mg of protein.

**Nuclear Fragmentation:** Nuclear condensation/fragmentation of Hoechst 33342 (1 μg/ml)-labeled cells was evaluated as described previously (Uthaisang, Nutt et al. 2003). Cells were scored using a fluorescence microscope (Nikon ECLIPSE TE 200, Tokyo, Japan) equipped with a digital Hamamatsu CCD camera (C4742-95-12NBR).

**Phagocytosis of HL-60 Cells by RAW 264.7 Macrophages:** RAW 264.7 macrophages were seeded into an 8-well chamber slide ($5 \times 10^4$ cells/well) and cultured overnight in Dulbecco's modified Eagle's medium containing 10% fetal bovine serum. Naïve or nitrosatively modified HL-60 cells (i.e. treated in the presence of SNCEE (50-300 μM) as described above) were loaded with Cell Tracker Orange™ (10 μM) for 10 min at 37 °C. Cells were then washed twice and co-cultured with macrophages for 1 h at 37 °C. To inhibit caspase activation, HL-60 cells were pretreated with a pan-caspase inhibitor, Z-VAD-fmk (10 μM, for 30 min at 37 °C). To prevent oxidative damage leading to nonspecific changes in membrane biophysical properties, HL-60 cells pretreated with Z-VAD-fmk were exposed to a potent lipid antioxidant, etoposide (50 μM, for 1 h at 37 °C). In the same experiments macrophages were stimulated by lipopolysaccharide (LPS, 0.1 μg/ml for 6 h at 37 °C) and zymosan (0.25 mg/ml for 1 h at 37 °C). After incubation, unbound target cells were washed three times with RPMI 1640 medium and three times with PBS and fixed with solution of 2% formaldehyde in PBS containing Hoechst 33342 (1 μg/ml) for 1 h at 4 °C. The cells were examined under a Nikon ECLIPSE TE 200 fluorescence microscope (Tokyo, Japan) equipped with a digital Hamamatsu CCD camera

(C4742-95-12NBR) and analyzed using the MetaImaging Series™ software version 4.6 (Universal Imaging Corp.,Downingtown, PA). A minimum of 300 macrophages was analyzed per experimental condition. Results are expressed as the percentage of phagocytosis-positive macrophages.

**Superoxide Production:** Intracellular production of $O_2$. was assessed using the dihydroethidium (DHE) oxidation assay (Zhao, Kalivendi et al. 2003). DHE has been specifically recommended for assessments of superoxide production in cells because of its relatively high specificity. Macrophages ($0.3 \times 10^6$/well) were preincubated with DHE-DA (10 μM for 10 min at 37 °C) and then stimulated by zymosan (0.25 mg/ml) for 1 h at 37 °C. At the end of incubation, cells were washed three times with PBS, fixed with a solution of 2% formaldehyde in PBS. Treated cells were then examined under a Nikon ECLIPSE TE 200 fluorescence microscope (Tokyo, Japan) equipped with a digital Hamamatsu charge-coupled device camera (C4742-95-12NBR) and analyzed using the MetaImaging Series™ software version 4.6 (Universal Imaging Corp.).

**Nitric Oxide Production:** Intracellular production of $NO^{\cdot}$ was assessed using the DAF-2DA oxidation assay (Jourd'heuil 2002). DAF-2DA has been extensively used for analysis of NO production in cells. In contrast to other NO scavengers, DAF-2 does not readily react with $NO^{\cdot}$ metabolites ($NO_2^-$ and $NO_3^-$) and reactive nitrogen and oxygen species ($O_2^{\cdot}$, $H_2O_2$, or $ONOO^-$) (Kojima, Nakatsubo et al. 1998). Acetylated DAF-2DA readily penetrates into cells and, after hydrolysis, acts as a sensitive and one of relatively specific fluorogenic reagents for $NO^{\cdot}$. Naïve and LPS-stimulated (0.1 μg/ml, for 6 h at 37 °C) macrophages ($0.3 \times 10^6$/well) were incubated with DAF-2DA (2 μM, for 1 h at 37 °C) and were then incubated in the presence of zymosan (0.25 mg/ml) for 1 h at 37 °C. At the end of incubation, cells were washed three times with PBS and fixed with a solution of 2% formaldehyde in PBS. Treated cells were then examined

under a Nikon ECLIPSE TE 200 fluorescence microscope (Tokyo, Japan) equipped with a digital Hamamatsu charge-coupled device camera (C4742-95-12NBR) and analyzed using the MetaImaging Series™ software version 4.6 (Universal Imaging Corp.).

**Statistics:** The results are presented as either mean ± S.E. or mean ± S.D. values from at least three experiments, and statistical analyses were performed by either paired/unpaired Student's t test or one-way ANOVA. The statistical significance of differences was set at $p < 0.05$.

## 3.3 RESULTS

### 3.3.1 Exposure of cells to SNCEE but not GSNO results in elevation of S-NO thiols and depletion of reduced thiols

In our initial studies, we employed two physiologically relevant transnitrosylating reagents, SNCEE (Clancy, Cederbaum et al. 2001) and GSNO (Stoyanovsky, Tyurina et al. 2005). The former readily enters cells and hence is expected to cause transnitrosylation of proteins within intracellular environments; the latter is poorly cell-permeable and therefore can trans-nitrosylate proteins in extracellular compartments. UV-induced decomposition of S-nitrosothiols quantitatively releases $NO^{\cdot}$ (Tyurin, Tyurina et al. 2002). Therefore, we utilized UV exposure and DAF-2 as a specific probe for released $NO^{\cdot}$ to assess S-nitrosylation in homogenates of HL-60 cells. We found that the endogenous level of S-nitrosothiols in HL-60 cells was low and did not exceed 50 pmol/mg protein, in line with data reported previously (Zhang and Hogg 2004; Stoyanovsky, Tyurina et al. 2005). Incubation of HL-60 cells with SNCEE (50-300 μM) for 30 min at 37 °C resulted in a robust and dose-dependent accumulation of intracellular S-nitrosothiols (Figure 3A). A 7-fold increase in the S-nitrosothiol content (to 349 ± 20 pmol/mg protein) was detected after exposure of cells to 300 μM SNCEE (Figure 1A). In contrast, HL-60 cells exposed to GSNO revealed no significant accumulation of S-nitrosothiols as compared with control untreated cells (Figure 3A). S-trans-Nitrosylation converts -SH cysteines in S-NO derivatives (Foster, McMahon et al. 2003; Hess, Matsumoto et al. 2005). Thus, a decrease in thiol content is expected as a result of S-nitrosylation. Indeed, we found that SNCEE at a concentration of 300 μM was able to significantly deplete low molecular weight thiols (GSH) (Figure 3B, panel a) as well as protein sulfhydryls (Figure 3B, panel b) in HL-60 cells. Notably, the loss of GSH and protein -SH

groups significantly exceeded the amounts of accumulated S-NO thiols on an absolute scale suggesting that other types of oxidative protein modification occurred during exposure of HL-60 cells to SNCEE. As expected, the content of cellular thiols remained unchanged after treatment with GSNO

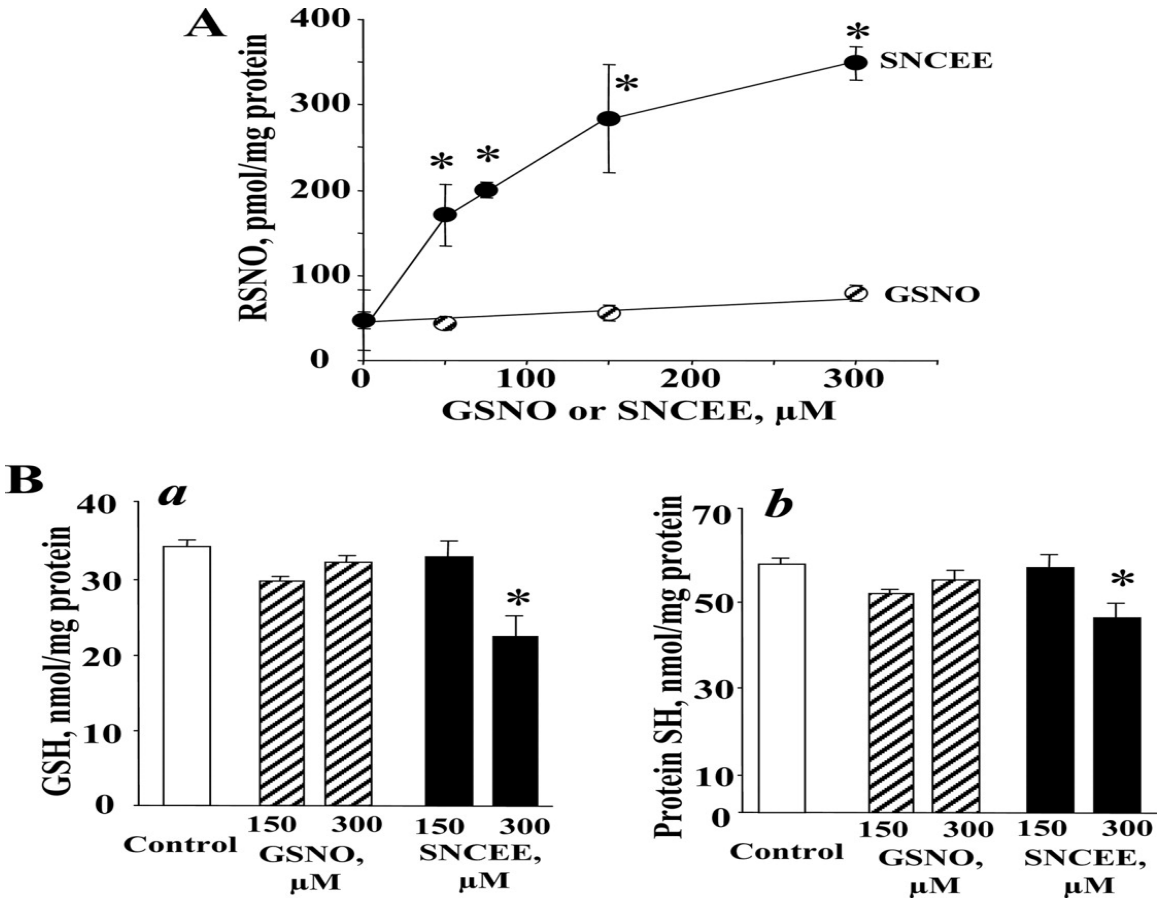


**Figure 3. Effect of SNCEE and GSNO exposure on the contents of reduced low molecular weight thiols, protein -SH groups, and S-nitrosothiols in HL-60 cells.** A, accumulation of S-nitrosothiols in HL-60 cells after treatment with SNCEE or GSNO. B, depletion of low molecular weight (panel a) and protein -SH (panel b) in HL-60 cells exposed to SNCEE or GSNO. HL-60 cells were incubated in the presence or absence of SNCEE and GSNO in serum-free RPMI 1640 medium without phenol red for 30 min at 37 °C. At the end of incubation, cells were washed with PBS, and reduced thiols and intracellular S-nitrosothiols were measured as described under "Experimental Procedures." (*, $p < 0.05$ versus untreated cells, mean ± S.E., ANOVA, n = 5).

### 3.3.2 SNCEE triggers PS externalization without activating the common apoptotic pathway

Furthermore, we were interested in determining the extent to which S-nitrosylation of cellular proteins and subsequent inhibition of APLT is associated with changes in PS externalization in HL-60 cells. To this end, cells were exposed to SNCEE (300 μM) for 30 min and subsequently co-stained with Hoechst 33342 (blue) and annexin V (green) for visualization of nuclear condensation and PS exposure, respectively. We found that cells readily externalized PS on their surface in response to SNCEE as evidenced by the appearance of typical patched fluorescent spots of annexin V (Figure 4A). No PS was detectable on the surface of nontreated cells (Figure 4A). To quantify the number of cells with externalized PS, we used flow cytometric analysis. Less than 4.8 ± 0.1% of control cells exposed PS on their surface. SNCEE caused a dose-dependent and a significant increase in the number of cells with externalized PS, 16.6 ± 1.3% of cells externalized PS 30 min after treatment with 300 μM SNCEE (Figure 4B). Next, we studied the time course of PS externalization. To this end, HL-60 cells were exposed to SCNEE (300 μM) for 30 min and then washed and further incubated in RPMI 1640 medium containing 12% fetal bovine serum for 0.5, 2, 4, 6, and 18 h at 37 °C in 5% $CO_2$.At the end of incubation, cells were examined for PS externalization. No further increase in the number of annexin V-positive cells was observed after 2, 4, 6, and 18 h of incubation (Figure 4C). In addition, no nuclear condensation or fragmentation was observed when HL-60 cells were exposed to SCNEE (Figure 4A). During apoptosis, PS externalization usually parallels caspase-3 activation (Vanags, Porn-Ares et al. 1996). However, no activation of caspase 3/7 was found in either SNCEE-treated cells (300 μM, 30 min) or in cells incubated for 0.5, 2, 4, 6, and 18 h after the SNCEE treatment (Figure 4C). Thus, at the time when SNCEE-induced externalization of PS was associated with phagocytosis of target cells, the caspase-dependent

pathways of apoptosis were not initiated. This is in line with the reported data indicating that in normal non-apoptotic cells caspase 3 is S-nitrosylated and that denitrosylation of caspase 3 is required for its catalytic activation (Mannick, Schonhoff et al. 2001). Therefore, SNCEE-induced PS externalization was disconnected from the common caspase-dependent pathway of apoptosis. No significant increase in the number of annexin V-positive HL-60 cells (versus nontreated controls) was observed after treatment with GSNO (Figure 4B).

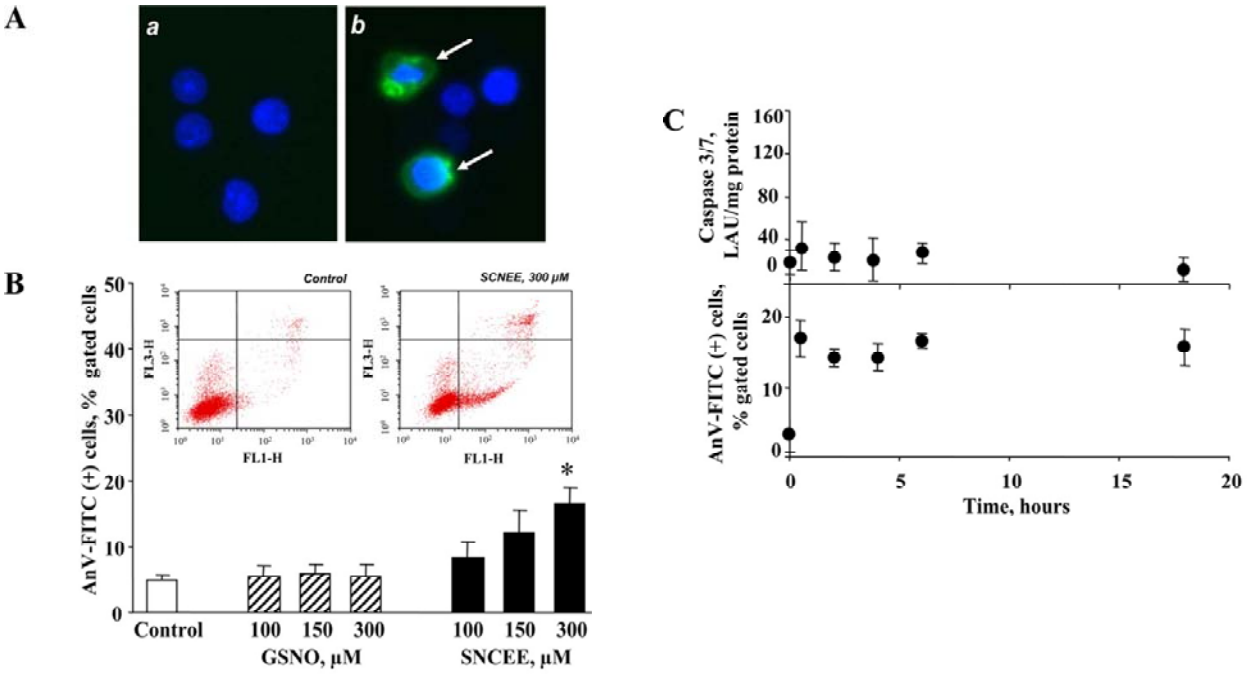


**Figure 4. PS externalization on the surface of HL-60 cells exposed to the trans-nitrosylating agent, SNCEE.** A, fluorescence micrographs of control HL-60 cells (panel a) and cells treated with SNCEE (300 μm) (panel b) for 30 min at 37 °C and stained with Hoechst 33342 (blue) and annexin V (green). Micrographs are representative of three experiments. Arrows show cells with externalized PS. B, flow cytometric detection of PS externalization in HL-60 cells treated with either SNCEE or GSNO. Control group represents cells without any stimulation. (*, $p < 0.05$, SNCEE versus control and GSNO exposed cells, mean ± S.D., ANOVA, n = 7.) Insets show typical flow cytometry results in the presence or absence of SNCEE (300 μm). C, caspase 3/7 activity (upper panel) and PS externalization (annexin V positivity, lower panel) in HL-60 cells treated with SCNEE (300 μm for 30 min at 37 °C), washed, and then incubated in RPMI 1640 medium containing 12% fetal bovine serum for 0.5, 2, 4, 6, and 18 h at 37 °C in 5% $CO_2$.

### 3.3.3 Dithiothreitol (DTT) reverses SNCEE-induced APLT inactivation and PS externalization in HL-60 cells

Recently, we have shown that vicinal di-thiols such as thioredoxin, dihydrolipoic acid, and DTT, in addition to their well known ability to reduce disulfides, can also de-nitrosylate S-nitrosylated proteins in live cells (Stoyanovsky, Tyurina et al. 2005). Thus, we hypothesized that inhibition of APLT activity and PS externalization on the cell surface induced by nitrosative stress can be reversed by DTT. Measurements of S-nitrosothiols revealed that ~65% of intracellular thiols were de-nitrosylated when DTT was added after SNCEE treatment (Figure 5C). Importantly, DTT was able to reverse SNCEE-induced inhibition of APLT up to 91% of its rate characteristic of control HL-60 cells (the rate of NBD-PS internalization was as high as 38.8 ± 1.5 pmol/min, insignificantly different from control HL-60 cells) (Figure 5A). DTT was also able to reverse SNCEE-induced PS externalization (Figure 5B). These results demonstrate that SNCEE-induced nitrosative/oxidative stress uncoupled from apoptotic caspase activation was responsible for the inactivation of APLT and externalization of PS in HL-60 cells.

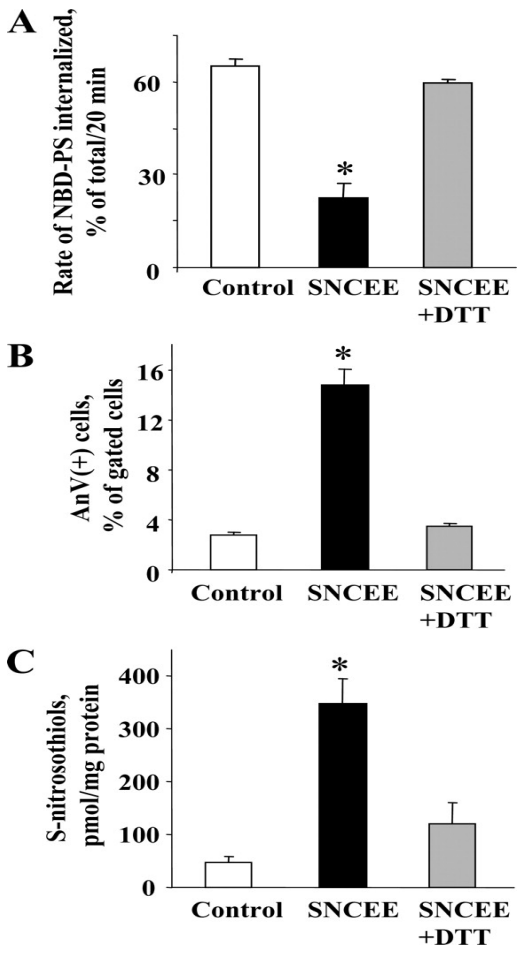


**Figure 5. Effect of DTT on APLT activity, externalization of PS, and reduction of S-nitrosothiols in HL-60 cells exposed to SNCEE.** HL-60 cells were exposed to SNCEE (300 μm) in serum-free RPMI 1640medium without phenol red for 30 min at 37 °C. At the end of incubation cells were washed with PBS, and the APLT activity (A), PS externalization (B), and content of S-nitrosothiols (C) were measured as described under "Experimental Procedures." (*, $p < 0.05$, SNCEE versus control and SNCEE + DTT, mean ± S.E., ANOVA, n = 5.)

### 3.3.4 RAW 264.7 macrophages elicit enhanced phagocytic activity toward "Nitrosylated" HL-60 cells

Because externalized PS is an important and universal recognition signal for engulfment of apoptotic cells by macrophages, we further tested whether exposure of non-apoptotic HL-60 cells to nitrosative stress would be sufficient for their phagocytosis. HL-60 cells pre-labeled with Cell Tracker Orange were treated with SNCEE (300 μM) and then co-incubated with RAW 264.7 macrophages. Relatively low levels of phagocytosis-positive macrophages (less than 2.0%) were detected when control (non-treated) HL-60 cells were co-incubated with RAW 264.7 macrophages (Figure 6A). In contrast, SNCEE-treated HL-60 cells were readily engulfed by RAW 264.7 macrophages (Figure 6A). The number of positive macrophages was dependent on the concentration of SNCEE and increased up to 15% after their co-incubation with HL-60 cells exposed to 300 μM of SNCEE (Figure 6B). To exclude potential minimal activation of caspases, HL-60 cells were pretreated with the pan-caspase inhibitor Z-VAD-fmk. We found that SNCEE caused a quantitatively similar pattern of engulfment by macrophages both in the absence and in the presence of Z-VAD-fmk. (Figure 6B). To further test whether oxidative damage potentially leading to nonspecific changes in membrane biophysical properties may be involved in recognition of nitrosylated cells by macrophages, we used etoposide, a previously reported potent inhibitor of lipid peroxidation in HL-60 cells (18, 52), along with Z-VAD-fmk. We found that etoposide/Z-VAD-fmk-pretreated cells incubated with SNCEE were effectively recognized and engulfed by RAW 264.7 macrophages (Figure 6B).

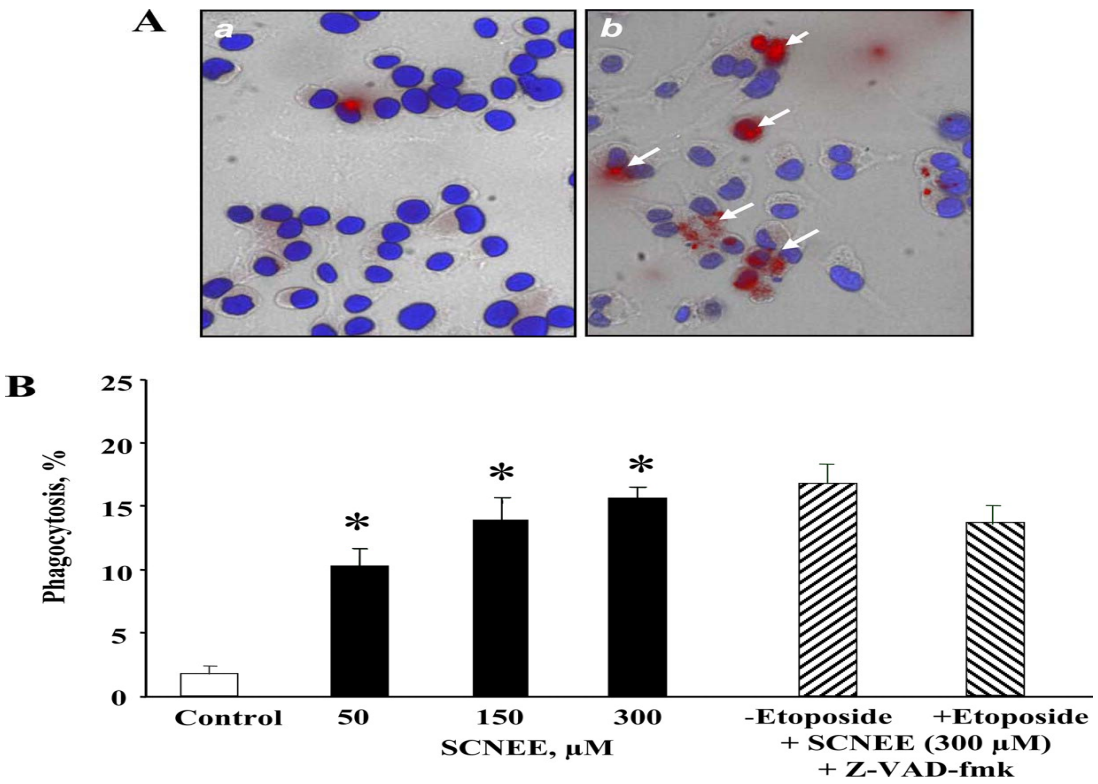


**Figure 6. Phagocytosis of HL-60 cells exposed to nitrosative stress by RAW 264.7 macrophages.** A, typical micrographs of engulfment of control HL-60 cells (panel a) and HL-60 cells exposed to 300 µm SNCEE (panel b) by RAW 264.7 macrophages (labeled with Hoechst 33342). Arrows show HL-60 cells engulfed by macrophages. B, percent of phagocytosis-positive RAW 264.7 macrophages (*, $p < 0.05$, SNCEE versus control, mean ± S.D., ANOVA, n = 7). HL-60 cells were labeled with Cell Tracker Orange™ and treated in the absence or presence of SNCEE for 30 min at 37 °C. In some experiments HL-60 cells were pretreated with a pan-caspase inhibitor, Z-VAD-fmk (10 µm, for 30 min at 37 °C). To prevent nonspecific oxidative damage, HL-60 cells pretreated with Z-VAD-fmk were exposed to etoposide (50 µm, for 1 h at 37 °C). The cells were co-incubated with RAW 264.7 macrophages for 1 h and subsequently analyzed for phagocytosis as described under "Experimental Procedures."

### 3.3.5 Activation of macrophages is associated with the generation of reactive oxygen species and reactive nitrogen species: Implications for PS externalization on target cells

Activation of macrophages is associated with the generation of reactive oxygen species and reactive nitrogen species known to cause both S-nitrosylation and oxidation of low molecular weight thiols and protein cysteines (Forman and Torres 2001). Therefore, we were anxious to further test our hypothesis in a physiologically more relevant environment by using activated RAW 264.7 macrophages and HL-60 cells as a source of nitrosative stress and target cells, respectively. First, we confirmed that LPS-stimulated and zymosan-treated RAW 264.7 macrophages indeed generate $O_2^{\cdot}$ and $NO^{\cdot}$. By using DHE-DA and DAF-2DA as specific probes for $O_2^{\cdot}$ and $NO^{\cdot}$, respectively (Jourd'heuil 2002; Zhao, Kalivendi et al. 2003), we found that generation of $NO^{\cdot}$ in LPS/zymosan-stimulated DAF-2DA-loaded RAW 264.7 macrophages was significantly increased (Figure 7A). Similarly, zymosan caused a robust intracellular production of $O_2^{\cdot}$ radicals as evidenced by the increased number of DHE-positive cells (Figure 7B).

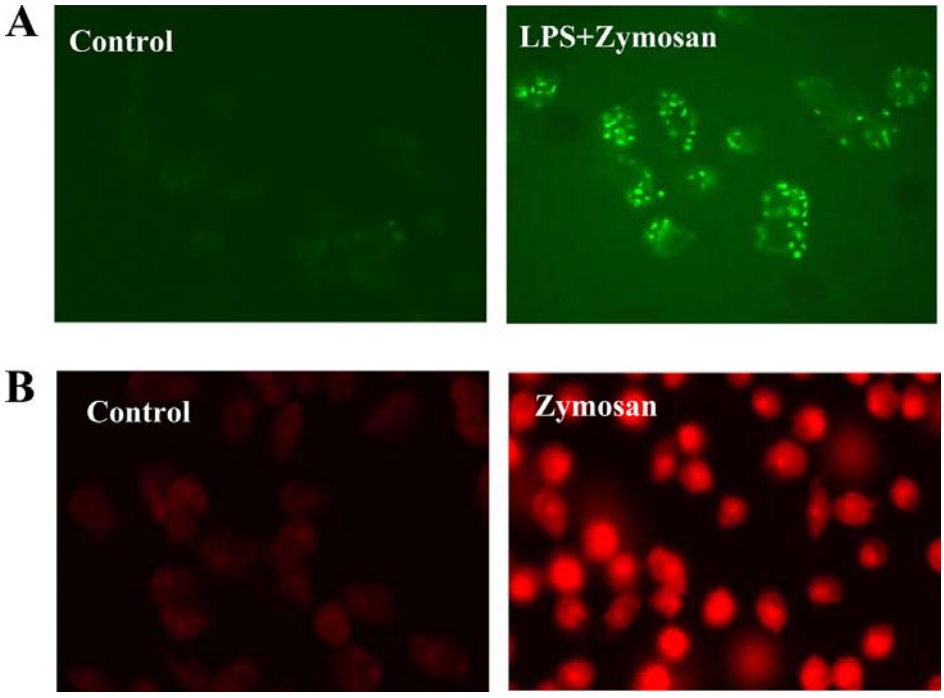


**Figure 7. Nitric oxide and superoxide production in LPS-stimulated zymosan-activated macrophages.** A, evaluation of the number of NO.-producing cells by fluorescence microscopy of DAF-2 oxidation to DAF-2 triazole. Naïve and LPS-stimulated (0.1 μg/ml, for 6 h at 37 °C) macrophages ($0.3 \times 10^6$/well) were incubated with DAF-2DA (2 μm, for 1 h at 37 °C) and were then treated with zymosan (0.25 mg/ml) for 1 h at 37 °C. At the end of incubation, cells were washed three times with PBS, fixed with a solution of 2% formaldehyde in PBS, and examined under a Nikon ECLIPSE TE 200 fluorescence microscope. B, evaluation of the number of $O_2$.-producing cells by fluorescence microscopy of DHE oxidation. Macrophages ($0.3 \times 10^6$/well) were preincubated with DHE-DA (10 μm for 10 min at 37 °C) and then stimulated by zymosan (0.25 mg/ml) for 1 h at 37 °C. At the end of incubation, cells were washed three times with PBS, fixed with a solution of 2% formaldehyde in PBS, and examined under a Nikon ECLIPSE TE 200 fluorescence microscope. Photomicrographs in A and B are representative of three independent experiments.

### 3.3.6 LPS-stimulated macrophages readily engulf HL-60 cells in the presence of zymosan

It was found that naïve HL-60 cells co-incubated with LPS-stimulated macrophages in the presence of zymosan for 1 h at 37 °C were readily engulfed (Figure 8A). The number of positive macrophages was increased to 26.4 ± 1.7% (versus 2% in control with nonstimulated macrophages without zymosan). The number of phagocytosis-positive macrophages was

significantly decreased when annexin V was added to the incubation medium confirming the participation of externalized PS as an essential recognition signal (Figure 8B). Moreover, DAF-2, a non-cell-permeable scavenger of $NO^{\cdot}$, added to the incubation system was able to quench $NO^{\cdot}$ produced by activated macrophages, which released 54 ± 12 pmol of $NO^{\cdot}/10^6$ cells. Importantly, DAF-2 significantly inhibited the phagocytosis of HL-60 target cells by RAW 264.7 macrophages (Figure 8B), thus supporting the notion that macrophage-generated $NO^{\cdot}$ contributes to efficient phagocytosis of target cells.

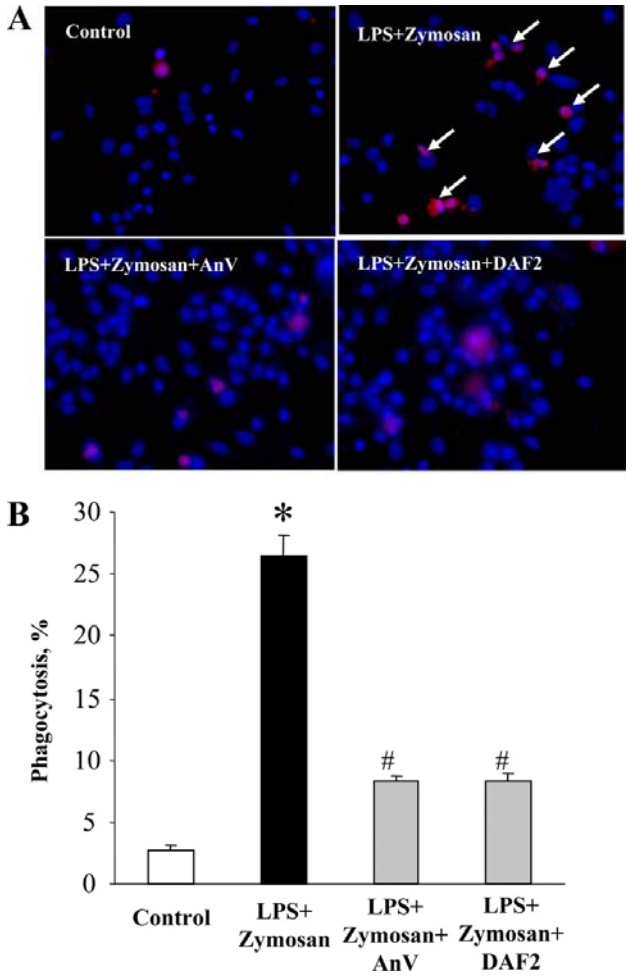


**Figure 8. Effect of nitrosative stress induced by stimulated RAW 264.7 macrophages on the phagocytosis of HL-60 cells.** A, typical microphotographs of engulfment of HL-60 cells by LPS + zymosan-stimulated RAW 264.7 macrophages (arrows, upper right panel). In the presence of annexin V (AnV, lower left panel) or DAF-2 (lower right panel) phagocytosis of HL-60 cells by LPS + zymosan-stimulated RAW 264.7 macrophages is decreased. B, effect of

annexin V and DAF-2 on number of phagocytosis-positive LPS-stimulated RAW 264.7 macrophages (*, $p < 0.05$, LPS + zymosan versus control; #, $p < 0.05$, LPS + zymosan + annexin V and versus LPS + zymosan + DAF-2 versus LPS + zymosan; mean ± S.E., ANOVA, n = 5). HL-60 cells were labeled with Cell Tracker Orange™ (10 μm for 10 min at 37 °C). Then cells were co-incubated with LPS-stimulated RAW 264.7 macrophages in the presence of zymosan for 1 h and subsequently analyzed for phagocytosis as described under "Experimental Procedures."

## 3.4 CONCLUSIONS

This work demonstrates for the first time that nitrosative stress causes inhibition of APLT, externalization of PS on the cell surface, and subsequent elimination of these cells by macrophages. The physiological significance of these findings is underscored by the importance of effective apoptotic cell clearance, whose success provides for safe elimination of unwanted cells without accompanying excessive inflammation and/or autoimmunity. Thus, paradoxically, $NO^{\cdot}$, a well known participant of inflammatory and immune responses, acts also as a regulator of these responses via controlling the process of phagocytosis. Moreover, the role of this regulatory nitrosative stress-driven pathway is also evident from the independence of PS externalization on the common pathway of caspase-mediated apoptosis. Of note, numerous studies have shown that S-nitrosylation of the active-site cysteine residue of caspases results in the inhibition of their catalytic activities (Dimmeler, Haendeler et al. 1997; Melino, Bernassola et al. 1997; Torok, Higuchi et al. 2002), and only denitrosylation of caspases allows the catalytic site to function (Mannick, Schonhoff et al. 2001). These findings are in line with our previous studies showing that oxidative stress inactivates caspases in human neutrophils, yet induces the simultaneous caspase-independent PS externalization (Fadeel, Ahlin et al. 1998). Because the engulfment and removal of dying cells define the "meaning" of cell death (Savill and Fadok 2000), one may argue that nitrosative/oxidative stress is ultimately a pro-death event or, at any rate, a pro-clearance event, which could have important implications for the resolution of inflammation. In conclusion, our work has established that nitrosative/oxidative modification of APLT enhances PS externalization in target cells by inhibiting APLT activity and promotes the disposal of these cells by macrophages. Thus, nitrosative/oxidative stress may significantly contribute to the clearance of effete cells and, hence, to the resolution of inflammation. These findings suggest that nitric

oxide produced by activated macrophages, through its effects on PS-dependent phagocytosis of neighboring target cells, is engaged in a feedback mechanism limiting excessive inflammatory responses.

We and others have demonstrated that the PS signaling pathway turns off the production of pro-inflammatory cytokines and reactive oxygen and nitrogen species by activated macrophages (Huynh, Fadok et al. 2002; Serinkan, Gambelli et al. 2005). Thus, nitrosative stress realized via $NO^{\cdot}$-dependent macrophage processes and causing PS externalization in target cells acts as a novel mechanism for regulation of the inflammatory response. In line with this, therapy of inflammatory conditions using $NO^{\cdot}$-releasing drugs has shown considerable promise. Indeed, addition of an NO moiety to non-steroidal anti-inflammatory drugs sufficiently reduced their toxicity and enhanced their therapeutic effects (Davies, Roseth et al. 1997; Wallace 2006). Nanoparticles, especially SWCNT, are widely utilized for improvements of drug delivery and therapeutic efficacy of drugs (Bianco, Hoebeke et al. 2005). Non-functionalized SWCNT, however, are poorly recognized by macrophages. Hence, we hypothesize that coating of SWCNT with PS will result in a remarkable improvement in their recognition by macrophages. In the studies described in the above chapter we found that PS acts as an eat-me signal on the surface of apoptotic cells and predict that PS coating may also act the same on nanotubes. PS-coated nanotubes may also be utilized as a novel tool for the regulation of inflammatory responses.

# 4 CHAPTER 4 - PHOSPHATIDYLSERINE AS AN "EAT-ME" SIGNAL ON SWCNT FOR PROFESSIONAL PHAGOCYTES

## 4.1 INTRODUCTION

Broad applications of single-walled carbon nanotubes (SWCNT) dictate the necessity to better understand their health effects. Poor recognition of non-functionalized SWCNT by phagocytes is prohibitive towards controlling their biological action. Specific interfacing of SWCNT with phagocytic cells of the immune system – macrophages, microglia, and neutrophils - is important for several reasons. The first one is that SWCNT can be used for simultaneous targeted delivery of several different regulators/inhibitors with a potential to release them in temporally and spatially predetermined ways to control the bioactivity of a specific cell population during physiologically critical events. Subsequently the complete clearance of therapeutic SWCNT from the body majorly relies up on their uptake by phagocytic cells. Also, as macrophages can host a number of pathogens (Celli 2006; Houben, Nguyen et al. 2006), nanocarriers can also be used for specific delivery of pro-apoptotic agents to aid in the defense against intracellular pathogens (Lecaroz, Gamazo et al. 2006). Furthermore, macrophages and microglia are the major executors of pro-/anti-inflammatory responses, and - along with antigen-presenting dendritic cells - are important components of immune reactions (Twigg 2004; Serhan and Savill 2005; Grayson 2006). Specific targeting of cargoes/regulators to these cells could be exploited for therapeutic regulation of numerous immune functions, including the enhancement of immune responses to prophylactic or therapeutic allergen-specific vaccines through the coupling of allergens to nanocarriers. Finally, SWCNT are among the most commonly used nanomaterials with explosively expanding research and commercial applications (Service 2004). Because the production and employment of industrial quantities of

SWCNT are becoming a reality, health risk concerns, particularly due to occupational and environmental exposures, are emerging. Not only an unusually large surface area, but also unique physical and chemical characteristics, redox features as well as significant decoration with transition metals alert to a possibility of unanticipated bioresponses resulting from interactions of SWCNT with cells, tissues, and biofluids. In fact, recent studies have demonstrated significant pulmonary and cardiovascular toxicity of SWCNT associated with a robust inflammatory response and early onset of fibrotic transition in mice (Lam, James et al. 2004; Shvedova, Kisin et al. 2005; Shvedova, Kisin et al. 2008). In this context, the enhancement of phagocytic recognition and uptake of SWCNT through PS-functionalization may be important in order to reduce the potential cytotoxicity of SWCNT.

## 4.2 METHODS

**Atomic force microscopy (AFM)-**After sonication, 20 μL of SWCNT in 25 mM HEPES buffer (pH 7.4) was placed on a freshly cleaved mica which was subsequently rinsed with DI water while being spun at 950 rpm to remove the excess of the buffer solution. The samples were air-dried prior to imaging. AFM images were collected in a tapping mode with a Multimode Nanoscope IIIa microscope (Digital Instruments, Santa Barbara, CA) in air.

**Coating of SWCNT with phospholipids and other cargoes-**In all presented experiments, the SWCNT subjected to chemical cutting by $H_2SO_4$ plus $H_2O_2$ have been utilized. The morphology of thus obtained SWCNT preparations was assessed by TEM, SEM as well as AFM. Following the chemical cutting of SWCNT, the nanotubes were used for coating with cargoes (phospholipids, cyt c). Therefore, neither phospholipids nor cyt c were exposed to aggressive environments employed for the SWCNT cutting protocol. SWCNT were sonicated with either 2.5 mM DOPC or 5 mM DOPC: DOPS at the ratio of 1:1 (3 cycles 30 s), then washed 4 times with 25 mM HEPES, pH 7.4. After each washing, samples were centrifuged at 50,000 g for 30 min at 4°C. To prepare fluorescently labeled nanotubes, SWCNT were sonicated with either PC or PC/PS liposomes containing NBD-PC or NBD-PS (10% of total phospholipids), respectively. For the PS-coated Annexin V treated SWCNT, PS-coated SWCNT were incubated with Annexin V (25 mg/mg SWCNT) in Annexin V binding buffer for 5 min at room temperature and then washed twice with 25 mM HEPES, pH 7.4 to remove non-bound Annexin V. After each washing, PS-coated/Annexin V treated SWCNT were centrifuged at 50,000 g for 15 min. To prepare PS/cyt c/SWCNT, nanoparticles (0.3 mg/ml) were incubated in 25 mM HEPES buffer, pH 7.4 with 50 μM cyt c for 30 min at room temperature. To remove non-bound cyt c, SWCNT were washed twice with 25 mM HEPES buffer pH 7.4 and centrifuged at 50,000 g for 30 min at 4°C. After that, cyt c/SWCNT were

sonicated in the presence of 3 mM PC:PS liposomes (at the ratio of 1:1) 3 cycles for 30 s and then washed 4 times with 25 mM HEPES. After each washing, samples were centrifuged at 50,000 g for 30 min at 4°C. Coated SWCNT were finally suspended in 25 mM HEPES pH 7.4 (containing a transition metal chelator, DTPA (100 μM) to prevent oxidative damage to lipids and protein) using the same volume as the original suspension. Endotoxin content in SWCNT suspensions and its amounts present in the medium during incubations were approximately 300–500 times lower than those causing stimulation of macrophages.

**Determination of phospholipid content-**Phospholipids from coated SWCNT were extracted using Folch procedure (Folch, Lees et al. 1957) and separated by one dimensional HPTLC. Spots of PS or PC were visualized by exposure to iodine vapors and compared with authentic standards. Phospholipid phosphorus was determined using sub-micro method.

**Animals-**Specific-pathogen-free adult female C57BL/6 mice (7–8 wk) were supplied by Jackson Lab (Bar Harbor, ME) and weighed 20.3±0.2 g at time of use. Animals were individually housed in AAALAC-approved NIOSH animal facilities in microisolator cages for one week prior to use. Autoclaved Beta Chip bedding (Northeastern Products Corp., Warrensburg, NY) was changed weekly. Animals were supplied with water and Harlan Teklad, 7913, NIH-31 Modified Mouse/Rat Diet, Irradiated (Harlan Teklad, Madison, WI) and housed under controlled light, temperature and humidity conditions. Experiments were conducted under a protocol approved by the Animal Care and Use Committee of the NIOSH. Mice were randomized into three experimental groups treated either with non-coated SWCNT, PC-coated SWCNT or PS-coated SWCNT on day 0. Animals were sacrificed on day 1 following exposures.

**Particulate Instillation-**Pharyngeal aspiration was used for particulate administration to C57BL/6 mice. Briefly, after anesthization with ketamine and xylazine anesthesia (62.5 and

2.5 mg/kg, respectively), the mouse was placed on a board in a near vertical position. The animal's tongue was extended with lined forceps and a suspension of particulates (50 µl, non-coated SWCNT, PC-coated SWCNT or PS-coated SWCNT at a dose of 40 µg/mouse) was placed in the posterior of pharynx. The tongue was held until the suspension was aspirated into the lungs. All mice in particle and PBS groups survived this exposure procedure. This technique provides good distribution of particles widely disseminated in a peri-bronchiolar pattern within the alveolar region (Rao, Tinkle et al. 2003). Animals treated with the particulates recovered easily after anesthesia with no behavioral or negative health outcomes.

**Bronchoalveolar lavage-**Mice were weighed and euthanized with intraperitoneal injection of sodium pentobarbital (SPB, Fort Dodge Animal Health, Fort Dodge, Iowa) (>100 mg/kg). The trachea was cannulated with a blunted 22 gauge needle, and BAL was performed using cold sterile $Ca^{2+}$+$Mg^{2+}$-free PBS at a volume of 0.9 ml for first lavage (kept separate) and 1.0 ml for subsequent lavages. Approximately 5 ml of BAL fluid per mouse was collected and pooled in sterile centrifuge tubes. Pooled BAL cells were washed in $Ca^{+2}$+$Mg^{+2}$-free PBS by alternate centrifugation (800×g for 10 min at 4°C) and resuspension.

**Cells-**Primary microglia was isolated from brains of postnatal day 5 rats as described (Bettinger, Thanos et al. 2002). More than 80% of the cell population was represented by microglia as evidenced by immunostaining with the microglia CD11 (mouse monoclonal anti-CD11 antibody were from Novus Biologicals, Inc. (Littleton, Colorado, USA); Alexa Fluor 488 goat anti-mouse secondary antibody were from Molecular Probes (Eugene, Oregon USA).HeLa cells and RAW264.7 macrophages (American Tissue Culture Collections; ATCC) were grown in DMEM supplemented with 10% heat inactivated fetal bovine serum (FBS), 100 units/ml penicillin and 100 µg/ml streptomycin.SH-SY5Y neuroblastoma cells (ATCC) were

kept in DMEM:F12 (1:1) supplemented with 2 mM glutamine, 1% non essential amino acids and 15% fetal bovine serum (FBS).

**Cell exposure to particles-**Cells (at density of $0.3\times10^6$/ml for RAW 264.7 macrophages and HeLa cells, $0.5\times10^6$/ml for HMDM and MDDC, $3\times10^5$/ml for microglia and SH-SY5Y neuroblastoma cells) were exposed to non-coated SWCNT or PC-coated SWCNT, PS-coated SWCNT (0.02 mg/ml, calculated by concentration of SWCNT, or 0.1 mg/ml for HMDM and MDDC) for 2 h (and 24 h for some experiments using MDDC) in serum-free medium, except for primary human phagocytes which were maintained in cell culture medium supplemented with 10% heat-inactivated serum so that cell viability was not compromised. For the purpose of uniformity we present the condition of exposure to SWCNT using the ratios of SWCNT (μg)/$10^6$ cells. The ratios SWCNT to cells were 125–150 μg/$10^6$ cells. In the experiments with cyt c/PS-coated SWCNT chloroquine (100 μM) was applied as endosome disruptor and cells were incubated for 15 min at 37°C. Cells were washed once with DMEM medium and then incubated in DMEM medium containing 10% FBS for additional 2 h. At the end pointed incubation, cells were washed with PBS, collected and used for assessment of caspase 3/7 activity and externalized of PS. Cytotoxicity was confirmed using Trypan blue exclusion as well as LDH release (with CytoTox-ONE™ Homogeneous Membrane Integrity Assay (Promega, WI) kit).

**Assessment of cytokines-**RAW macrophages were seeded at $2.5\times10^5$ cells/well 12 h before treatment. Cells were incubated with 0.25 mg/ml zymosan in the presence or absence of SWCNT, PS-coated SWCNT or PC-coated SWCNT (all at the level of 150 μg/$10^6$ cells) in normal culture medium for different time periods. At the end of incubation, the medium was collected and subjected to 50,000 g centrifugation at 4°C for 30 min to remove nanoparticles from the solution. The supernatant was then used to measure cytokines. R&D Quantikine ®

immunoassay kit (R&D system Inc. Minneapolis, MN) was used for measurements according to the manufacturer's manual.

**Caspase 3/7 activity**-was measured using Caspase-Glo 3/7 Assay kit (Promega, Madison WI, USA).

**PS exposure**-was determined by fluorescently microscopic detection of annexin V as outlined in the annexin V-FITC apoptosis detection kit (BioVision Research Products, Mountain View, CA). Cells were analyzed under a Nikon ECLIPSE TE 200 fluorescence microscope (Tokyo, Japan) equipped with a digital Hamamatsu CCD camera (C4742-95-12NBR) using the MetaImaging Series™ software version 4.6 (Universal Imaging Corp., Downingtown, PA). A minimum of 300 cells were analyzed per experimental condition.

**Fluorescent microscopy-**Cells were seeded on cover slides 18 h before treatment, 20 μg/ml of various functionalized SWCNT were added and incubated in DMEM with no phenol red at 37°C for 2 h. At the end of incubation cells were gently washed 3 times with PBS, fixed by 2.5% paraformaldehyde at RT for 5 min and examined under a Nikon ECLIPSE TE 200 fluorescence microscope (Tokyo, Japan) equipped with a digital Hamamatsu charge-coupled device camera (C4742–95-12NBR) and analyzed using the MetaImaging Series™ software version 4.6 (Universal Imaging Corp., Downingtown, PA).

**Confocal microscopy-**RAW 264.7 macrophages were seeded on LabTek chamber slides at a density of $5\times10^5$ cells per well the previous day. The normal DMEM medium was replaced with phenol red free RPMI 1640 medium the next day and incubated with LysoTracker Red-DND99 (50 nM) for 1 h to label lysosomes. Prior to incubation with LysoTracker Red, RAW 264.7 macrophages ($5\times10^5$ cells per well) were incubated with cocktail of endocytosis inhibitors containing a mixture of nystatin (25 μg/ml), genistein (200 μM), chlorpromazine (6 μg/ml) and brefeldin A (10 μg/ml) for 30 min as described [40]. Cells were then washed twice

with PBS followed by addition of various functionalized SWCNT (150 μg/$10^6$ cells). The cells were incubated with particles for 5 minutes for the purpose of confocal microscopy. Cells were then washed three times with PBS and fixed using 2% paraformaldehyde. Nuclei were stained with Hoechst 33342. Cells were imaged using Olympus Fluoview 1000 confocal microscope. Following incubation for 2 or 24 h with NBD-labeled SWCNT, MDDCs were fixed in 4% formaldehyde for 15 min. Staining of cell membranes was carried out using anti-HLA-DR mAb (Becton Dickinson). A secondary goat anti-mouse mAb labeled with Alexa Fluor 546 (Molecular Probes, Eugene, OR) was used for detection. Slides were mounted with anti-fading Vectashield mounting medium (Vector laboratories, Burlingame, CA). Fluorescent images were acquired on a confocal laser-scanning microscope (TCS SP2; Leica Microsystems, Mannheim, Germany) equipped with one argon and two HeNe lasers. NBD was excited with a 488-nm laser line detecting light in the wavelength region of 560–700 nm. Alexa 546 was excited by a 543-nm laser line with detection of light in the region of 560–700 nm.

**Scanning Electron Microscopy-**Macrophages fixed in cold 2.5% glutaraldehyde were rinsed in PBS, post-fixed in 1% Osmium Tetroxide (Electron Microscopy Sciences, Hatfield, PA) with 0.1% potassium ferricyanide (Fisher Scientific, Pittsburgh, PA) dehydrated through a graded series of ethanol, from 30 to 100%, and then critical point dried in a critical point dryer, Emscope CPD, (EMScope Lab, Ashford, Great Britain). Following critical point drying, the samples were attached to aluminum SEM specimen mounting stubs (Electron Microscopy Sciences) and then sputter coated with a gold palladium alloy (Sputter Coater 108 Auto, Cressington Scientific Instruments, Cranberry Township, PA). Following processing, samples were analyzed using a JEM 6330F microscope (JEOL, Peabody, MA).

**Transmission Electron Microscopy-**Macrophages were fixed in 2.5% glutaraldehyde for 1 h, pelleted, and re-suspended in 3% gelatin in PBS, olidified at 4°C, and then re-fixed for 15 min.

Pellets were washed 3 times in PBS and then postfixed in 1% $OsO_4$ and 1% $K_3Fe(CN)_6$ for 1 hour. After 3 PBS washes, the pellet was dehydrated through a graded series of 30% to 100% ethanol then incubated in Polybed 812 epoxy resin (Polysciences, Warrington, PA) for 1 h. After several changes of 100% resin over 24 h, pellet was cured at 37°C overnight with additional hardening at 65°C for 48 h. Ultrathin (60 nm) sections were collected on 200 mesh grids and stained with 2% uranyl acetate in 50% methanol for 10 min followed by 1% lead citrate for 7 min. Sections were observed on a JEM 1210 electron microscope (JEOL, Peabody, MA) at 80 kV.

**Statistics-**The results are presented as mean±s.d. values from at least three experiments, and statistical analyses were performed by either paired/unpaired Student's t-test or one-way ANOVA. The statistical significance of differences was set at $p< 0.05$.

## 4.3 RESULTS

### 4.3.1 Physico-chemical characterization of functionalized SWCNT

We prepared SWCNT coated with DOPC, as a control (PC-coated SWCNT), or a mixture of DOPS, plus PC (PS-coated SWCNT) by incubating nanotubes in the presence of liposomes containing these lipids (PC or a mixture of PS plus PC at a molar ratio of 1:1). Successful integration and the content of PS and PC associated with SWCNT were confirmed by direct assessment of the phosphorus content after HPTLC separation of phospholipids (Figure 9Aa). We found that PC-coated SWCNT contained 462 ± 33 nmol PC/mg SWCNT. Analysis of PS-coated SWCNT revealed that amounts of integrated PS and PC on nanotubes were approximately similar: 198 ± 14 and 223 ± 13 nmol of phospholipids/mg SWCNT, respectively (Figure 9Ab). Additionally, the presence of PS on the surface of SWCNT was verified using FITC-conjugated PS-specific protein, Annexin V, by measuring its characteristic fluorescence (Figure 9B). After treatment of PS-coated SWCNT with FITC-conjugated Annexin V, the appearance of a robust fluorescence response was observed.

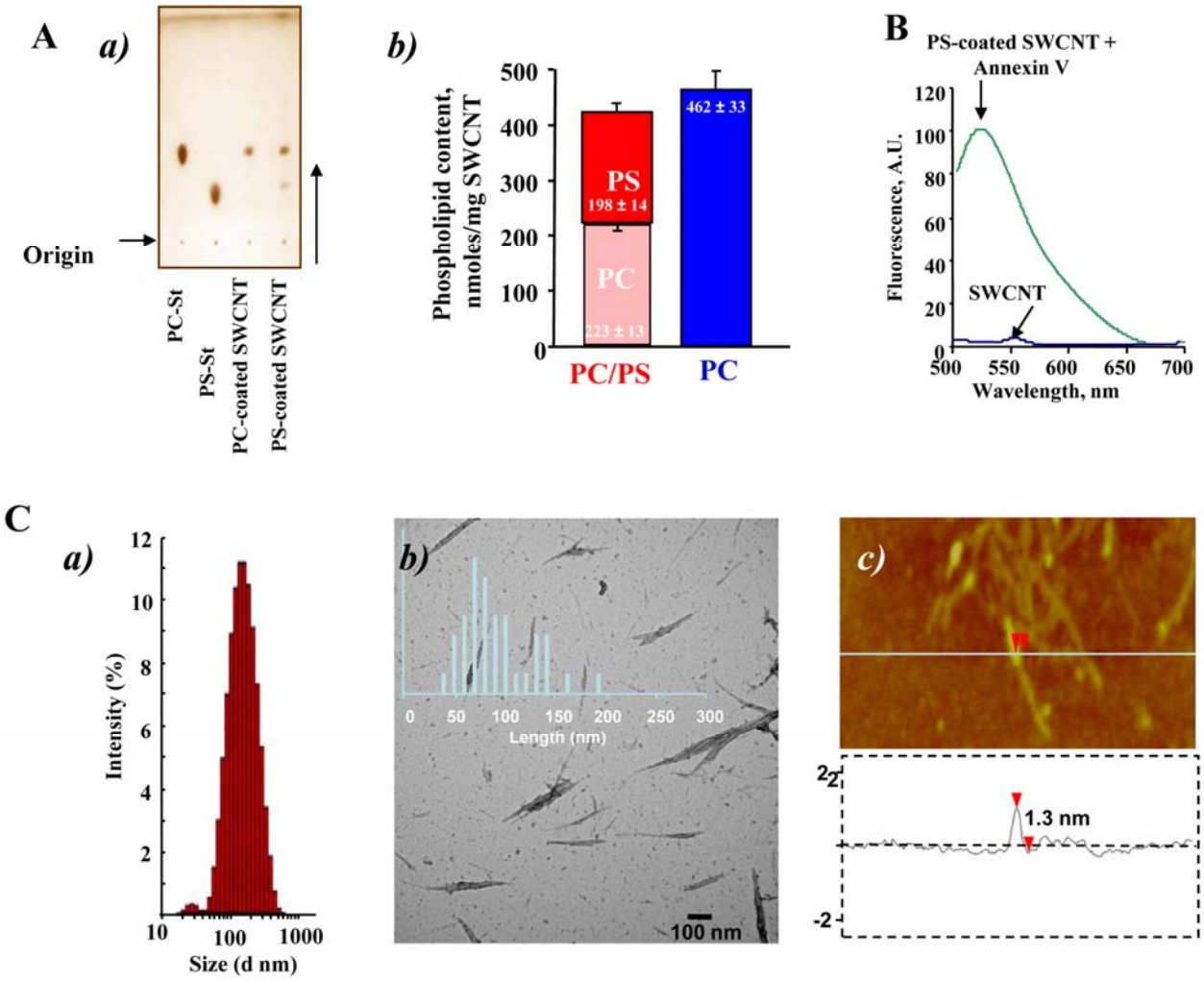


**Figure 9. Physico-chemical characterization of SWCNT.** A. Evaluation of phospholipid content of PC-coated or PS-coated SWCNT. a) Typical one-dimensional HPTLC of phospholipids extracted from PC-coated or PS-coated SWCNT. b) Phospholipid content of phospholipid-coated SWCNT. B. Typical fluorescence spectrum of Annexin V bound to PS-coated SWCNT. Note that a robust fluorescence response (Annexin V-FITC binding) was recorded from PS-coated but not from non-coated or PC-coated SWCNT. C. Physico-chemical characterization of bare SWCNT. a) Typical histograms of size distribution assessed by dynamic light scattering; b) AFM images of bare SWCNT deposited on mica substrates; c) The height cross section analysis of bare SWCNT.

### 4.3.2 Scanning and Transmission electron microscopic evaluation of SWCNT-Phagocyte interactions

To investigate interactions of SWCNT with the surface of macrophages, we performed SEM imaging (Figure 2A). We found that PS-coated SWCNT were actively recognized and tethered to the surface of RAW264.7 macrophages. At higher magnifications (Figure 10Aa), we were able to detect the presence of SWCNT fibers on the surface of macrophages. Numerous filopodia – budding off the macrophages surface – associated with their major functions such as phagocytosis and substrate adhesion were observed in RAW264.7 macrophages exposed to PS-coated SWCNT. In contrast, non-coated (Figure 10Ab), PC-coated (Figure 10Ac) and PS-coated Annexin V treated (Figure 10Ad) SWCNT were ingested to a lesser extent by macrophages, and the presence of these types of SWCNT on the surface of RAW264.7 macrophages was observed much less frequently. TEM evaluations of the uptake of SWCNT showed that RAW264.7 macrophages readily phagocytozed PS-coated SWCNT (Figure 10Ba) while a significantly less pronounced engulfment of PC-coated and non-coated SWCNT was documented (Figure 10Bc). At higher magnifications (Figure 10Ba), PS-coated SWCNT fibers within phagosomes could be seen. To distinguish SWCNT from autophagic bodies inside of phago-lysosomes we used a high magnification TEM imaging (100,000×). Further, in order to better identify nanoparticles in cells we performed TEM imaging of nanotubes alone which were processed in a fashion similar to that of cells for electron microscopy. SWCNT alone appear as “bamboo shoots” and resemble SWCNT that have been engulfed by RAW264.7 macrophages (Figure 10Bab). Markedly less of “bamboo shoot”-like material was detected in RAW264.7 macrophages exposed to PC-coated or non–coated SWCNT (Figure 10Bc). Quantitative assessments of the number of nanotubes present in an endosome within a 60 nm ultrafine section of cells could be complicated by the fact that the same SWCNT could be cut

1, 2 or more times, especially SWCNT bundles or “bird's-nest”-like aggregates. Therefore, we presented the data as a plot of percentage of active phagocytes in analyzed samples. We considered as active macrophages those that engulfed at least one nanoparticle. We found that amongst the various treatment groups, 70% macrophages treated with PS-coated SWCNT showed active phagocytosis with nanoparticles inside, which was approximately twice the phagocytosis-positive population of cells co-incubated with PC-coated SWCNT. Annexin V that masks PS (van Engeland, Nieland et al. 1998) and affects its recognition (Vermes, Haanen et al. 1995) effectively blocked the recognition by 50% as indicated by a lower cell population with active phagocytes (Figure 10Bc).

### 4.3.3 Effect of SWCNT on cytokine release by RAW264.7 macrophages

Apoptotic cells with externalized PS quench the production and release of pro-inflammatory cytokines by macrophages (Huynh, Fadok et al. 2002; Serinkan, Gambelli et al. 2005). To assess whether PS-coated SWCNT display a similar effect, we employed a standard stimulation of TNF-α formation in RAW264.7 macrophages by zymosan (Vadiveloo 1999; Underhill 2003) and evaluated the effects of SWCNT. PS-coated SWCNT were more potent in inhibiting TNF-α production by stimulated macrophages than PC-coated or non-coated SWCNT (Figure 10C). Thus, uptake of PS-SWCNT is accompanied by typical PS-dependent suppression of the pro-inflammatory macrophage response. It should be noted that macrophages stimulated with SWCNT alone - in the absence of zymosan - showed a significant increase in the TNF-α production up to 497 ± 24 pg/ml vs. 40±10 ($^{\#\#}$ $P<0.05$) in the control. Notably, in PS-coated SWCNT, TNF-α levels dropped to 368 ± 33 pg/ml. No significant changes in the content of TNF-α was found after SWCNT coating with PC (445 ± 21 pg/ml). In contrast, the production of anti-inflammatory cytokines is known to be stimulated

by PS-dependent pathways (Hoffmann, Kench et al. 2005). Stimulation of RAW264.7 macrophages by zymosan resulted in the accumulation of TGF-β and IL-10 at 4 hrs after the challenge. The production of anti-inflammatory IL-10 and TGF-β by zymosan-stimulated macrophages subsequently treated with PS-coated-SWCNT increased 1.5- and 2-fold respectively, compared with the effect of zymosan alone (Figure 10C). This enhancement of IL-10 and TGF-β production was not observed after exposure of zymosan-stimulated RAW264.7 macrophages to either non-coated SWCNT or PC-coated SWCNT.

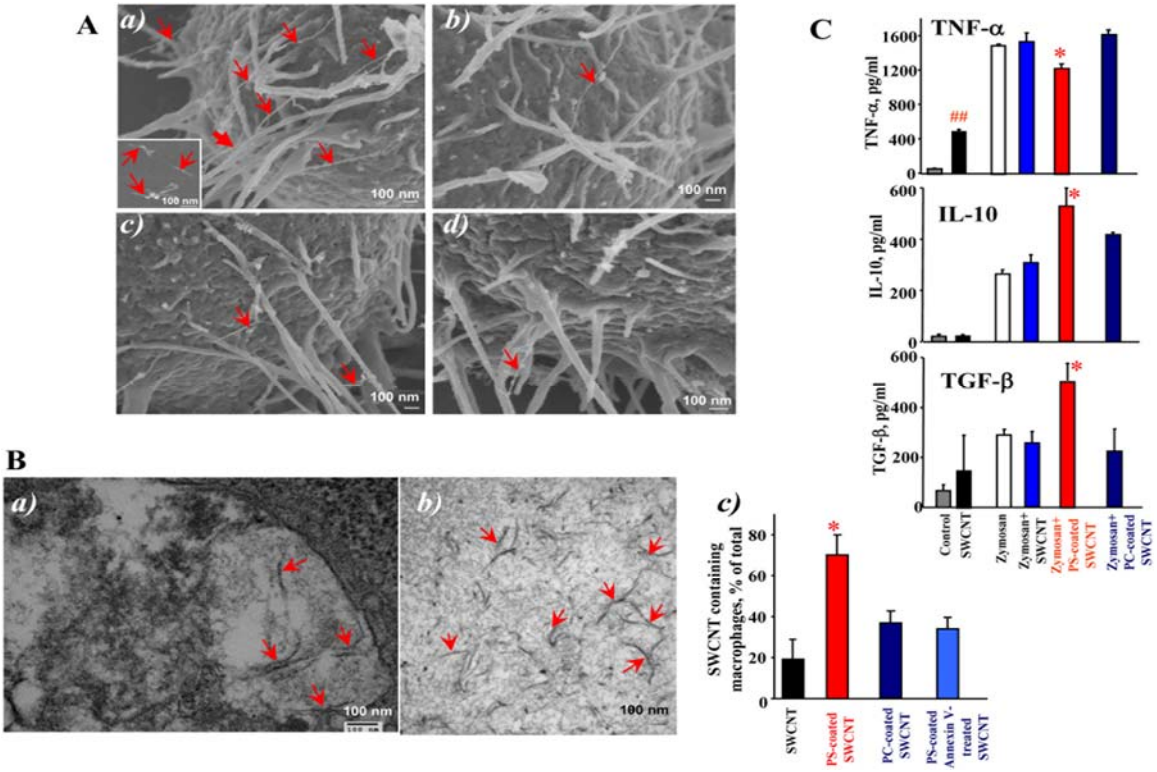


**Figure 10. SWCNT functionalized with PS but not with PC engulfed by murine RAW264.7 macrophages.** A, Scanning electron micrographs of RAW264.7 macrophages treated with SWCNT in vitro. RAW264.7 macrophages (0.3 x $10^6$ cells/ml) were incubated for 2 h with noncoated, PC- or PS-coated SWCNT. At the end of incubation macrophages were washed and fixed for SEM. a) Recognition of PS-coated SWCNT by RAW264.7 macrophages; (Note: The red arrows in all the electron micrographs in figure 2 point SWCNT. Sub-panel A-a represents scanning electron micrograph of SWCNT alone.) b) PC-coated SWCNT, c) non-coated, d) PS-coated Annexin V treated SWCNT are poorly recognized by macrophages. A total of 150 cells from each sample type were analyzed by SEM. B. Transmission electron

micrographs of RAW264.7 macrophages treated with SWCNT in vitro. RAW264.7 macrophages (0.3 x $10^6$ cells/ml) were incubated for 2 h with non-coated, PC- or PS-coated SWCNT. At the end of incubation macrophages were washed and fixed for TEM. a) A high-power image of the macrophage with engulfed PS-coated SWCNT. b) A typical TEM image of PS-coated SWCNT. Samples of SWCNT for TEM imaging were processed in a fashion similar to that of cells for electron microscopy. Arrows indicate SWCNT. Representative TEM images are presented. c) Quantitative assessments of SWCNT phagocytosis by RAW 264.7 macrophages. A total of 150 cells from each sample type were analyzed by TEM. Data are mean ± S.D., n = 3, *p,0.05, PS-coated SWCNT vs. SWCNT, PC-coated SWCNT and PS-coated Annexin V-treated. C. Effect of SWCNT on cytokine production by zymosan-stimulated RAW 264.7 macrophages. Macrophages were seeded at 2.5 x $10^5$ cells/well in 48 well plates and co-incubated with zymosan (0.25 mg/ml) in the presence of non-coated, PC-coated and PS coated SWCNT (150 μg/$10^6$ cells). At the end of 2 hr incubation, TNF-α was measured in the medium. IL-10 and TGF-β were measured after 4 hr incubation. The cytokines were measured using R&D Quantikine H immunoassay kit. Data are mean ± s.d., n = 3. ## $p<0.05$, SWCNT vs control. *$p<0.05$, PS-coated plus zymosan vs SWCNT plus zymozan and PC-coated plus zymosan.

### 4.3.4 Intracellular localization of PS-coated SWCNT

Visually, we observed accumulation of "black" (SWCNT-containing) pellets after sedimentation of cells. To quantitatively characterize this effect, we performed measurements of optical density of cell suspensions incubated with PS-coated SWCNT and PC-coated SWCNT. A broad absorbance of SWCNT with characteristic maxima at 1050–1060 and 1260–1270 nm was detected. The intensity of absorbance at 1050–1060 nm was 1.3-fold higher in PS-coated SWCNT than in PC-coated SWCNT samples. We further used fluorescently-labeled phospholipids to characterize the presence of phospholipid-coated SWCNT in cells. We found that NBD-PS coated SWCNT co-incubated with RAW 264.7 macrophages yielded a higher fluorescence response from cell suspensions than NBD-PC coated SWCNT (Figure 11Ca). Further, the majority of fluorescence was associated with the cytosolic fraction (containing endo-lysosomal vesicles) and was minimal in the fraction of nuclei and cell debris (Figure 11Cb). We isolated the endo-lysosomal fraction from RAW 264.7 macrophages loaded with NBD-PS-coated SWCNT and found that 77 ± 18 % (n = 3) of the fluorescence response was

associated with this fraction. This is in line with the recent demonstration of deposition of SWCNT in endo-lysosomal compartments of macrophages upon prolonged incubation (Porter, Gass et al. 2007). Additionally, to prove co-localization of SWCNT with phagolysosomes we used confocal microscopy. To this end, we treated RAW 264.7 macrophages ($5\times10^5$ cells/well) with either NBD-PS-coated SWCNT or NBD-PC-coated SWCNT (150 μg/$10^6$ cells). We found that NBD-PS-coated SWCNT were readily taken up by macrophages. As shown in Figure 11Da,b,c a robust intracellular fluorescence of NBD-PS (but not of NBD-PC) was co-localized, at least in part, with a lysosomal marker, Lyso-Tracker Red. Moreover, after pre-treatment of macrophages with the cocktail of inhibitors of endocytosis (nystatin (25 μg/ml), genistein (200 μM), chlorpromazine (6 μg/ml) and brefeldin A (10 μg/ml)), the intensity of intracellular NBD-PS fluorescence was drastically reduced (Figure 3Dd,e,f). No fluorescence was detected after treatment of macrophages with NBD-PC-coated SWCNT (data not shown). This suggests that NBD-PS-coated SWCNT were effectively taken up by macrophages through an endocytosis-mediated process resulting in their significant accumulation in endo-lysosomes.

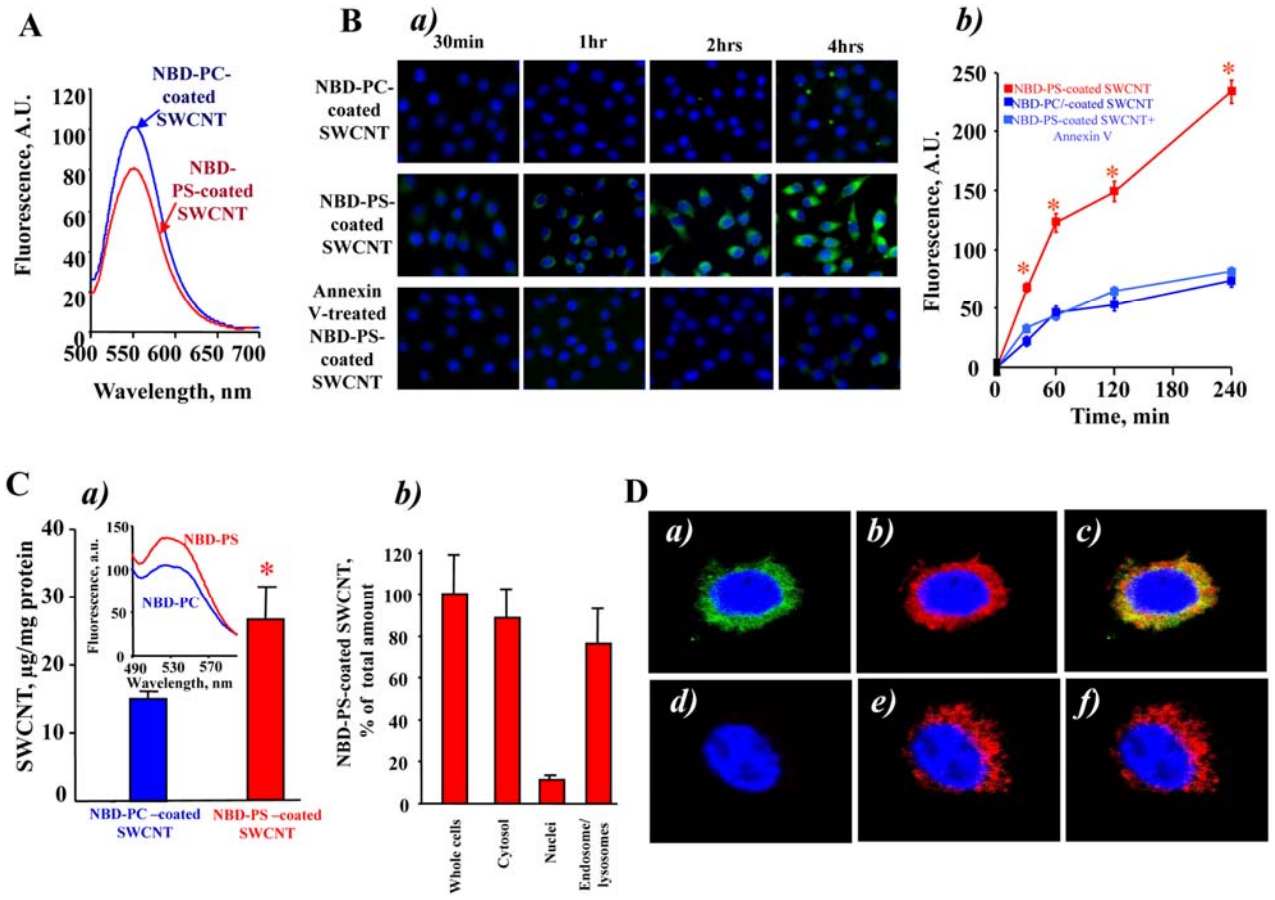


**Figure 11. In vitro assessment of uptake of NBD-PS-coated or NBD-PC-coated SWCNT by RAW264.7 macrophages.** A, Typical fluorescence spectra obtained from NBD-PC- and NBD-PS-coated SWCNT. B. Time-dependent uptake of NBD-PS-coated but not NBD-PC-coated SWCNT. a) RAW264.7 macrophages ($0.3\times10^6$ cells/ml) were incubated for up to 4 hrs with NBD-PC- or NBD-PS-coated SWCNT. Annexin V prevents engulfment of NBD-PS-coated SWCNT by RAW264.7 macrophages. Overlapped blue and green fluorescence images are presented. b) Quantitative evaluation of cell number with engulfed SWCNT. Data are mean ± s.d., n = 3. *$p<0.05$, NBD-PS-coated vs NBD-PC-coated SWCNT and NBD-PS-coated Annexin-V treated SWCNT. C. Assessment of NBD-phospholipid-coated SWCNT in whole cells and subcellular fractions isolated from RAW264.7 macrophages. a) Uptake of PS-coated and PC-coated SWCNT by RAW264.7 macrophages. Data are mean ± S.D., n = 3, *$p<0.05$, NBD-PS-coated SWCNT vs NBD-PC coated SWCNT. Inset: typical fluorescence spectra obtained from endosomal/lysosomal fraction isolated from RAW264.7 macrophages. b) Intracellular localization of PS-coated SWCNT in RAW264.7 macrophages. Macrophages were incubated with PC-coated or PS-coated SWCNT for 15 min at 37°C. At the end of incubation, subcellular fractions were isolated and examined for the presence of NBD fluorescence. D. Typical confocal microscopy images of RAW 264.7 macrophages with NBD-PS-coated SWCNT. RAW macrophages were treated with NBD-PS-coated SWCNT in the presence of Lyso-Tracker Red for 5 min at 37°C (a,b,c). In the experiments with inhibitors of

endocytosis, macrophages were pretreated with a mixture containing nystatin (25 μg/ml), genistein (200 μM), chlorpromazine (6 μg/ml) and brefeldin A (10 μg/ml) for 30 min prior to incubation with NBD-PS-coated SWCNT (d, e, f). a and d - green fluorescence is from NBD-phospholipid coated SWCNT; b and e - red fluorescence is from Lyso-Tracker Red, c and f - overlay of green and red fluorescence.

### 4.3.5 PS-coated SWCNT deliver cyt c into RAW264.7 macrophages

We further determined whether PS-coated SWCNT could be employed for the delivery of physiologically active agents to macrophages. Because cyt c released from mitochondria into the cytosol acts as an effective activator of caspases and a death-signal (Kagan, Tyurin et al. 2005) we chose to use it as a cargo. Given that positively charged cyt c readily interacts with negatively charged surfaces we assumed that SWCNT coated with anionic PS would effectively bind to cyt c. Indeed, the binding of cyt c to PS-SWNT was confirmed by direct measurements of specific cyt c absorbance as well as by atomic force microscopy (AFM). Section analysis of bare SWCNT (Figure 12Cc) demonstrated that the diameter of non-coated SWCNT was 1.3 nm (typically these SWCNT have diameters in the range of 0.6–1.5 nm. Figure 12Aa shows AFM image of cyt c adsorbed on SWCNT sidewalls. AFM image revealed the presence of globular structures of cyt c on the surface and in the contact with SWCNT (measured height ~1 nm). This image is similar to previously reported (Kam and Dai 2005) picture of SWCNT functionalized with proteins and in particularly with cyt c. AFM of SWCNT functionalized with PS/PC and cyt c displayed a significantly different image (Figure 12Ab), where distinct PS/PC molecules were not seen; rather a layer of PS/PC was spread on the SWCNT surface thereby demonstrating lipid adsorption onto SWCNT. Such an event is likely due to a greater retention of PS/PC aggregation, resulting into multiple PS/PC layers over SWCNT, while individual globular structures of cyt c are still clearly visible on the nanotube sidewalls. The height cross section of the SWCNT functionalized with PS/PC and cyt

c (Figure 12Ac) shows that the diameter of the structures is 3.5 nm which is significantly larger than bare SWCNT. Importantly, cyt c-loaded PS-SWCNT caused a marked increase of caspase activity (Figure 12Ba) in RAW264.7 macrophages upon co-treatment with a disruptor of endosomes, chloroquine. This is in line with previous reports where acid-oxidized SWCNT were utilized for delivery of cyt c into cancer cell lines (Kam and Dai 2005). PC-coated or non-coated SWCNT pre-incubated with cyt c were ineffective in inducing caspase-3 activation in macrophages. In addition, we found that delivery of cyt c into macrophages resulted in significantly increased numbers of Trypan Blue positive cells (Figure 12Bb) compared to cells treated with PS-SWCNT with no cyt c attached. Thus, PS-coating makes PS-SWCNT loaded with a protein cargo recognizable, facilitates their uptake by macrophages, and could hence be envisaged as a promising tool for targeted delivery of regulators of macrophage activity/survival.

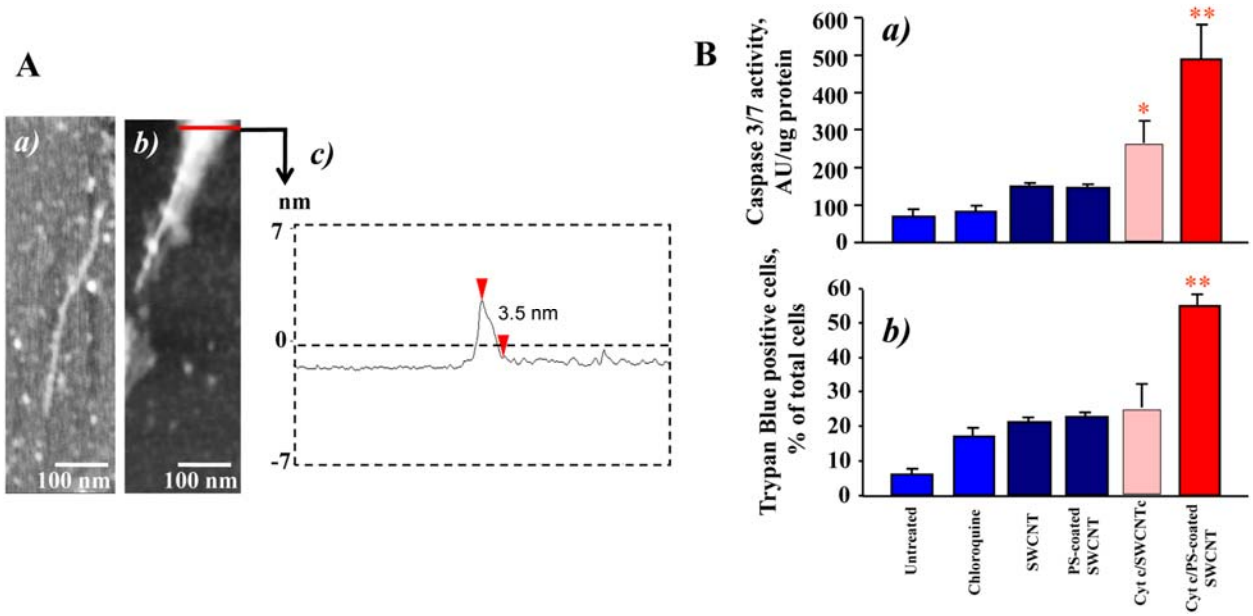


**Figure 12. PS-coated SWCNT effectively bind cyt c, deliver it into RAW264.7 macrophages, and activate apoptotic pathways (caspase 3/7), and cell death.** A, AFM images of various SWCNT samples deposited on mica substrates: a) SWCNT with cyt c; b) SWCNT with cyt c and PS/PC. c) The height cross section of the functionalized SWCNT in image b. B. Cyt c delivered into macrophages by PS-coated SWCNT activates caspase 3/7 (a) and increases the number of Trypan Blue positive cells (b). SWCNT were treated with 50 mM cyt c, washed twice and then were coated with PS and PC alone. Cells were incubated with protein/lipid/SWCNT conjugates in the presence of 100 mM chloroquine to trigger endosomal rupture. Data are normalized versus SWCNT/chloroquine. Note that under experimental conditions used chloroquine alone (100 mM, 15 min incubation) did not induce any significant activation of caspase 3/7. The data represent mean6s.d (standard deviation), n = 5, *p,0.05, PS-coated plus cyt c vs PS-coated SWCNT, non-coated SWCNT plus cyt c and SWCNT alone.

### 4.3.6 Recognition of PS-coated SWCNT by microglia

To determine whether PS-coated SWCNT can be recognized and taken up by other types of professional phagocytes, we performed experiments using microglia from rat brain. The experiments using SEM (Figure 13A) and TEM (Figure 5Ba) demonstrated that, similarly to RAW264.7 macrophages, microglia effectively engulfed PS-coated (Figure 13Bb), but not PC-coated or non-coated SWCNT. Essentially in samples in which PS-coated SWCNT were treated with Annexin V the number of SWCNT positive microglial cells was not different from SWCNT controls or from PC-coated SWCNT (Figure 13Bb). This was confirmed by

quantitative assessments of NBD-PS-SWCNT uptake by fluorescence microscopy (Figure 13C).

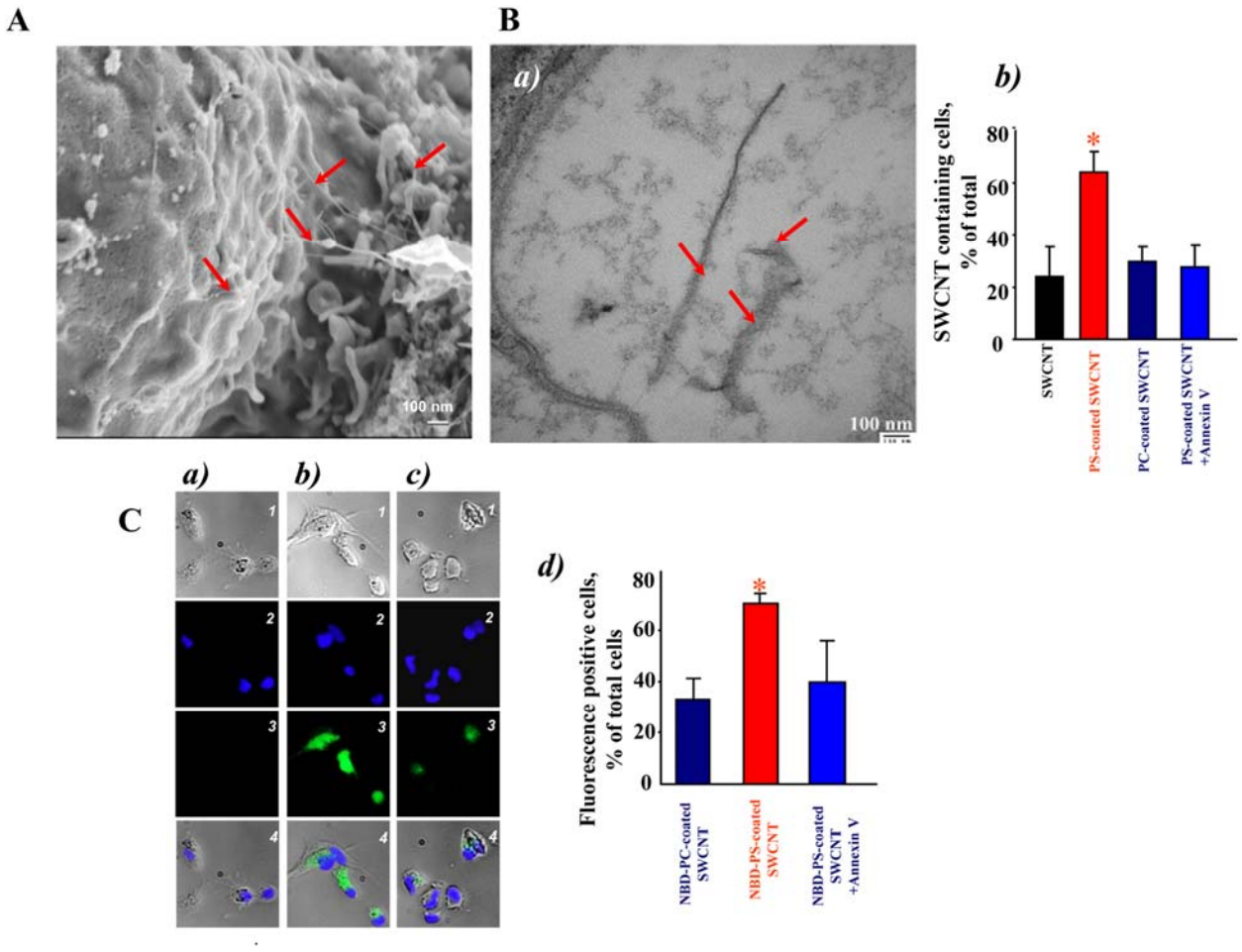


**Figure 13. Primary rat microglia recognized SWCNT functionalized with PS but not with PC.** A, Scanning electron micrographs of microglia treated with PS-coated SWCNT in vitro. Microglia ($1.5\times10^5$ cells/ml) were incubated for 2 h with PC- or PS-coated SWCNT. At the end of incubation macrophages were washed and fixed for SEM. (Note: The red arrows in all the electron micrographs in figure 5 point SWCNT). B. Transmission electron micrographs of primary microglia exposed to SWCNT in vitro. Microglia ($1.5\times10^5$ cells/ml) were incubated with PC- or PS-coated SWCNT. At the end of incubation microglia was washed and fixed for TEM. a) Microglia exposed to PS-coated SWCNT; b) Quantitative assessments of SWCNT phagocytosis by Microglia cells. A total of 60 cells from each sample type were analyzed by TEM. Data are mean ± S.D., n = 3, *$p<0.05$, PS-coated SWCNT vs SWCNT, PC coated SWCNT and PS-coated Annexin V–treated SWCNT. C. In vitro assessment of uptake of SWCNT coated with NBD-PS or NBD-PC by microglia. Microglia ($1.5\times10^5$ cells/ml) were incubated with NBD-PC- (a), NBD-PS-coated SWCNT (b) or NBD-PS-coated/Annexin V

treated SWCNT (c). 1 – Bright field image; 2 – blue fluorescence image, Hoechst 33342; 3 – green fluorescence image, NBD-labeled phospholipids; 4 – overlap of blue and green fluorescence images with image under bright field. d) Annexin V treatment of NBD-PS-coated SWCNT prevents their engulfment by microglia. Quantitative evaluation of cell number with engulfed SWCNT. Data are mean ± s.d., n = 4. *$p<0.05$, NBD-PS-coated SWCNT vs NBD-PC-coated SWCNT and NBD-PS-coated Annexin V treated SWCNT.

### 4.3.7 Interaction of PS-coated SWCNT with HeLa cervical carcinoma cells and SH-SY5Y neuroblastoma cells

While ingestion of apoptotic cells is not absolutely specific to phagocytes, the rates of uptake by professional phagocytes - macrophages and microglial cells – are significantly higher compared to non-professional phagocytes (such as endothelial, epithelial cells and fibroblasts) (Parnaik, Raff et al. 2000). Typical fluorescence micrographs of cervical carcinoma HeLa cells (Figure 14Aa) and neuroblastoma SH-SY5Y cells (Figure 14Ba) demonstrate preferential uptake of NBD-PS-coated SWCNT vs NBD-PC-coated SWCNT by both cell types. Quantitative assessments revealed that PS-coated SWCNT were ingested more actively than NBD-PC-coated SWCNT by HeLa cells, and SH-SY5Y cells, respectively (Figure 14Ab and

Figure 14Bb). However, uptake of NBD-PS-coated SWCNT by these cells was 2.4 times and 2.6 times less effective, respectively, than their ingestion by RAW 264.7 macrophages.

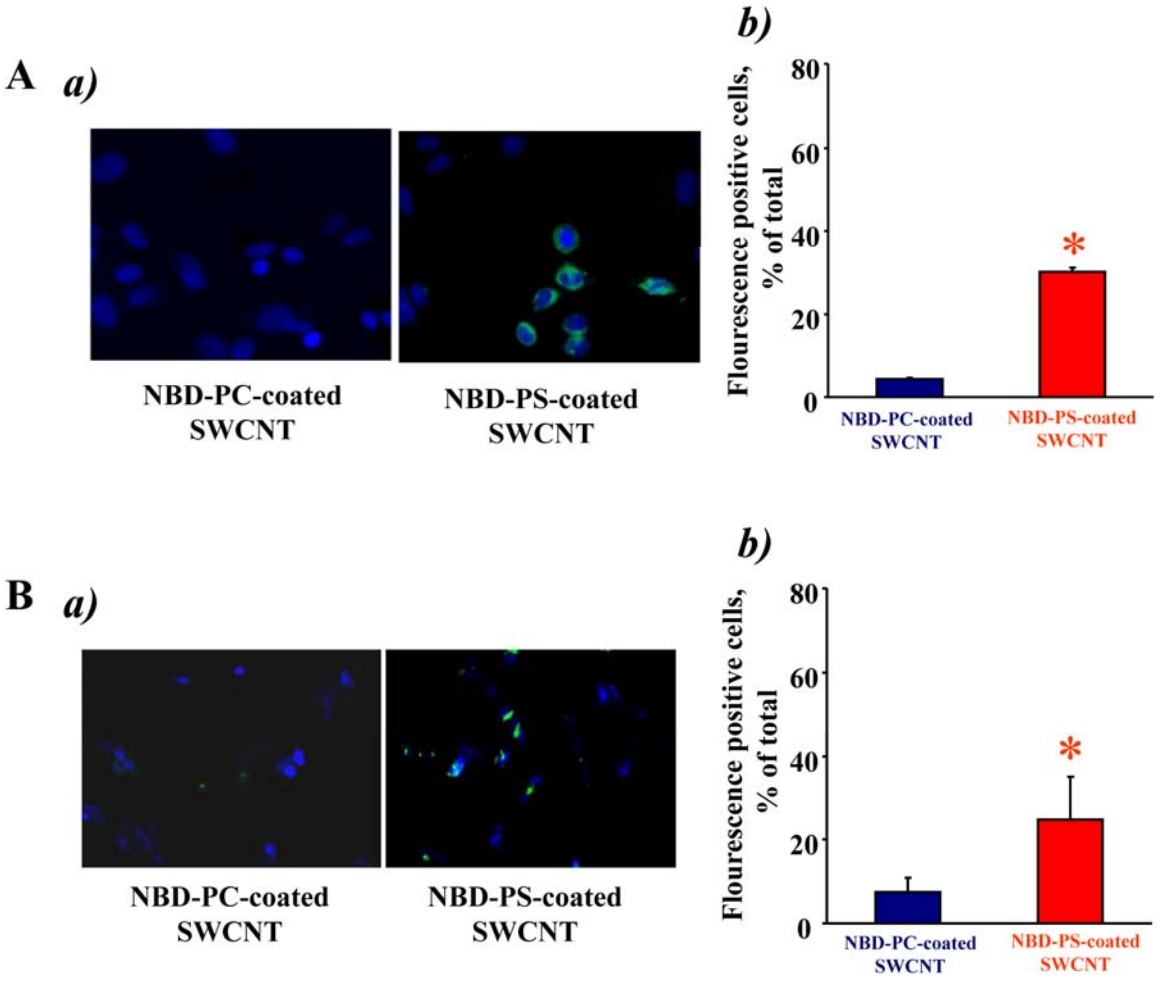


**Figure 14. HeLa cervical carcinoma cells and SH-SY5Y neuroblastoma cells interact with PS-coated (but not with PC-coated) SWCNT**. A, In vitro assessment of uptake of SWCNT coated with NBD-PS or NBD-PC by HeLa cells. a) Overlay of blue and green fluorescence images. b) Quantitative evaluation of cell with engulfed SWCNT. Data are mean ± s.d., n = 4. *p<0.05, NBD-PS-coated SWCNT vs NBD-PC-coated SWCNT. B. In vitro assessment of uptake of SWCNT coated with NBD-PS or NBD-PC by SH-SY5Y neuroblastoma cells. a) Overlay of blue and green fluorescence images. b) Quantitative evaluation of cells with engulfed SWCNT. Data are mean ± s.d., n = 4. *p<0.05, NBD-PS-coated SWCNT vs NBD-PC-coated SWCNT.

### 4.3.8 Recognition of PS-coated SWCNT by alveolar macrophages in vivo

As PS is an important recognition signal for alveolar macrophages in the lung (Huynh, Fadok et al. 2002), we reasoned that PS-coated SWCNT could be effectively phagocytozed in vivo. To this end, we used an established mouse model of SWCNT pulmonary exposure through pharyngeal aspiration. Mice were exposed to PS-coated-, PC-coated-, or non-coated SWCNT using procedures described previously (Kisin, Jurray et al. 2005). A high magnification TEM image of alveolar macrophages obtained from animals exposed to PS-coated SWCNT clearly demonstrates the presence of "bamboo shoot"-like material (Figure 15A). We also performed quantitative assessments of phagocytosis by counting SWCNT-positive alveolar macrophages using TEM images. Macrophages with at least one nanoparticle engulfed were considered as phagocytosis-positive. The data are presented as a plot of percentage of active phagocytes for each condition (Figure 15B). BAL obtained from PS-coated SWCNT–exposed mice revealed 72 ± 8.4 % of phagocytosis-positive alveolar macrophages. In contrast, only 40 ± 10 % and 18 ± 8 % of macrophages isolated from mice exposed to PC/SWCNT or non-coated SWCNT contained nanoparticles. Thus, PS-coated SWCNT were ingested at a significantly higher rate in vivo as compared to PC-coated or non-coated SWCNT by alveolar macrophages.

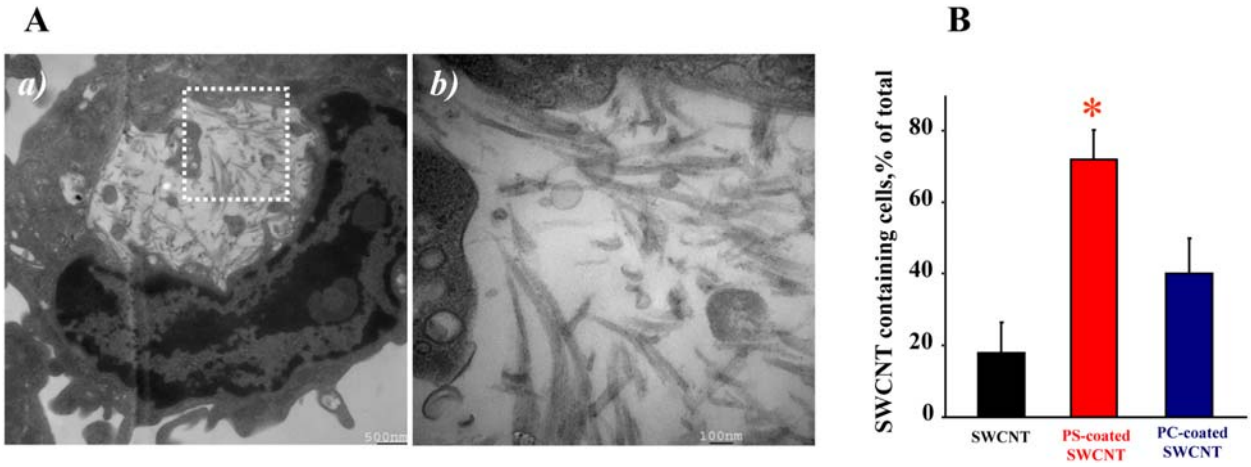


**Figure 15. SWCNT functionalized with PS but not with PC engulfed in vivo by murine alveolar macrophages**. A, a) Transmission electron micrographs of bronchoalveolar macrophages isolated from C57BL/6 mice exposed to PS-coated SWCNT; b) high magnification image of the area shown in (a). B. Alveolar macrophages preferentially phagocytoze PS-coated SWCNT in vivo. TEM images were used to calculate the percent of phagocytosis-positive macrophages. At least 150 cells were counted for each treatment. Data are mean ± s.d., *p,0.05, PS-coated SWCNT vs noncoated or PC-coated SWCNT. C57BL/6 female mice, 7–8 weeks old, were exposed to SCWNT (40 mg/mouse) by pharyngeal aspiration. Twenty-four hours following exposure, mice were sacrificed using sodium pentobarbital. Mice were lavaged with sterile PBS. The lavage fractions were pooled and centrifuged to obtain the cellular fraction. Cells were then fixed for TEM.

## 4.4 CONCLUSIONS

The goal of our work was to employ the naturally occurring "eat-me" signal, PS as a specific ligand that is recognized by professional phagocytes. We provide evidence that the uptake is specific, since nanotubes functionalized with PC are not recognized as readily as PS-coated nanotubes and because the PS-binding protein, Annexin V, can prevent uptake of PS-coated nanotubes. Previous studies from our and other laboratories have established high-affinity binding of cyt c with PS (Jiang, Kini et al. 2004). After the coating, binding of positively-charged cyt c was likely associated with abundant negatively-charged PS. We also provide evidence that the mechanism of uptake is specific and occurs through endocytosis. Finally, we show that a relevant cargo (pro-apoptotic cyt c) can be delivered into macrophages, and upon disruption of endosomes, the cargo is released and can perform its biological function (activation of the caspase cascade). Taken together, our findings highlight a novel strategy for the controlled delivery of relevant cargoes into specific cell populations. Further developments of the novel principle established in the current study, i.e. PS-coating of SWCNT for recognition and ingestion, may exploit cargoes covalently-conjugated with specific linkers that are hydrolysable extracellularly by activated macrophages (eg. superoxide-sensitive linkers) or intracellularly (eg. esterase-sensitive conjugates) for targeted delivery and release to regulate life-span and activity of phagocytes.

# 5 CHAPTER 5 - TARGETING OF SWCNT TO PROFESSIONAL PHAGOCYTES FOR BIODEGRADATION IN VITRO

## 5.1 INTRODUCTION

Chemical degradation of carbon nanotubes – used for the cutting of nanotubes to defined sizes - is often based on protocols employing oxidative modification of nanotubes by strong acids in the presence of oxidants, eg, $H_2SO_4$ plus $H_2O_2$ (Wei, Kondratenko et al. 2006). Furthermore, a halogen oxoanion, NaOCl, has been shown to strongly adsorb to and modify the surfaces of nanotubes by generating carboxyl and hydroxyl groups (Wu 2007; Yoon, Kim et al. 2008). This suggests that strong oxidants such as hypochlorous acid and oxoferryl species may be effective in biodegrading nanotubes. It was recently demonstrated that nanotubes can be catalytically biodegraded by horseradish peroxidase (HRP) over a period of several weeks (Allen, Kichambare et al. 2008). However, the involvement of peroxidase intermediates generated in mammalian (human) cells and/or biofluids in nanotubes biodegradation has not yet been explored. Polymorphonuclear leukocytes (PMNs) are bone marrow-derived cells of the innate immune system and they play a key role in the disposal and killing of invading microorganisms (Dale, Boxer et al. 2008). To this end, these cells express oxidant-generating enzymatic activities, including the phagocyte NADPH oxidase and myeloperoxidase (MPO) as well as numerous proteolytic enzymes. The hMPO is highly concentrated in the so-called azurophilic granules in neutrophils and is released into the extracellular compartment in an inflammatory setting (Winterbourn, Vissers et al. 2000). Human MPO (hMPO) generates potent reactive intermediates and hypochlorous acid. The standard redox potentials of hMPO and its oxoferryl intermediates (compound I/native hMPO, compound I/compound II of hMPO, and compound II/native hMPO) have been determined to be 1.16 V, 1.35 V, and 0.97 V

respectively (at pH 7 and 25°C) (Arnhold, Furtmuller et al. 2003). The reactive radical intermediates and hypochlorous acid (HOCl) has been shown previously to probably contribute in the degradation of implantable polymeric materials such as poly(ester-urea-urethane) (Sutherland, Mahoney et al. 1993). We reasoned that potent hMPO oxidants from azurophilic granules of nautrophils could also biodegrade nanotubes.

The body's response to nanoparticles may depend upon the physico-chemical properties of the particles, the amount initially entering the system, and the bio-persistence of the particles in the system. Clearance from the body involves particle transport as well as the action of phagocytic cells in different organ systems. Particle-laden professional phagocytes may migrate to different organs, but an important mechanism of clearance is the dissolution of particles within phagocytic compartments and the subsequent translocation of dissolved materials to the blood. In the inflammatory response to particulate matter in lungs depends not only on the amount of particles deposited but also on the amount retained over time. Bio-persistent particle amount is the amount of particles present in the lungs at any time and equals deposited mass minus cleared mass. In the respiratory system the clearance of particles may represent either bulk, mechanical transport from the airways and parenchyma, or solubilization and the removal of particles by body fluids. Both the amount of particles retained within a specific lung region over time and those properties of the retained particles determine the magnitude of the inflammatory response (Borm, Klaessig et al. 2006). Phagocytic cells, in particular macrophages and neutrophils, are the major two orchestrators of inflammatory and immunologic reactions in the lung. Amongst the two phagocytic cell types, macrophages represent the majority of phagocytes in the lower respiratory tract and respond to environmental factors and account for most of the clearance of particles and pathogens in the

distal airways and the alveolar spaces. The phagocytic and lytic abilities of these cells contribute for microbicidal properties of the lungs. The normal distal airways generally contain a small number of neutrophils, but the pulmonary vascular bed represents a large reservoir of this particular phagocytic cell type. A minor population of cells is in intimate contact with the endothelium, referred as marginating pool of neutrophils. Macrophages share many of the cellular composite features similarly with neutrophils, like granule-associated proteins which are similar to those of neutrophils. Monocyte derived macrophages have an inherent ability to augment production of granule proteins through new protein synthesis, a feature absent in mature neutrophils (Dale, Boxer et al. 2008). Also, macrophages have a greater ability to synthesize cytokines compared to neutrophils. When a neutrophil comes in contact with a particle, the pseudopodium flows round the particle. Its extensions fuse, grab and contain the particle within the phagosome. Silverstein observed the phagocyte membrane adheres firmly to particles it ingests and surrounds the particle in a zipperlike fashion (Griffin, Griffin et al. 1975). Neutrophils kill invading microorganisms by using their oxidant- generating enzymes, such as nicotinamide adenine dinucleotide phosphate-oxidase (NADPH oxidase), myeloperoxidase and proteases (Hampton, Kettle et al. 1998).

Although, both macrophages and neutrophils varyingly phagocytoze particles with any surface chemistry, the efficacy of phagocytosis is, however, increased by coating the surface of the particles with signaling biomolecules such as opsonins-immunoglobulins (IgG) and complement components etc (Moghimi, Muir et al. 1993). Antibody coated particles are recognized and internalized by Fcγ receptor mediated endocytosis. Neutrophil granules serve as reservoirs for digestive and hydrolytic enzymes prior to delivery into the phagosome (Dale, Boxer et al. 2008). Studies by Spitznagel, Elsbach and Weiss et al indicated that azurophilic

granule contents possess microbicidal activity and in inflammatory regulation (Spitznagel, Dalldorf et al. 1974; Weiss, Elsbach et al. 1992). Phagosome, which is an organelle of plasma membrane origin, usually fuses with lysosomes, forming phagolysosomes, wherein the ingested materials are degraded (Hart and Young 1975; Knapp and Swanson 1990). However, the fate of ingested particles in the intracellular compartments of phagocytes depends on the particle chemistry. Recently, a study by Liu X et al, 2010 showed that single-walled nanotubes with carboxylated surfaces were unique in their ability to under go 90-day degradation in a phagolysosomal simulant leading to length reduction and accumulation of ultrafine solid carbonaceous debris (Liu, Hurt et al.). However, the biodegradation routes of these nanomaterials remain unknown. As both these cell types are critical determinants in particle bioperistsence and particle mediated lung injury, we hypothesized that coating of SWCNT with biomolecules which would render it capable of being bound and ingested by phagocytic cells would also eventually cause particle biodegradation (Figure 16). As we demonstrated that coating of SWCNT with bio-molecules such as phospholipid PS enhances the uptake by macrophages, we examined if particles underwent biodegradation upon phagocytosis in professional phagocytes.

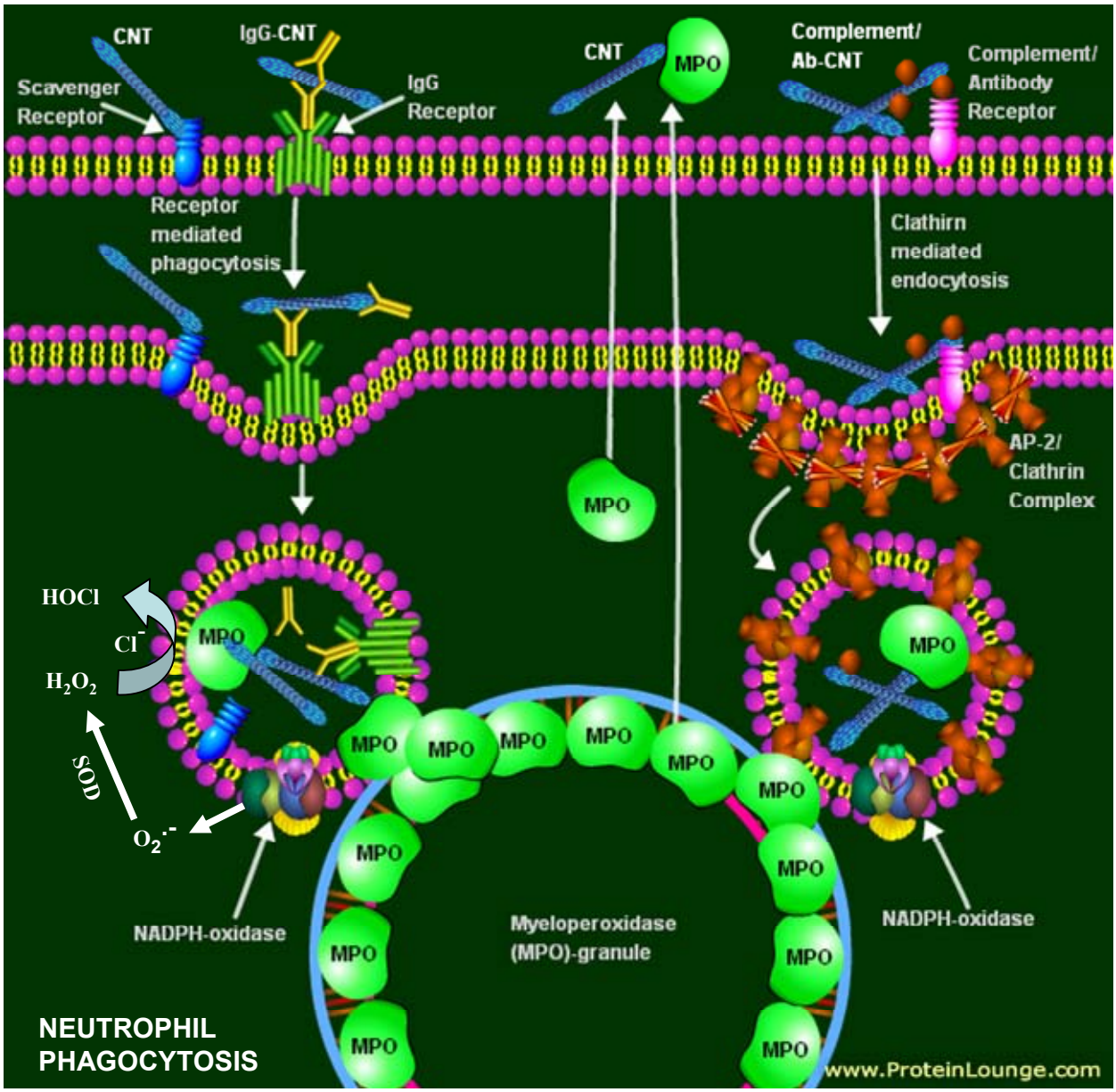


**Figure 16. Uptake of nanotubes by neutrophils and macrophages for biodegradation.**

As part of the innate cellular immune response, neutrophil granulocytes and monocytes/macrophages phagocytoze particles and readily eliminate pathogens (Mollinedo, Borregaard et al. 1999; Schwarzer, De Matteis et al. 1999). In circulation, human neutrophils are in a range of 4000− 7000 cells per µL of blood and much higher in number compared to monocytes, but the latter can differentiate into longer-lived cell types such as dendritic cells or

macrophages with various subtypes (Auffray, Sieweke et al. 2009) that are present in various tissues. Hubeau et al reported the surface area infiltration of neutrophils in the different regions of human lung under normal and disease conditions (Hubeau, Lorenzato et al. 2001). The quantitative analysis showed that neutrophil infiltration was 199 ± 54 cells/mm$^2$/segmental under diseased conditions versus normal 27 ± 7 cells/mm$^2$/segmental. Under normal conditions, the macrophage population in lung represents about 3-5 % of all the cells in the alveolar region of the lungs and the cells reside on the alveolar epithelial surface and defend against deposited particles. Previous studies with inhaled particles have demonstrated that about 70 % of the particles in the lavage fluids are associated with phagocytes (Bice, Harmsen et al. 1990). Studies showed that during the first 7 days after instillation, most of the particles in the pulmonary tract were associated with neutrophils and at 14 days and later, most of the particles were associated with macrophages. Circulating monocytes have been shown to generate hypochlorous acid by activation of MPO, and thereby increase oxidative stress. Phagocytosis of particles is an essential step to contain particles within the cellular compartments of phagocytes and for subsequent particle clearance. Surface functionalization of particles is important for recognition and subsequent clearance. Particle opsonization has been shown to improve particle internalization in phagocytic cells. Uptake of IgG-coated cells, particles and microorganisms is mediated by receptors for the Fc portion of IgG (Fcγ receptors) expressed on monocytes/macrophages and neutrophils (Ravetch and Kinet 1991; McKenzie and Schreiber 1998). Based on these concepts, we designed experiments to test the uptake and biodegradation of nanotubes by neutrophils that are cells rich in MPO content as well as by monocyte derived macrophages which also contain a relatively very low content of MPO compared to neutrophils.

## 5.2 METHODS

**$HOCl/H_2O_2$/hMPO/SWCNT incubation system**: Mixtures contained 30 μg of hMPO with activity of 1.1 U/μg (Sigma, St. Louis, MO, USA) per 300 μg of SWCNT suspended in 300 μl of 50 mM phosphate buffer containing 140 mM NaCl and 100 μM DTPA, a transition metal chelator. Hydrogen peroxide was added at the rate of 200 μM per hour for 5 hrs. Because of loss of activity of hMPO in the incubation system, the enzyme was replenished after 5 hrs and the enzyme/SWCNT/$H_2O_2$ system was maintained at 37$^oC$ for 24 hrs. To the experimental group with SWCNT plus OCl-, NaOCl was added every hour to give concentrations of 200 μM for 24 hrs at 37 $^oC$.

**Computational Modeling:** The 3D structure of SWCNT was generated using Nanotube Modeller software (http://www.jcrystal.com/products/wincnt/index.htm) to contain a diameter of 1.1 nm using the chirality parameters m and n as 14 and 0. For carboxylated SWCNT, one of the ends of the nanotube was carboxylated using the Builder tool, provided by Pymol (DeLano 2002) visualization software. Carboxylated and noncarboxylated SWCNT (pristine) were docked to the hMPO X-ray crystal structure (PDB ID: 1CXP, chains A & C), using the Lamarckian Genetic Algorithm provided by AutoDock4.0 software, as described previously (Yanamala, Tirupula et al. 2008) with the following modifications. The entire surface of the target was searched for possible binding sites without bias. The grid maps representing the protein were calculated using AutoGrid option. A cubic box was built around the protein with 126 × 126 × 126 points. A spacing of 0.41 Å between the grid points was used, placing the center of the protein to be the center of the cube. 17 Docking simulations were carried out with an initial population of 300 structures, and a maximum number of 50,000,000 energy evaluations. The resulting top 25 minimum energy orientations that have less than or equal to 2.0 Å root mean

square deviation were clustered. AutoDock4.0 software was run via distributed computing (www.pittgrid.pitt.edu).

**Dynamic light scattering analysis:** A Malvern Zetasizer Nano (Malvern Instruments, Westborough, MA, USA) was used. The analysis was conducted according to standard operating procedures as previously described (Allen, Kichambare et al. 2008). Particle sizes were determined on the basis of the refractive index of carbon as the particle and DMF as the carrier fluid.

**AFM imaging of hMPO/nanotubes interaction** was performed on freshly cleaved mica treated with Poly – L- Lysine. Approximately 10 μL from the sample (aq) containing nanotubes and hMPO incubated for an hour in 50 mM phosphate buffer was spin-coated at 1,400 r.p.m. and allowed to dry in ambient air for 45 mins prior to imaging.

**Gas chromatography-mass spectroscopy (GC-MS) of $CO_2$:**Approximately 2 μL of sample headspace from a typical incubation medium containing nanotubes plus hMPO and H2O2 was injected into a Shimadzu QP5050A GC-MS unit (Shimadzu Instruments, Columbia, MD, USA) with an XTI-F capillary column (30 m, 0.25 mm i.d., 0.25 μm film thickness). A basic temperature program was run starting at 100 °C held for one minute, followed by temperature ramping at a rate of 10 °C/min until a maximum of 325 °C was achieved and held for an additional 10 min. CO2 (with m/z 44) intensities were observed relative to N2 (28 m/z) and analyzed for their maximum concentration.

**Transmission electron microscopy:** A FEI-Morgani TEM instrument (Tokyo, Japan) was operated at 80 KV equipped with a soft imaging system charge-coupled device (CCD) camera. TEM samples were prepared by drop casting the solution on a copper grid and the excess drawn off with filter paper. Alternatively, one drop of the aliquot was then placed on a lacey

carbon grid (Pacific-Grid Tech, CA,USA) and allowed to dry in ambient conditions for 2 hrs prior to TEM imaging (FEI Morgagni, 80 keV).

**Raman spectroscopy:** Samples suspended in ethanol were prepared by drop-casting approximately 20 μL on a quartz microscope slide and allowed to dry. A Renishaw inVia Raman microscope spectrometer (Renishaw, Gloucestershire, UK) with an excitation wavelength of 633 nm was used for all samples, while scanning 1000 – 1800 $cm^{-1}$ to visualize D and G band intensity changes throughout the degradation process. Spectra were collected with a 15 second exposure time and averaged across 5 scans per sample.

**Vis−NIR Spectroscopy**: Aqueous samples (150 μL) were analyzed using a Lambda 900 spectrophotometer (Perkin-Elmer) and 0.20 mL quartz cuvettes (path length: 1 cm, World Precision Instruments, Inc.). Carbon nanotubes were scanned from 600 to 1300 nm. All samples were used without any further treatment or purification.

**Determination of nanotubes biodegradation products by GS-MS:** The biodegradation products of nanotubes were extracted from incubation media and detected using GS-MS as described by Zeinali et al. (Zeinali, Vossoughi et al. 2008) and Meckenstock et al. (Meckenstock, Annweiler et al. 2000). Incubation medium without nanotubes was used as a control sample. Briefly, biodegraded nanotubes products were extracted twice with three volumes of ethyl acetate. The extracts were evaporated under nitrogen, dissolved in hexane:ethyl acetate (99:1 v/v) and derivatized with reagent (99% N,O-bis(trimethylsilyl)-trifluoroacetamide (BSTFA)+1% trimethylchlorosilane (TMCS)) at 60 °C for 40 min. The GC-MS analysis was performed on GC-2010 gas chromatograph (Shimadzu, Japan) equipped with a DB-225MS capillary GC column (30 m, 0.25 mm i.d., 0.25 μm film thickness, Agilent Technologies, Santa Clara, CA) and coupled to a GCMS-QP2010S mass spectrometer. GC temperature program was 280 °C interface temperature, 100 °C (2 min isothermal), 100-250 °C

(at 10 °C/min) and 250 °C (3 min isothermal). Helium was used as a carrier gas at a flow rate of 0.97 ml/min. GS-MS conditions: positive electron ionization (EI+); ionization electron energy, 70 eV; source temperature, 200 °C and mass range m/z 45-800. The mass spectra of individual total ion peaks were identified by comparison with mass spectra database (Shimadzu, Japan).

**Neutrophils isolation:** Human neutrophils were isolated by a procedure utilizing Histopaque (Sigma, St. Louis, MO, USA). Briefly, human buffy coat (Central blood bank, Greentree, PA, USA) was layered on top of a density gradient (Histopaque1.077/1.119, Sigma, St. Louis, MO, USA) and subjected to centrifugation as described in the manual (700 g 45 min at room temperature without brake). The neutrophil-rich supernatant (between the layers of Histopaque) was carefully aspirated and washed twice with calcium and magnesium free PBS; thus obtained cells were suspended in RPMI and adjusted to $25\times10^6$ cells/ 3ml before use.

**Isolation of monocyte-derived macrophages** was performed essentially as described (Boynton, Waddell et al. 2000) . In brief, mononuclear cells were prepared from buffy coats obtained from healthy adult blood donors by density gradient centrifugation using Histopaque1.077/1.119. Cells were washed and resuspended in RPMI-1640 medium. Monocytes were separated by adhesion to tissue culture plastic for 1 hr at $37^oC$ with a 5 % $CO_2$ atmosphere and non-adherent cells were removed by several washes with PBS.

**hMPO contents in cells and its release:** Levels of hMPO in cells were determined by ELISA kit (Alpco Diagnostics, NH, USA) after 30 min incubation with either fMLP with cytochalasin B or SWCNT (Zipfel, Carmine et al. 1997). Neutrophils were centrifuged at 1000 g for 10 min. The supernatant and pellet were obtained and used separately for hMPO measurements according to the manufacturer's manual. The amounts of hMPO were expressed as pg/mL.

**Superoxide generation:** Oxidation-dependent fluorogenic dye, dihydroethidium (DHE, Molecular Probes, Eugene, OR, USA) was used to evaluate intracellular production of superoxide radicals. Briefly, 0.3 x 106 cells were incubated with 5 μM DHE for 10 min prior to treatments. After washing with PBS, cells were incubated with IgG-nanotubes or nanotubes (25 μg) for 30 min. fMLP (10 nM) was used as a control to trigger ROS generation in cells. Subsequently, treated cells were either collected or fixed for fluorescence microscopy. Cells were examined under a Nikon ECLIPSE TE 200 fluorescence microscope (Tokyo, Japan) equipped with a digital Hamamatsu charge-coupled device camera (C4742-95-12NBR). Extracellular superoxide generated by neutrophils was measured in incubation medium by an SOD-inhibitable cytochrome creduction assay as described by Pick and Mizel (1981) (Pick and Mizel 1981).

**Hydrogen peroxide generation:** Amplex Red assay was applied for assessments of hydrogen peroxide production in neutrophils as described previously (Lekstrom-Himes, Kuhns et al. 2005). Cells (3.6 x $10^6$/mL) were incubated with either fMLP or nanotubes together with 50 μM Amplex Red (Molecular Probes, CA, USA) and horseradish peroxidase 0.1 U/mL at 37 oC for 30 min followed by centrifugation to remove the pellet. Fluorescence of resorufin (Amplex Red oxidation product) was measured at 590 nm using a spectrofluorometer (RF-5301-PC, Shimadzu, Japan). The 2′,7′-dichlorofluorescein diacetate (DCF-2DA) assay for intracellular $H_2O_2$ detection was performed by incubating 2.5 x $10^6$ cells with 20 μM DCF-2DA 30 min prior to the initial addition of stimulants for experiments lasting 2 hr. For experiments lasting longer time, the DCF-2DA was added 30 min prior to the cell harvest. Cells were washed twice with PBS, fixed using 2.5 % paraformaldehyde and cytospinned on glass slide for imaging.

**Coating of SWCNT with IgG:** SWCNT (200 μg) in HEPES buffer (pH 7.4) were incubated with purified human IgG (Invitrogen, Carlsbad, USA) in 1:1 ratio (w/w) for 48 hrs at 37 $^{o}$C with sonication for 10 min every 5 hrs in a water bath sonicator.

**Raman microscopy of SWCNT in neutrophils**: cells incubated with SWCNT preparations were fixed using 2.5 % paraformaldehyde and cyto-spinned on 1.5 mm thick cover glass (Fisher Scientific, PA, USA). A Renishaw inVia Raman spectroscopic microscope was used, with a cobalt solid state laser operating at a wavelength of 473 nm. All Raman spectra were recorded for 2 secs, at 10% laser power using a 100x oil immersion objective. For each spectrum a static grating (2400 l/mm) scan was taken over the range 678.28 $cm^{-1}$ to 2231.82 $cm^{-1}$ (centered at 1500 $cm^{-1}$). Detection of the Raman scattered light was performed using a peltier cooled CCD detector. Calibration was carried out daily using a piece of silicon to ensure the 520 $cm^{-1}$ line of silicon was not out by more than 1 $cm^{-1}$. From each of the samples an average of 20 spectra was recorded.

**Processing of Neutrophils for Vis-NIR spectroscopy**: Neutrophils incubated with SWCNT preparations were harvested from culture plates after 24 hrs of incubation along with the incubation medium. The cell suspensions were further subjected to harsh sonication for 1 hr using the ultrasonic probe tip sonicator (Cole-Palmer Ultrasonic Homogeneizer, 20 kHz) and then using Vis-NIR spectrophotometer (Perkin-Elmer) the spectra were recorded in the samples.

**Statistics:** The results are presented as means ± S.D. values from at least three experiments, and statistical analyses were performed by one-way ANOVA. The statistical significance of differences was set at $p < 0.05$.

## 5.3 RESULTS

### 5.3.1 Purified human myeloperoxidase biodegrades SWCNT

Firstly, we examined if purified hMPO in a cell free system could catalyze the biodegradation of carbon nanotubes. We prepared short-cut carboxylated single-walled carbon nanotubes by chemical cutting and used them throughout the study unless specified otherwise (Note: All our previous studies also included short-cut carboxylated single-walled carbon nanotubes). Upon incubation with hMPO and $H_2O_2$, the nanotubes degraded over time, and the suspension turned translucent after 24 h (Figure 17a). Neither hMPO alone nor $H_2O_2$ alone caused nanotube degradation. Incubation of hMPO with nanotubes alone, without $H_2O_2$, did not inactivate the enzyme (Figure S1a). In the presence of $H_2O_2$, however, hMPO retained 50% of its activity over 2.5 h but decayed after 5 h (Figure 17C). We therefore added fresh hMPO and $H_2O_2$ to the nanotube suspensions every 5 h. Dynamic light scattering of nanotubes treated with hMPO and $H_2O_2$ showed several peaks that corresponded with a reduction in the size of the treated nanotubes compared to untreated controls (Figure 17D). Native agarose gel electrophoresis showed that the majority of non-degraded carbon nanotubes remained as a dark congested band in the loading well or migrated as a smear in the presence of albumin/bromophenol blue. In contrast, no detectable bands were found on native gels when biodegraded carbon nanotubes were electrophoresed under similar conditions (Figure 17E).

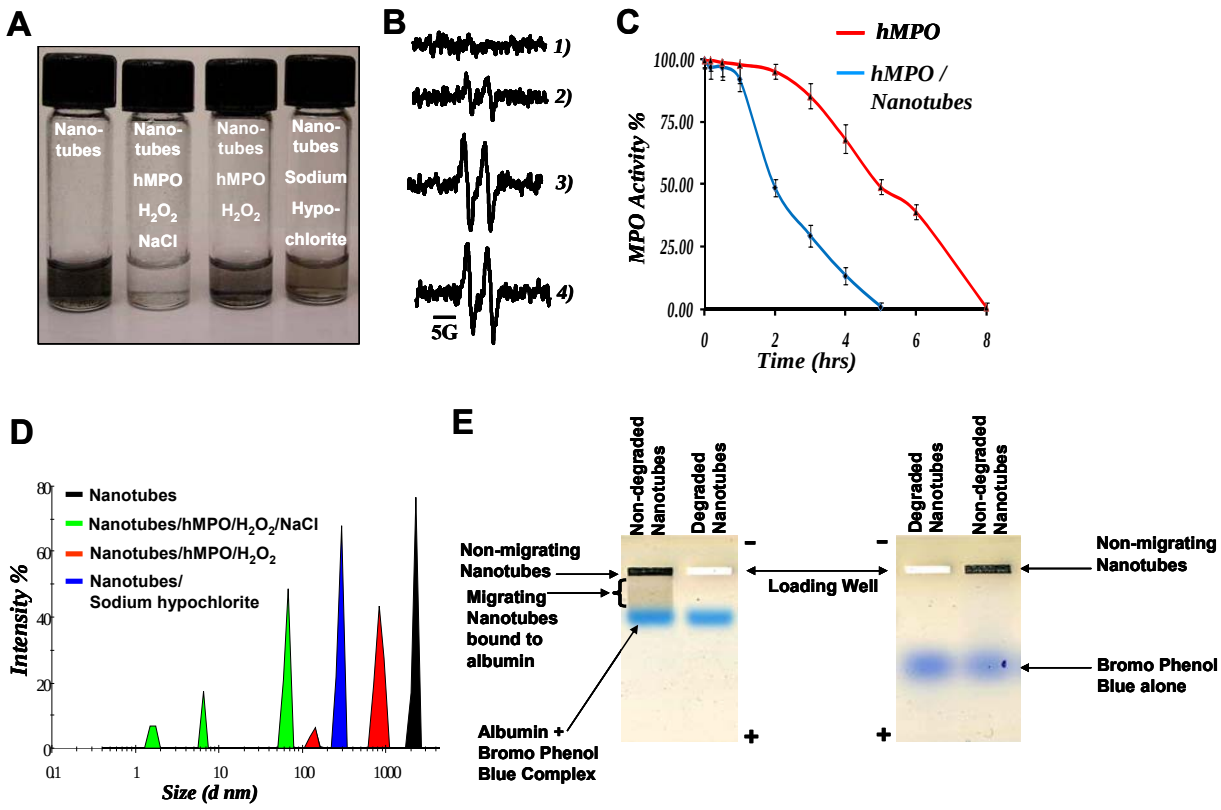


**Figure 17. Human myeloperoxidase (hMPO) mediated degradation of nanotubes in vitro.** A, Photograph of different short-cut nanotubes suspensions after 24 hrs. B. EPR spectra of ascorbate radicals characterizing peroxidase activity of hMPO in the presence and absence of nanotubes. 1) nanotubes alone, 2) hMPO and nanotubes, 3) hMPO and $H_2O_2$ and 4) nanotubes, hMPO and $H_2O_2$. Addition of nanotubes to the incubation mixture did not change the EPR signal of ascorbate radical. In the absence of hMPO or $H_2O_2$, the magnitude of the signal was several-fold lower thus confirming that oxidation of ascorbate occurred mainly via the peroxidase reaction. C. hMPO activity measurements in the presence and absence of nanotubes based on standard guaiacol assay. D. Dynamic light scattering shows multiple smaller peaks corresponding to biodegraded nanotubes. E. Agarose gel electrophoresis showing mobility profiles of non-biodegraded and biodegraded material in 0.5 % agarose. Electrophoresis was performed in TAE buffer (40 mM Tris acetate and 1 mM EDTA) and the wells were loaded with 20 µL of the material.

### 5.3.2 Visible-near infrared and Raman spectroscopic evaluation of hMPO catalyzed nanotube biodegradation

Spectroscopic evaluation of hMPO biodegraded nanotubes: Visible–near infrared (Vis–NIR) absorbance spectra of hMPO/$H_2O_2$ treated nanotubes showed that the characteristic metallic band (M1) and semiconducting (S2) transition band were suppressed during incubation (Figure 18A). The disorder-induced D-band at 1,250–1,350 $cm^{-1}$ increased in the Raman spectra, whereas the tangential-mode G-band decreased with incubation time, suggesting that the graphene sidewall was oxidized (Figure 18B).

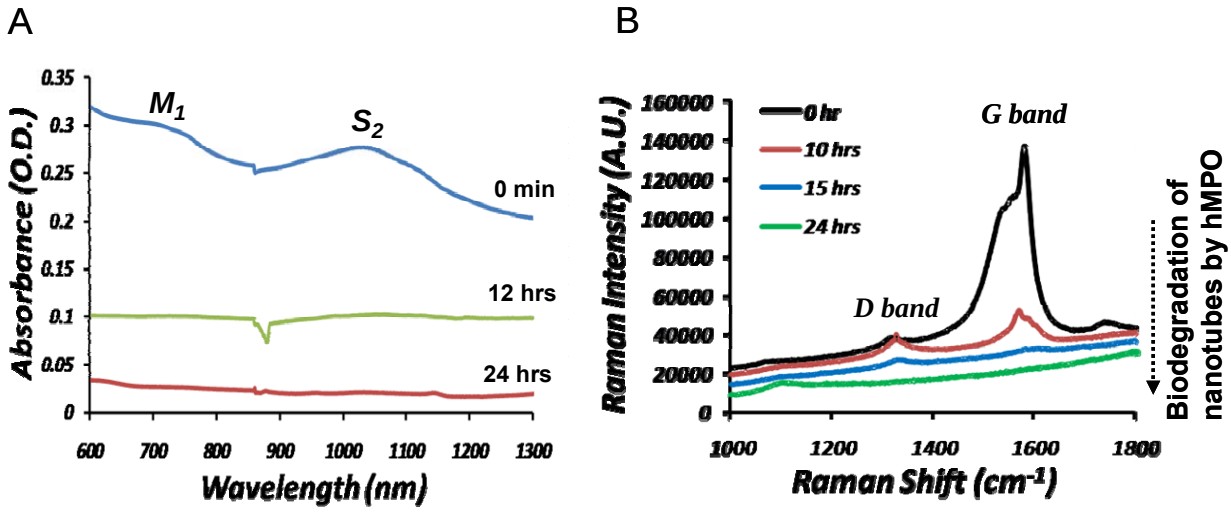


**Figure 18. Spectroscopic evaluation of human myeloperoxidase (hMPO) mediated degradation of nanotubes in vitro.** A, Infrared spectra show loss of M1 and S2 bands as nanotubes are degraded in the presence of hMPO and $H_2O_2$. B. Raman spectra (633 nm excitation) of ethanol dried nanotubes (black) and hMPO and $H_2O_2$ treated nanotubes showing loss of the characteristic G-band followed by appearance and decay of the D-band over time.

### 5.3.3 Electron microscopic characterization of human myeloperoxidase (hMPO) mediated degradation of nanotubes in vitro

Drastic changes in nanotube morphology were further confirmed by transmission (TEM) and scanning electron microscopy (SEM). The characteristic fibrillar structure of intact nanotubes was completely lost, and the bulk of the nanotubes was no longer present after 24 h of incubation (Figure 19A,B ). Only a few visual fields showed evidence of residual carbonaceous material (Figure 19C).

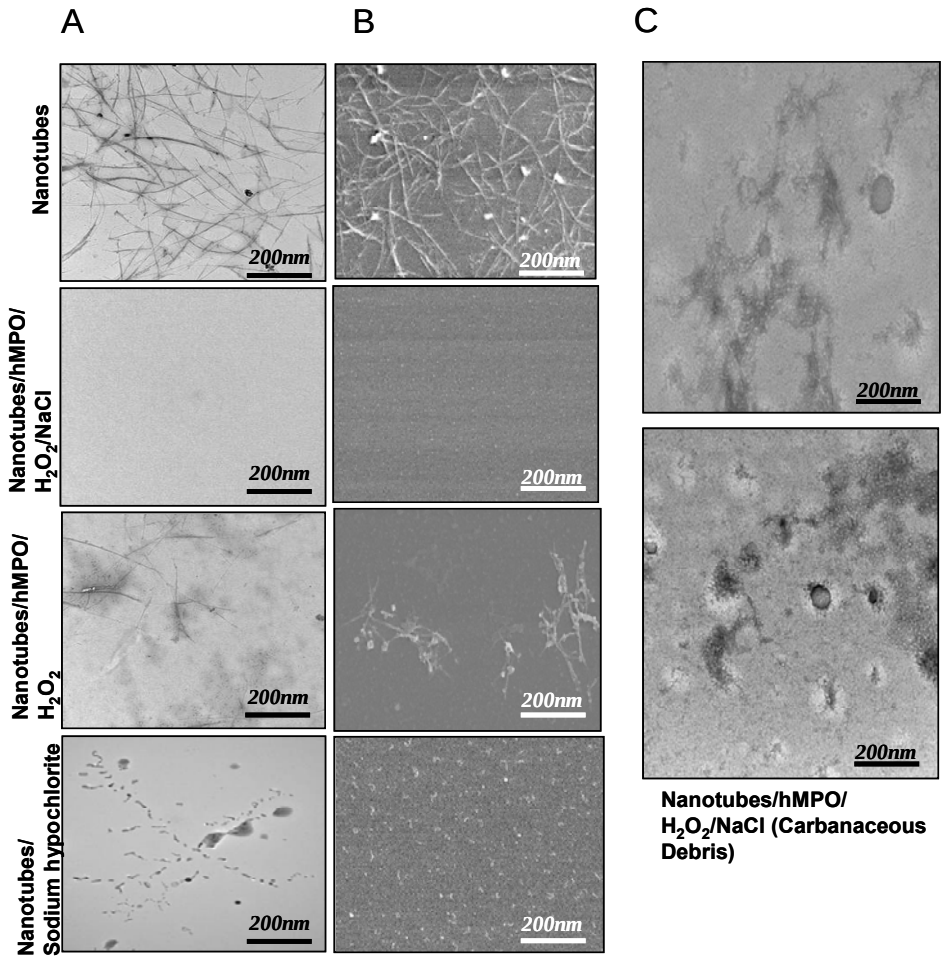


**Figure 19. Electron micrographs of carbon nanotubes.** TEM (A) and SEM (B) analyses, tracking the biodegradation of carbon nanotubes after 24 h. C, TEM images of biodegraded nanotubes showing fields with globular carbonaceous amorphous material.

### 5.3.4 Determination of nanotubes biodegradation products by gas chromatography-mass spectrometry

After 12 h of incubation of the nanotubes with hMPO and $H_2O_2$, gas chromatography–mass spectrometry (GC–MS) revealed several major products, including short-chain tri-carboxylated alkanes and alkenes, and molecular ions of di-carboxylated short-chain and mono-carboxylated products (Figure 20). Analysis of the products extracted from fully biodegraded nanotubes demonstrated the presence of short-chain carboxylated alkanes and alkenes. These results are in agreement with previous studies showing carboxylation of nanotubes on acid treatment (Kuznetsova, Popova et al. 2001). Furthermore, a 60% increase in $CO_2$ levels was detected in biodegraded nanotubes compared to nanotubes incubated with hMPO alone or $H_2O_2$ alone.

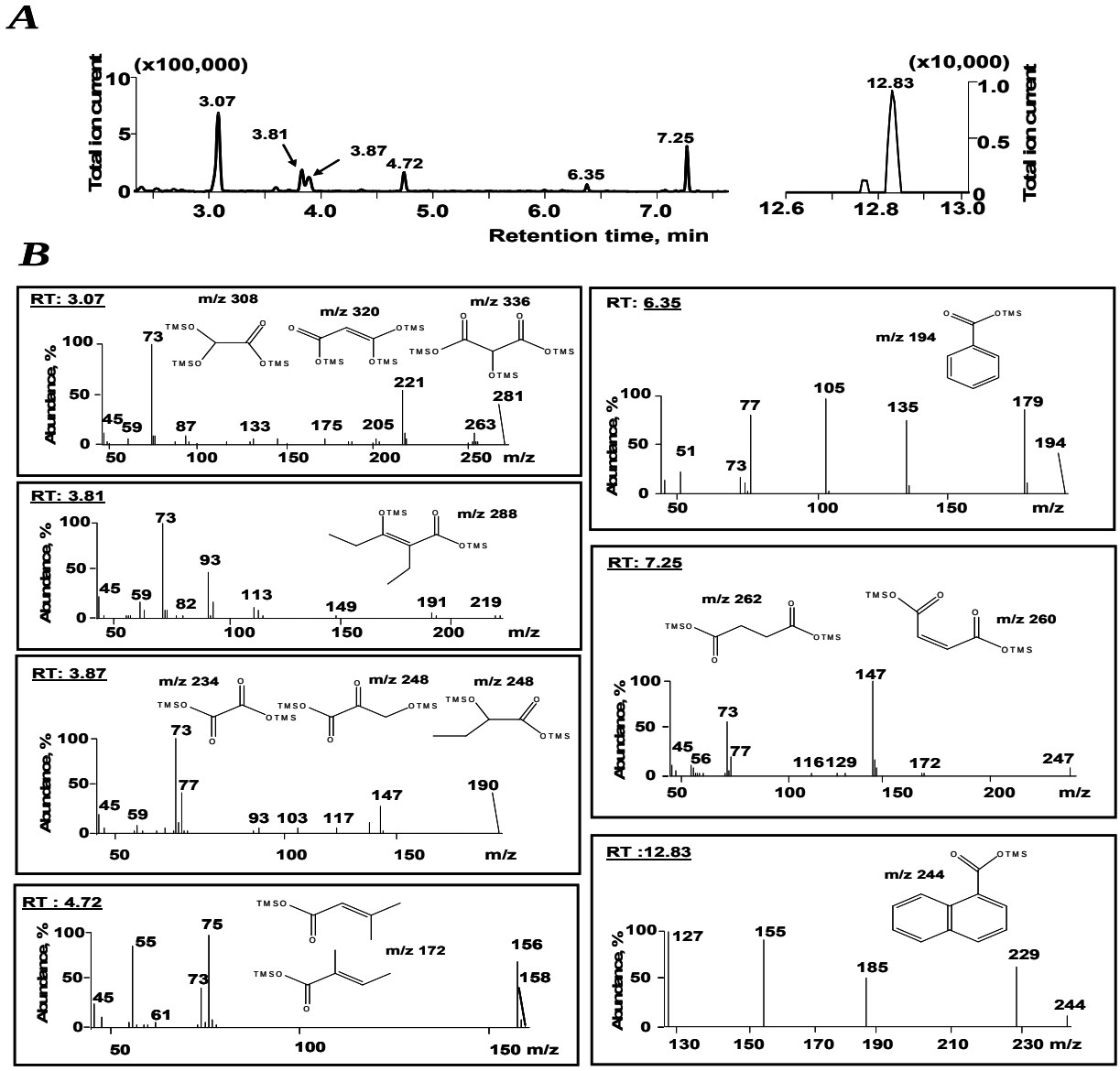


**Figure 20. GC-MS analysis of SWCNT biodegradation products.** A, Typical GS-MS chromatogram of products obtained from partially degraded nanotubes. B, MS-fragmentation patterns of major nanotubes biodegradation products (chemical formulas are presented on the respective panels) corresponding to characteristic peaks with retention times shown on Figure 4A. The short-chained tri-, di- and mono- carboxylated alkanes and alkenes (retention time 3.07 min, 3.81 min, 3.87 min, 4.72 min, 7.25 min), benzoic acid (retention time 6.35 min) and naphthoic acid (retention time 12.83 min) are shown.

### 5.3.5 Elucidating the components of hMPO responsible for biodegradation of nanotubes

Reactive radical intermediates of hMPO and hypochlorite could be two oxidants involved in nanotube biodegradation (Panasenko, Chekanov et al. 2005). Both are formed when hMPO is incubated with $H_2O_2$ in the presence of sodium chloride (NaCl), whereas only peroxidase reactive radical intermediates are generated in the absence of NaCl. Myeloperoxidase ($MPO^{3+}$) reacts with $H_2O_2$ to form the redox intermediate compound I, which oxidizes chloride by a single 2-electron transfer to produce the hypochlorous acid (HOCl). In order to elucidate which of the two components was essential in catalyzing the biodegradation of nanotubes, we incubated the nanotubes with hMPO and $H_2O_2$ in the presence and absence of NaCl. Biodegradation of nanotubes occurred during their incubation with hMPO and $H_2O_2$ in the absence of NaCl, although it was markedly suppressed compared to results obtained for incubation with hMPO and $H_2O_2$ plus NaCl (Figure 21). Taurine, a scavenger of HOCl (Kearns and Dawson 2000), also impeded the biodegradation of nanotubes. The effect was similar to that achieved in a NaCl-free medium (Figure 21). When nanotubes were exposed to HOCl alone, the biodegradation of nanotubes was markedly attenuated. Overall, these data imply that both the peroxidase reactive intermediates and hypochlorite contributed to biodegradation.

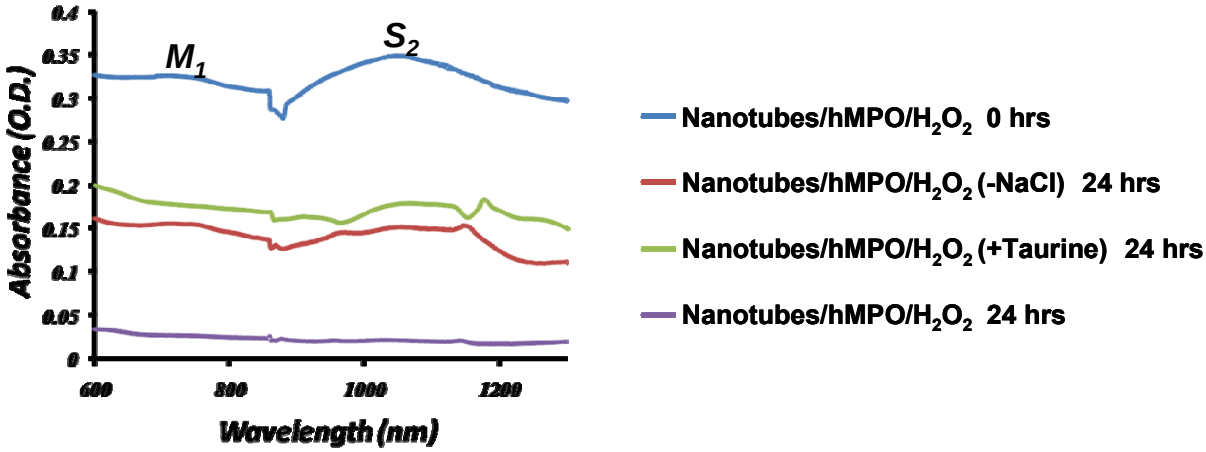


**Figure 21. Effect of taurine on biodegradation of nanotubes.**Vis-NIR spectroscopic evaluation of nanotubes biodegradation when incubated with hMPO/H2O2 in the standard incubation buffer containing 140 mM NaCl either in the presence of 10 mM taurine (green) or when incubated in buffer without NaCl (red).

### 5.3.6 Molecular modeling to understand the interaction of oxidized sites on carbon nanotube with critical residues in the active site of hMPO

We further sought to identify interaction sites of hMPO with SWCNT by molecular modeling. In particular we were interested in determining whether carbon nanotubes would interact with hMPO in proximity to the heme and catalytically essential amino acid residues on hMPO, such as Tyrosine (Tyr) and Tryptophan (Trp) (Olivier and Paul 2000). We generated models of carboxylated and non-carboxylated nanotubes and docked them to the hMPO crystal structure (see Methods). The top 25 rank ordered conformations were found to be clustered between two sites on hMPO in both cases (Figure 22A). One binding site, preferred based on minimum energy (see below), was located at the proximal end of the heme group involving the proposed catalytically active Tyr293 (Figure 22A, left) and the second site was located at the distal end of the heme group on the opposite side of the molecule (Figure 22A, right). The simulation model pointed to a strong interaction of positively charged residues on hMPO with the

carboxyl surface of (14,0) nanotubes, in line with the previous study by Kam et al (Kam and Dai 2006) which attributed interactions of nanotubes with proteins to attractive forces between the carboxyl groups on the nanotube surface and positively charged domains on the proteins. The conformation where carboxylated nanotubes is most buried has a minimum energy of -15.7 kcal/mol as compared to the second binding site which was only observed in 9 of the 25 top-ranked conformation and had a lesser minimum energy of -11.2 kcal/mol. Analysis of the residues located within 5 Å distance from the docked carboxylated SWCNT revealed the presence of Tyr293, Arg294, Arg307, Tyr313, Trp513, Trp514 and Arg507 in close proximity to SWCNT thus emphasizing their potential involvement in the catalytic act (Figure 22B, C). Notably, radicals of the above Tyr and Trp residues have been identified as possible catalytic intermediates of the peroxidase reaction (Olivier and Paul 2000). Experimental data obtained by atomic force microscopy (AFM) of the enzyme co-incubated with SWCNT (Figure 22D), demonstrated interaction/attachment of hMPO to the surface of carboxylated carbon nanotubes. We thus propose a site-localized reaction in which hMPO positive charges favour the binding of nanotubes, and radical-supporting aromatic groups participate in the cleavage of the nanotubes. Notably, pristine nanotubes underwent less effective biodegradation by hMPO both in the presence and absence of NaCl (Figure 22E).

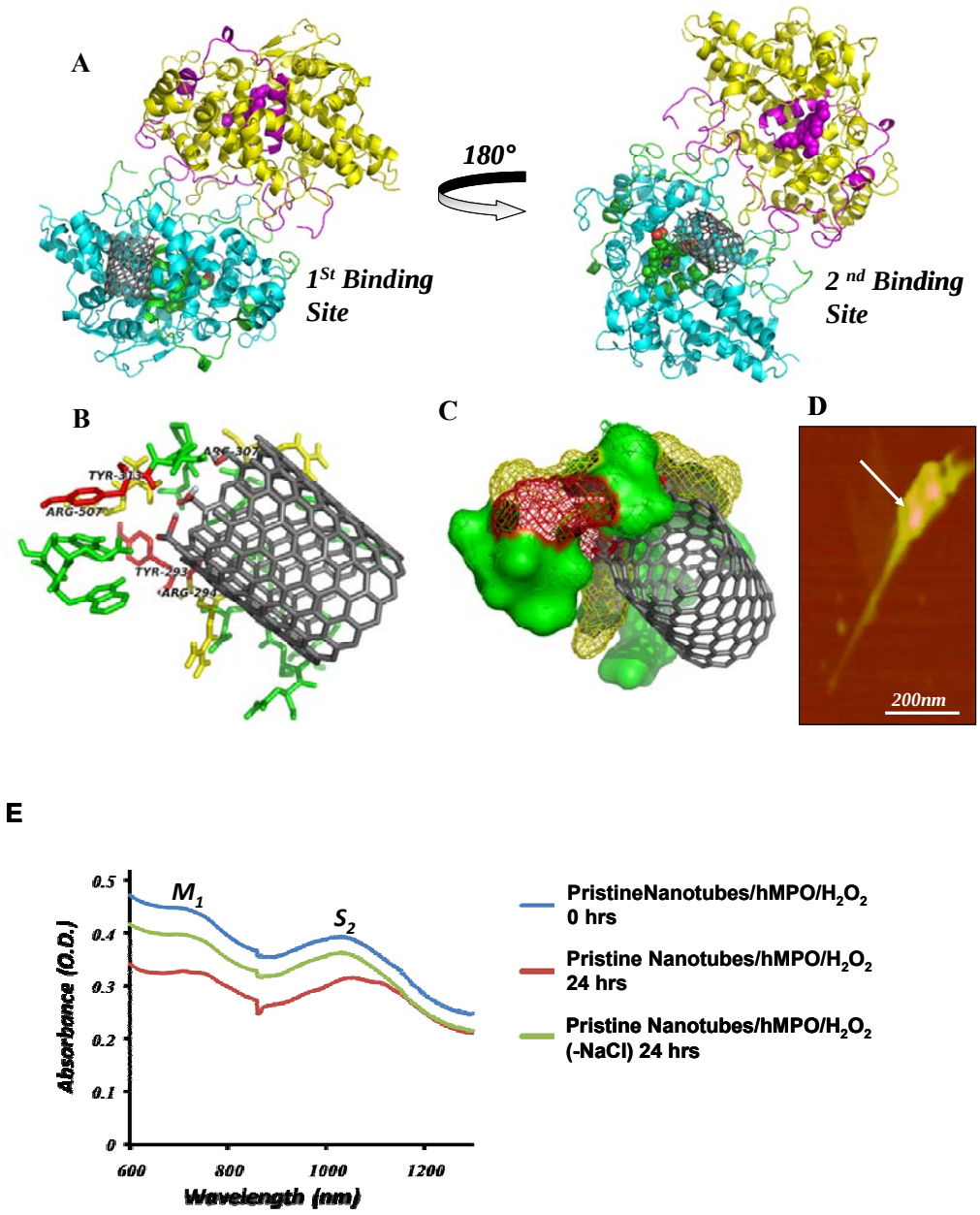


**Figure 22. Molecular modeling, demonstrating possible nanotube interaction sites on hMPO.** A, Two putative binding sites for nanotubes on the hMPO monomer surface are located on each side of the protein. The best model site with lowest binding energy is shown for carboxylated short-cut nanotubes (left) and pristine nanotubes (right). B, Stabilization of the carboxylated ends of the nanotubes by arginine (yellow) and tyrosine residues (red) in hMPO in the first binding pocket (left). All residues shown are within 5 Å of nanotubes and are predicted to participate in the degradative catalysis of nanotubes. This includes Tyr293, Arg294, Arg307, Tyr313 and Arg507. C, As B, using space-fill representation. D, AFM image confirming the binding of a dimer of hMPO with a single nanotube. E, Vis-NIR spectroscopic analysis showing pristine nanotubes before (blue line) and after 24 hrs of enzymatic catalysis with hMPO/$H_2O_2$ in 50 mM phosphate buffer, without (green line) and with (red line) 140 mM NaCl.

### 5.3.7 Uptake of nanotubes by neutrophils

We evaluated the ability of neutrophils - short-lived immune cells that are a particularly rich source of hMPO - to recognize and engulf nanotubes. In this context we tried to assess the particle uptake in neutrophils isolated from human blood. We functionalized fluorescently labeled nanotubes (FITC-nanotubes) with phospholipids (PS and PC) and immunoglobulin-IgG and assessed the degree of particle uptake in neutrophils upon functionalizing with bio-molecules. We found that IgG-functionalized FITC-nanotubes were more efficiently engulfed by neutrophils compared to PS and PC functionalized nanotubes (Figure 23A, B, C).

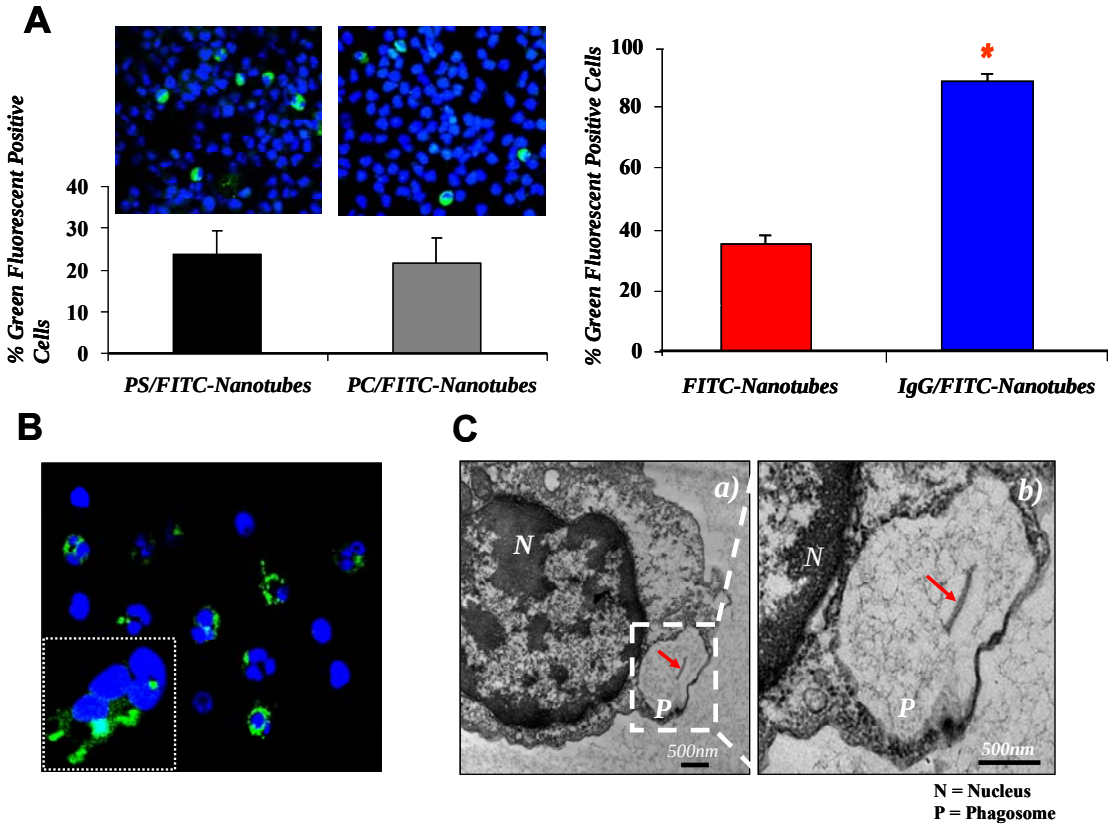


**Figure 23. Uptake of nanotubes conjugated with fluorescein isothiocyanate (FITC) (FITC-nanotubes) and functionalized with PS/PC or IgG by human peripheral blood neutrophils.** A, Quantitative uptake assessments of FITC-nanotubes coated with either phospholipids or IgG by neutrophils isolated from human blood after co-incubation for 2 hrs at 37°C. A total of 500 cells from each sample type were analyzed by fluorescence microscopy.

Data are mean values ± S.D. (n = 3, *p<0.05). B, Insert, confocal micrograph of neutrophils following incubation with IgG-functionalized FITC-nanotubes for 2 hrs. Blue: cell nuclei, Green: FITC-nanotubes. (Note: The insert also shows a magnified image of a neutrophil with internalized IgG functionalized FITC-nanotubes). C, Transmission electron micrograph of a neutrophil phagocytosing IgG-functionalized nanotubes. A higher magnification view of the neutrophil phagosome with IgG-functionalized nanotubes is also shown. (Arrows point to IgG-functionalized nanotubes).

### 5.3.8 Generation of oxidants and release of hMPO by activated human neutrophils

We next determined whether non-functionalized and IgG-functionalized nanotubes can stimulate oxidant generation and subsequently cause myeloperoxidase release in hMPO-rich human neutrophils. Stimulation of neutrophils was performed using a chemoattractant, N-formyl-methionylleucyl-phenylalanine (fMLP), in combination with a degranulation promoting agent, cytochalasin B. Cytochalasin B is known to increase the activity of hMPO and trigger its release (Zipfel, Carmine et al. 1997). During neutrophil activation, hMPO is translocated into phagosomes, in which the fully assembled, membrane-bound NADPH oxidase generates superoxide radicals (Hampton, Kettle et al. 1998). The latter dismutates to $H_2O_2$, which enables hMPO to produce reactive intermediates and HOCl. Dihydroethidium staining and cytochrome-c reduction assay confirmed the activation of neutrophils on stimulation with fMLP and cytochalasin B (Figure 24A,B). We observed that 75 % of the total hMPO remained inside the cells (Figure 24D), and only 25 % of the hMPO was released into extracellular environment upon neutrophil activation. Furthermore, we also observed sustained basal generation of oxidants (for up to 12 h) by neutrophils incubated with IgG–functionalized nanotubes as assessed by 2′,7′- dichlorofluorescein-di-acetate and Amplex Red assays (Figure 24 C, E, F, G).

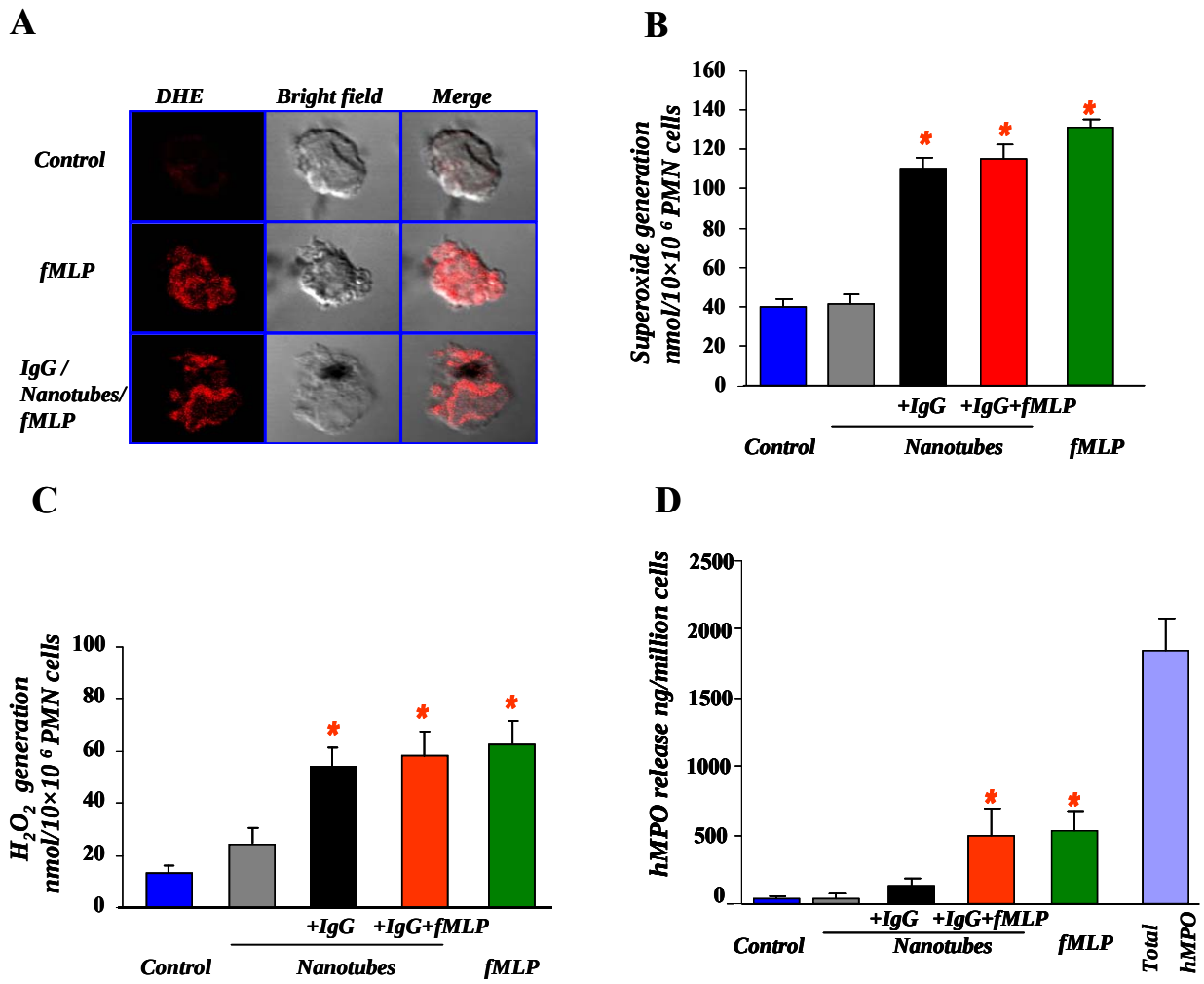


**Figure 24. IgG-functionalized nanotubes induce the release of hMPO and the generation of reactive oxygen species in human peripheral blood neutrophils.** A, Assessments of intracellular superoxide in neutrophils treated with fMLP and cytochalasin B (CyB) alone or plus IgG–functionalized nanotubes for 30 min at 37 °C. Representative confocal micrographs of neutrophils stained with dihydroethidium (DHE) to detect superoxide generation are shown. B, Quantitative assessment of extracellular generation of superoxide radicals. C, Generation of extracellular $H_2O_2$ 30 min after challenge with nanotubes assessed by the Amplex red assay. D, Extracellular release of hMPO in response to fMLP, cytochalasin B and IgG–functionalized nanotubes Data shown in panels B–D are from three independent experiments performed with neutrophils obtained from different donors and are expressed as mean values ± s.d. (*P,0.05, groups versus control). Error bars in B–D represent standard deviations (s.d.).

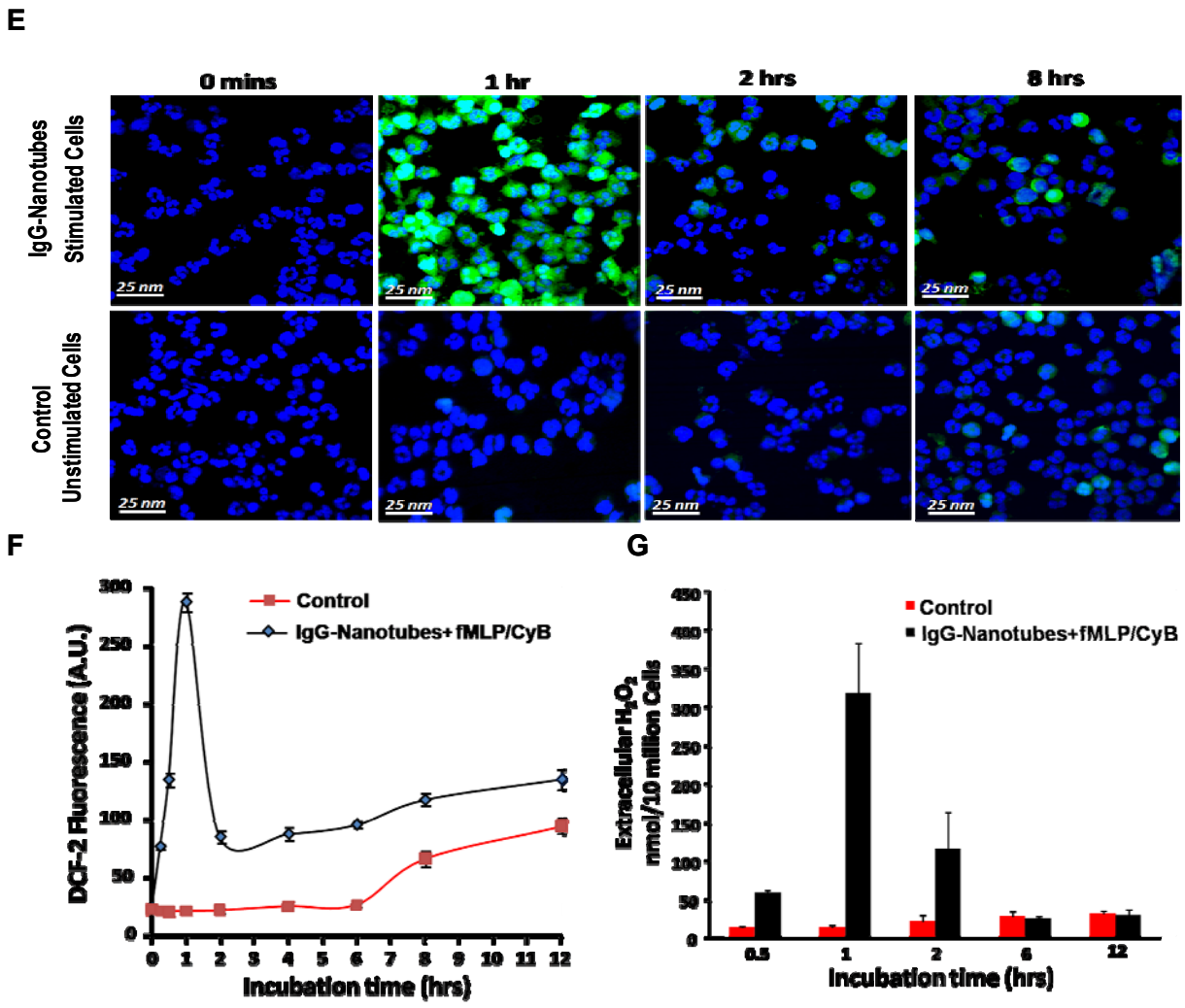


**Figure 24 (contd). Generation of H2O2 in stimulated neutrophils.** E, micrographs exhibiting 2,7-dichlorofluorescein (DCF) fluorescence (as a measure of intracellular $H_2O_2$) of intracellular $H_2O_2$ production in human neutrophils at different time points. DCF fluorescence was captured using laser confocal scanning microscope (excitation at 488 nm). Blue: cell nuclei, Green: DCF fluorescence. F, Time-course of mean DCF fluorescence (as a measure of intracellular $H_2O_2$) using MetaMorh software (Universal imaging). Data points represent mean fluorescence values ± S.D. of 200 cells from 3 determinations, and G, measurements of extracellular $H_2O_2$ from neutrophils stimulated with fMLP/cyB and incubated with IgG-functionalized nanotubes using Amplex red.

### 5.3.9 Biodegradation of nanotubes by human phagocytic cells

We next evaluated whether oxidative biodegradation of nanotubes can be executed by hMPO-rich human neutrophils and in human monocyte derived macrophages which contain relatively lower levels of hMPO (13 ng hMPO per $10^6$ macrophages, compared with 1.8 mg hMPO per $10^6$ neutrophils). Stimulation of neutrophils and macrophages was performed as described above using a chemo-attractant, N-formyl-methionylleucyl-phenylalanine (fMLP), in combination with a degranulation promoting agent, cytochalasin B. Because 75 % of the total hMPO remained inside the cells (Figure 8D), we targeted nanotubes to neutrophils by using IgG functionalization. Under these conditions, IgG–functionalized nanotubes underwent 100 % degradation, whereas only 30 % of non-IgG-functionalized nanotubes were degraded in neutrophil suspensions, as was made evident by infrared spectroscopy (Figure 25A). Inhibitors of hMPO (4-aminobenzoic acid hydrazide) (Kettle, Gedye et al. 1997) and NADPH oxidase (apocynin) (Touyz 2008) attenuated the degradation process (Figure 25B). This finding suggests that both hMPO and NADPH oxidase were essential for nanotube biodegradation by neutrophils. Raman microscopy of IgG-functionalized nanotubes inside neutrophils showed a marked loss of the G-band and appearance of a strong D-band. This is characteristic of oxidatively modified nanotubes (Figure 25 C, D) and demonstrates that the uptake of IgG-functionalized nanotubes by neutrophils resulted in an hMPO-driven biodegradation process in activated cells. Infrared spectroscopic assessments revealed only negligible degradation of IgG–functionalized nanotubes by macrophages after 6 h of incubation and 13 % degradation at 12 h (compared with 30 % and 100 % biodegradation of IgG–functionalized nanotubes by neutrophils at 6 and 12 h, respectively; Figure 25B). More pronounced (50 %) biodegradation of IgG–functionalized nanotubes by macrophages occurred only after 48 h. As described previously (Dou, Destache et al. 2006; Batrakova, Li et al. 2007) these results suggest that

hMPO activity is an important determinant of the biodegradation of nanotubes as well as other nano-formulations.

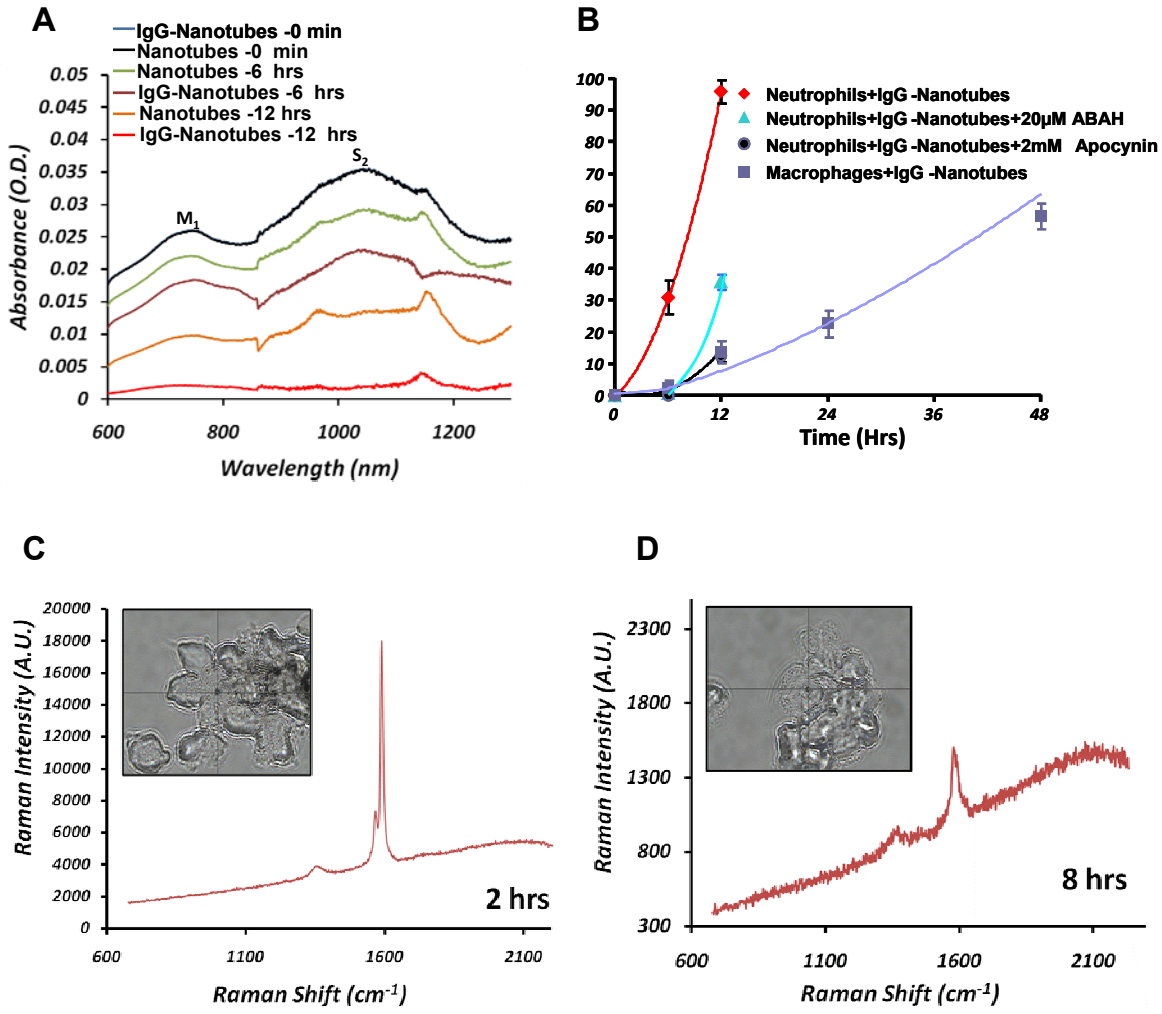


**Figure 25. Biodegradation of nanotubes in phagocytes evaluated by infrared and Raman spectroscopy.** A,Vis–NIR spectra showing biodegradation of nanotubes and IgG–functionalized nanotubes by human neutrophils after 0, 6 and 12 h. O.D., optical density. B, biodegradation of IgG-functionalized nanotubes by neutrophils and macrophages at different time points is plotted as percentage (n=3) assessed by the intensity magnitudes of both the characteristic semi-conducting (S2) and the metallic (M1) peaks of nanotubes present in the recorded Vis-NIR spectra. Cells (25 x $10^6$) were incubated with 25 μg of IgG-nanotubes for 12-48 hrs (12 hrs for Neutrophils and up-to 48 hrs for macrophages) and the extent of biodegradation was assessed. Neutrophils were pre-treated with either 20 μM 4-aminobenzoic acid hydrazide (ABAH) or 2 mM apocynin for 1 hr prior to the addition of IgG-nanotubes. C, D, Raman spectra (excitation, 473 nm) recorded from different areas of neutrophils containing

IgG–functionalized nanotubes at 2 h (C) and 8 h (D). Inset shows bright-field image of the neutrophils with engulfed IgG–functionalized nanotubes. The Raman spectra (red lines) with their corresponding G- and D-bands recorded from different areas of neutrophils are indicated by the crosswire on the bright-field images.

## 5.4 CONCLUSIONS

In conclusion, we provided here compelling evidence of the biodegradation of carbon nanotubes by myeloperoxidase/Nacl/$H_2O_2$ system in both cell free and cell based system involving neutrophils and macrophages. We have used biochemical model systems as well as contemporary methods of analytical biochemistry - ranging from atomic force microscopy and conventional transmission electron microscopy (TEM), scanning electron microscopy (SEM) to different types of spectroscopies including Raman, near-infrared (NIR) - to demonstrate that biodegradation indeed occurs due to action of oxo-ferryl intermediates and hypochlorous acid derived from hMPO on carbon nanotubes. We characterize the products ranging from short chained carboxylated alkanes and alkenes to aromatic derivatives formed during the process of SWCNT biodegradation using gas chromatography-mass spectroscopy (GC-MS). We also employed molecular modeling to study interactions of pristine and carboxylated carbon nanotube with residues in the of hMPO and found that a basic amino acid rich region in hMPO is involved in binding of carboxylated nanotubes and proposed a radical transfer mechanism through tyrosine and tryptophan residues bridging heme site with nanotube binding site. We evaluated the ability of neutrophils - short-lived immune cells that are a particularly rich source of hMPO, and macrophages low in hMPO content- to recognize, engulf and biodegrade SWCNT via their oxidative modification and found that neutrophils recognized and biodegraded nanotubes better than macrophages. We also evaluated the contributions of hMPO reactive intermediates and hypochlorous acid in nanotubes oxidative biodegradation and report that both these components are essential for effective biodegradation of nanotubes. We have shown a novel route of enzymatic biodegradation of single-walled carbon nanotubes relevant to potential respiratory exposures during the production and handling of carbon nanotubes.

# 6 CHAPTER 6 - BIODEGRADATION OF CARBON NANOTUBES IN VIVO

## 6.1 INTRODUCTION

Engineered nanomaterials, as exemplified by carbon nanotubes, can cause robust and unusual inflammatory responses in vivo with a rapid transition from the acute inflammatory phase to a chronic fibrotic phase; genotoxic effects have also been documented indicating that the realization of these events into a carcinogenic process may be possible. These toxic features of SWCNT limit their numerous industrial and biomedical applications. Studies of potential biodegradation pathways for nanotubes, although are clearly required, are lacking. The proposed projects will fill this gap by investigating the role and mechanisms through which MPO in neutrophils can catalyze biodegradation of nanotubes in vivo. Discovery of enzymatic mechanisms for "green" biochemistry of nanotubes biodegradation may revolutionize the ways to regulate their distribution in the body and contribute to a roadmap to new effective approaches to decrease their potential toxicity. The major goal of the next series of experiments is to determine the extent to which nanotubes biodegradation occurs in vivo. To delineate the specific role of MPO in catalysis of nanotubes biodegradation in vivo of nanotubes exposed (via pharyngeal aspiration) animals, MPO k/o mice and C57BL6 control mice (available from the Jackson Laboratory) were utilized. Previously the lab has developed two animal models of exposure to nanotubes - pharyngeal aspiration and inhalation (Shvedova, Kisin et al. 2008). In both cases, similar reactions that combined a robust pulmonary inflammatory response with unusually short acute phase and early onset of fibrosis were observed. Using these models, we were able to experimentally address the following issues: i) Can hMPO-catalyzed biodegradation process convert nanotubes into products that are inactive in eliciting the characteristic inflammatory pulmonary responses in vivo in mice; ii) Using MPO k/o mice, to

quantitatively evaluate participation and role of the enzyme in nanotubes biodegradation and modulation of inflammatory response. We used our established mouse model of pharyngeal aspiration of nanotubes and assessed the numbers of neutrophils, and the amount of pro-inflammatory (TNF-α) and anti-inflammatory (IL-6) cytokines in broncheoalveolar lavage (BAL) obtained from mice at 1 day and 7 day post-exposure. Essentially, the same experiments as in in vitro studies were performed and detailed analysis of nanotubes in tissue sections (using Raman spectroscopy/microscopy, transmission electron microscopy, histological analysis and hyperspectral imaging technology) was conducted. In addition, characterization of inflammatory response - including the numbers of inflammatory cells (neutrophils on days 1 and 7 after the exposure), the amount of pro-inflammatory (TNF-α) and anti-inflammatory (IL-6) cytokines in BAL and extent of collagen deposition on day 28 lung samples was evaluated.

## 6.2 METHODS

**Particulate instillation:** Pharyngeal aspiration was used for particulate administration to C57BL/6 and MPO knock out mice. Briefly, after anesthization with ketamine and xylazine anesthesia (62.5 and 2.5 mg/kg, respectively), the mouse was placed on a board in a near vertical position. The animal's tongue was extended with lined forceps and a suspension of particulates (50 μl, nanotubes at a dose of 40 μg/mouse) was placed in the posterior of pharynx. The tongue was held until the suspension was aspirated into the lungs. All mice in particle and PBS groups survived this exposure procedure. This technique provides good distribution of particles widely disseminated in a peri-bronchiolar pattern within the alveolar region. Animals treated with the particulates recovered easily after anesthesia with no behavioral or negative health outcomes.

**Bronchoalveolar lavage:** Mice will be weighed and euthanized with intraperitoneal injection of sodium pentobarbital (SPB, Fort Dodge Animal Health, Fort Dodge, IA, USA) (>100 mg/kg). The trachea will be cannulated with a blunted 22 gauge needle, and BAL will be performed using cold sterile $Ca^{2+}$/$Mg^{2+}$-free PBS at a volume of 0.9 ml for first lavage (kept separate) and 1.0 ml for subsequent lavages. Approximately 5ml of BAL fluid per mouse will be collected and pooled in sterile centrifuge tubes. Pooled BAL cells will be washed in $Ca^{2+}$/$Mg^{+2}$-free PBS by alternate centrifugation (800 × g for 10 min at 4 °C) and re-suspension.

**Histology:** In a separate set of animals, the lungs were excised and fixed in Karnovsk'y fixative. Paraffin-embedded sections were stained with hematoxylin and eosin (H&E) for light microscopic examination.

**Solubilization of lungs:** Lungs were homogenized using Biospec Products Inc, OK, USA tissue homogenizer in 500 μL of deionized water. Following homogenization, 1 % SDS was added to 300 μL of the aliquot and heated to 100$^{o}$C for 10 min. This was followed by

sonication using using the ultrasonic probe tip sonicator (Cole-Palmer Ultrasonic Homogeneizer, 20 kHz) for 15 min. After cooling the contents to room temperature, 100 μL of 50 mM Tris buffer (pH 8.0) was added to the aliquot. Finally, an 18 hour incubation of the material with 100 μg/mL of proteinase K was undertaken to completely solubilize the lung.

**Raman microscop/spectroscopy**: Solubilized lung material was vacuum filtered through double Polyvinylidene fluoride (PDVF) membrane. A Renishaw inVia Raman spectroscopic microscope was used, with a cobalt solid state laser operating at a wavelength of 633 nm. All Raman spectra were recorded for 10 secs, at 10% laser power using a 20x objective. For each spectrum a static grating (2400 l/mm) scan was taken over the range 678.28 $cm^{-1}$ to 2231.82 $cm^{-1}$ (centered at 1500 $cm^{-1}$). Detection of the Raman scattered light was performed using a peltier cooled CCD detector. Calibration was carried out daily using a piece of silicon to ensure the 520 $cm^{-1}$ line of silicon was not out by more than 1 $cm^{-1}$. From each of the samples an average of 20 spectra was recorded.

**Vis-NIR spectroscopy:** Solubilized lung aqueous samples (50 μL) were analyzed using a Lambda 900 spectrophotometer (Perkin-Elmer) and 60 μL quartz cuvettes (World Precision Instruments, Inc.). The samples were scanned from 600 to 1300 nm.

**Transmission electron microscopy:** Each tissue was fixed with Karnovsk'y fixative and then post fixed with aqueous 1% osmium tetroxide. The fixed sample was dehydrated and embedded with epon. The 50-nm ultrathin sections were cut and stained with 2% uranyl acetate and lead. The prepared sections were viewed with a JEOL 1210 TEM system (JEOL USA, Peabody, MA).

**Statistics:** The results are presented as means ± S.D. values from at least three experiments, and statistical analyses were performed by one-way ANOVA with tukey's post hoc analysis. The statistical significance of differences was set at $p < 0.05$.

## 6.3 RESULTS

### 6.3.1 hMPO-mediated biodegradation of nanotubes mitigates their pro-inflammatory effects in vivo

Pharyngeal aspiration or inhalation of nanotubes is known to induce a robust pulmonary inflammatory response in mice, with early onset of fibrosis (Shvedova, Kisin et al. 2005). To address whether the biodegradation process would render nanotubes non-inflammatory, we assessed the amounts of neutrophils and the levels of cytokines in broncheoalveolar lavage obtained from mice at day 1 (Figure 1A) and day 7 (Figure 1C) after nanotube exposure. The profiles of these inflammation markers in animals exposed to biodegraded nanotubes by pharyngeal aspiration were essentially indistinguishable from control values. In contrast, non-degraded short-cut nanotubes elicited an acute inflammatory response. Similar responses were seen with nanotubes pre-incubated with either hMPO or $H_2O_2$ alone (Figure 26A). Non-degraded nanotubes also induced the formation of tissue granulomas, but no granulomas were observed in the lungs of mice exposed to biodegraded nanotubes (Figure 26B). Partially degraded nanotubes obtained after 12 h of incubation with hMPO and $H_2O_2$ still retained some of their characteristic morphologic and spectral features, and induced less inflammation in mice than the non-biodegraded nanotubes (Figure 26D, E, F). Thus, hMPO-mediated biodegradation of nanotubes serves to mitigate the pro-inflammatory potential of these nanomaterials.

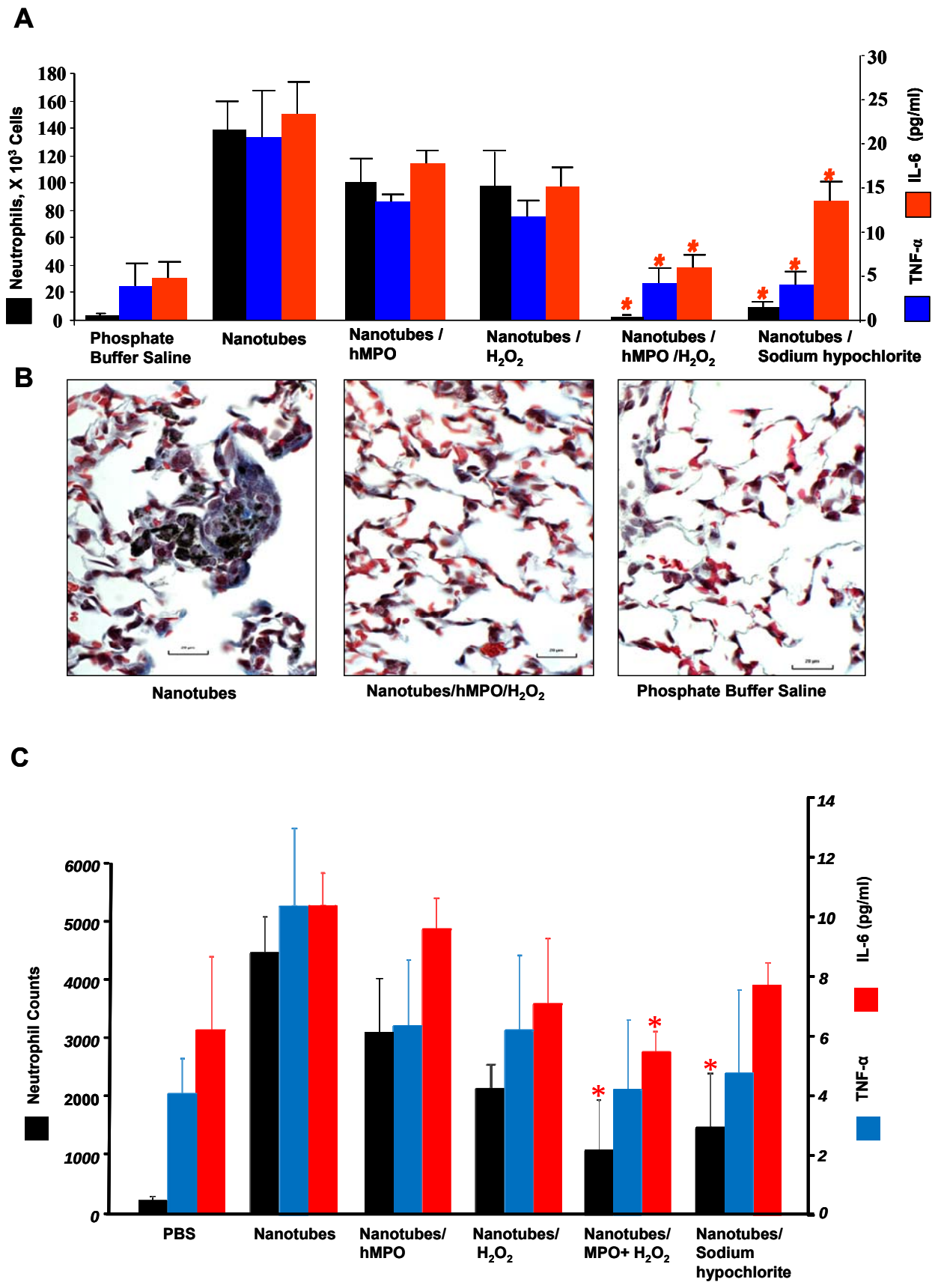
A
Neutrophils, X 10³ Cells
IL-6 (pg/ml)
TNF-α
Phosphate Buffer Saline
Nanotubes
Nanotubes / hMPO
Nanotubes / H2O2
Nanotubes / hMPO /H2O2
Nanotubes / Sodium hypochlorite
B
Nanotubes
Nanotubes/hMPO/H2O2
Phosphate Buffer Saline
C
Neutrophil Counts
IL-6 (pg/ml)
TNF-α
PBS
Nanotubes
Nanotubes/ hMPO
Nanotubes/ H2O2
Nanotubes/ MPO+ H2O2
Nanotubes/ Sodium hypochlorite

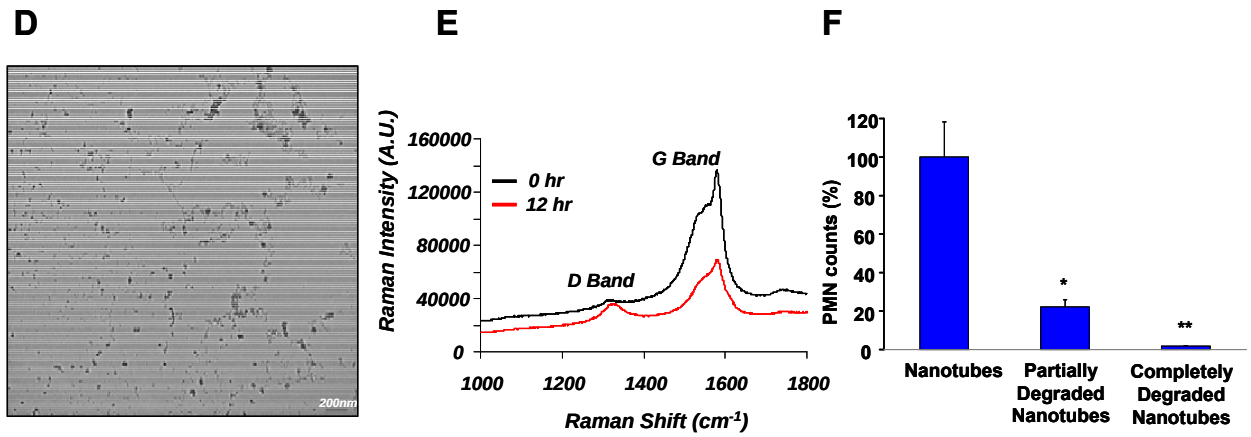


**Figure 26. Biodegraded nanotubes do not elicit a pro-inflammatory pulmonary response in C57BL/6 mice.** A, Neutrophil counts and expression of TNF-α and IL-6 in broncheoalveolar lavage fluid were measured 24 h after exposure to the indicated treatments by means of pharyngeal aspiration. Data represent mean values ± s.e. (n=6 mice per group). *P,0.05 groups versus nanotubes alone. B, Representative images of lung sections from mice exposed to 40 mg/animal nanotubes, showing granuloma formation on day 7 after pharyngeal aspiration. Similar to the results from control animals exposed to phosphate buffered saline, no granuloma formation is seen in the lungs of mice exposed to degraded nanotubes. Biodegradation of nanotubes was induced by their incubation with hMPO and $H_2O_2$. Error bars in a represent standard error (s.e.). C, Neutrophil counts and expression of TNF-α and IL-6 in broncheoalveolar lavage fluid were measured 7 days after exposure to the indicated treatments via the pharyngeal aspiration. *p < 0.05 vs. nanotubes alone. D, shows transmission electron micrograph of partially degraded nanotubes. The sample was prepared from an aliquot corresponding to 12 hrs incubation of nanotubes with hMPO/$H_2O_2$. E**,** Raman spectra showing lowering of G-band and an increase in the D-band in the partially degraded nanotubes (red line) compared to the untreated or non-degraded nanotubes (black line). E**,** Shows neutrophil counts from pharyngeal aspiration of nanotubes in BAL fluid from the exposed mice. Data are mean values ± S.D., n=6. *p<0.01, partially degraded nanotubes vs nanotubes; **p<0.001, completely degraded nanotubes vs nanotubes. (**Note:** Non-degraded implies to material not treated with hMPO/$H_2O_2$ and completely degraded nanotubes corresponds to the material from hMPO/$H_2O_2$/nanotubes incubation system at 24 hrs showing complete loss in the characteristic spectral and morphological features as presented in Figures 2 and 3 in previous section).

### 6.3.2 Differential degradative and inflammatory changes in wild type and myeloperoxidase null mice exposed to nanotubes

We then again employed our standard model of pharyngeal aspiration of nanotubes to assess their biodegradation in the lung tissue in the two different murine models at 1 day, 7 day and

28 days post exposure. Histopathological findings in lungs of mice on day 1 revealed marked nanotube congestion in lung parenchyma of myeloperoxidase kock-out (MPO-Ko) mice compared to wild type C57BL/6 wild type mice (Figure 27 A, upper panel). We found that while agglomerates of intact nanotubes remained entrapped in the largest airways in the MPO-Ko animals, nanotubes were much better dispersed in the lung tissues of wild type. MPO-Ko mice on day 28 showed relatively more and larger sized granulomatous areas (nanotubes-filled macrophage areas) in comparison to wild type mice (Figure 27A, lower panel). There was a significant increase (several fold) in the neutrophil counts in the BAL fluid following 24 hrs post nanotubes exposure in the wild type mice compared to MPO-Ko animals. Similarly, collage estimation following 28 day post exposure in animals revealed a significant increase in collagen deposition in MPO knock out mice compared to the wild type. Transmission electron microscopic evaluation on comparable lung areas indicates the presence and extracellular localization of nanotubes in both the mice types with predominantly more nanotubes laden areas in MPO-Ko mice (Figure 28A). Interestingly, the recognition and uptake of nanotubes by phagocytes was observed to be relatively higher in MPO-Ko mice compared to the wild type (Figure 29 B,D,C). Vis-near infrared spectroscopic studies on solubilized lung digests and estimates (quantification based on S2 and M1 peaks) showed significantly low amounts of nanotubes present in lungs of wild type mice compared to MPO-Ko after 28 days post exposure (Figure 28B,C and Figure 30B). Supportively, Raman spectroscopic analysis on solubilized lungs exhibited a significantly higher degree of biodegradation of nanotubes when compared to solubilized lungs from myeloperoxidase knock out mice as evaluated based on the D-band to G-band ratio (Figure 30A, C).

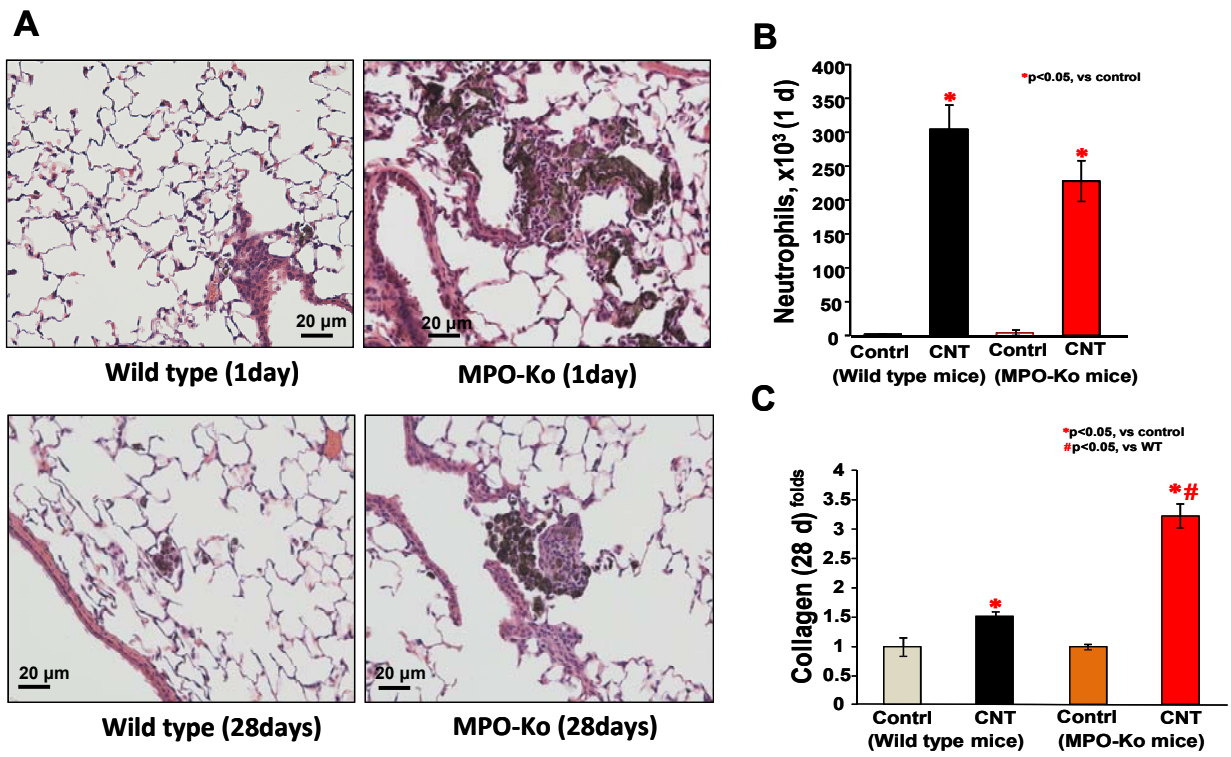


**Figure 27. Histopathological findings and inflammatory response in wild type and MPO-Ko animal lungs.** Representative micrographs of hematoxilin- and eosin-stained lung sections illustrating the pathologic changes observed in mice after 24 hours and 28 days post exposure to 40 ug nanotubes challenged by pharyngeal aspiration. Mice were sacrificed after challenge at 24 hrs (Fig A, upper panel) and 30 days (lower panel). Relatively, the alveolar parenchyma was occupied by compact aggregates of nanotubes in MPO-Ko lung tissues and appeared more dispersed in wild type after 24 hrs post exposure. At 28 days post exposure, nanotubes were surrounded by macrophages forming an interstitial granuloma and such areas laden with nanotubes were larger in MPO-Ko lung sections compared to wild type (A, lower panel). Counts of neutrophils (B) after 24 hrs and collagen content, a marker for pulmonary fibrosis (C) after 28 days post exposure were estimated in BAL fluid and lungs of mice respectively. Each bar represents the mean ± SD of 6-7 observations. *P < 0.05 vs. wild type (neutrophil counts); *# P < 0.05 vs. controls and wild type.

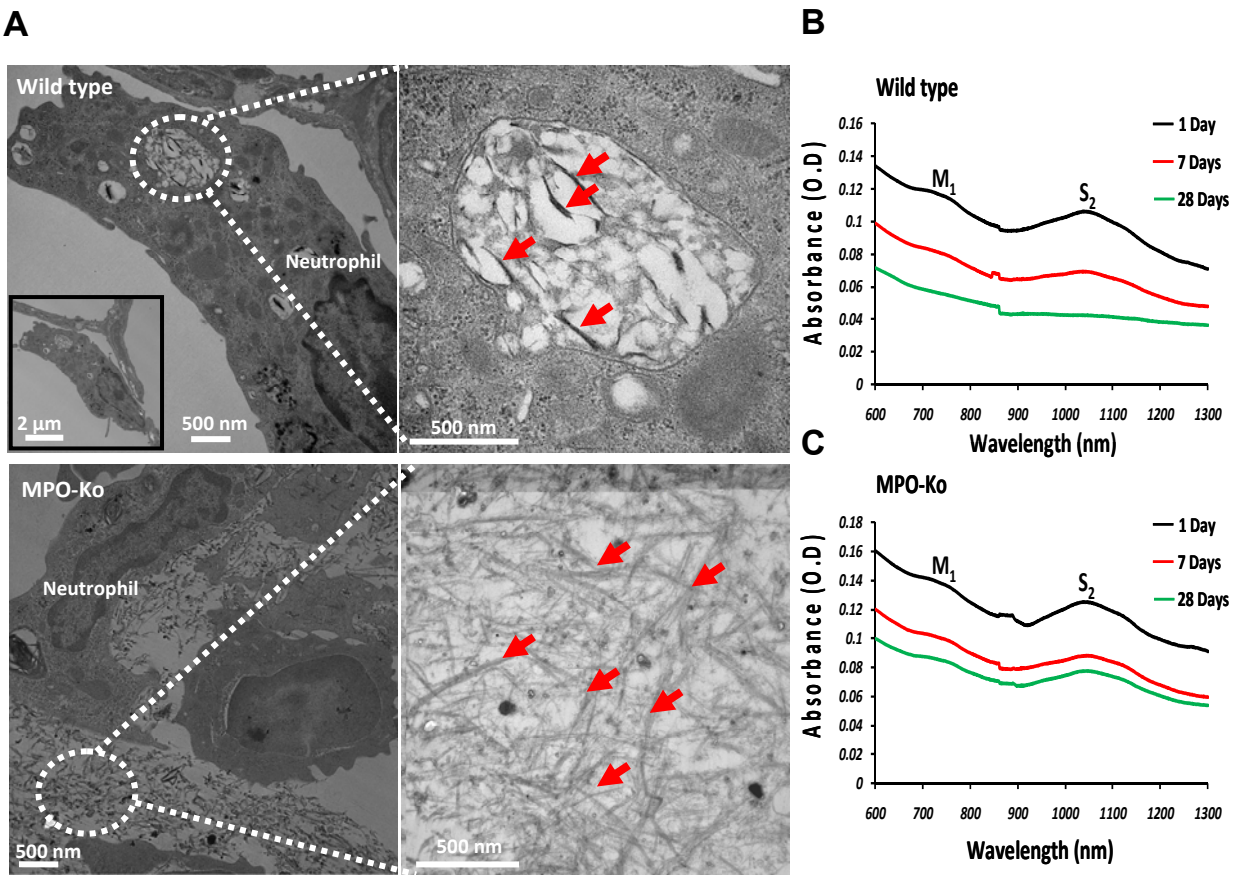


**Figure 28. Electron microscopic (TEM) images and Vis-NIR spectroscopy of nanotubes from lungs.** A, (upper panel), shows a neutrophil in a wild type lung with phagocytozed nanotubes and the corresponding high power image on the right shows the phagosome loaded with nanotubes. Lower panel shows the extra-cellular congested nanotubes in a MPO-Ko mice lung. B and C, Vis-NIR spectrum from solubilized lungs of animals belonging to wild type and MPO-Ko on days 1, 7 and 28 respectively.

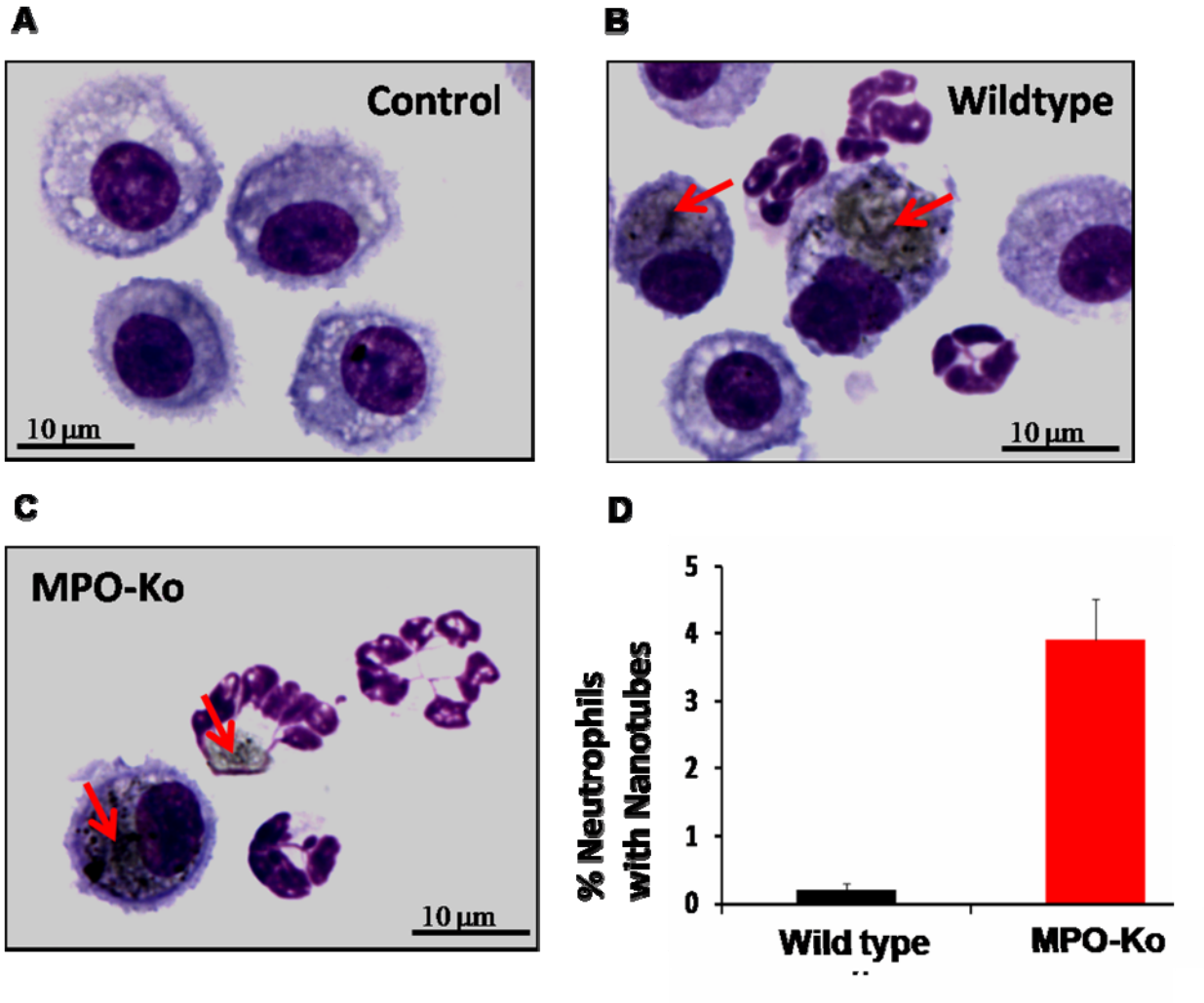


**Figure 29. Light microscopic images of BAL fluid cells collected from mice after 24 hours post nanotubes exposure.** A, control rats; B, nanotubes-exposed wild type mice, and C, nanotubes-exposed MPO-Ko mice. (The blackish–colored punctuate spots pointed by red arrows in (B) and (C) are nanotubes). D, the bar graphs depicting the percentage of neutrophils positive in nanotubes uptake. The data represent means ± S.D from 6 mice.

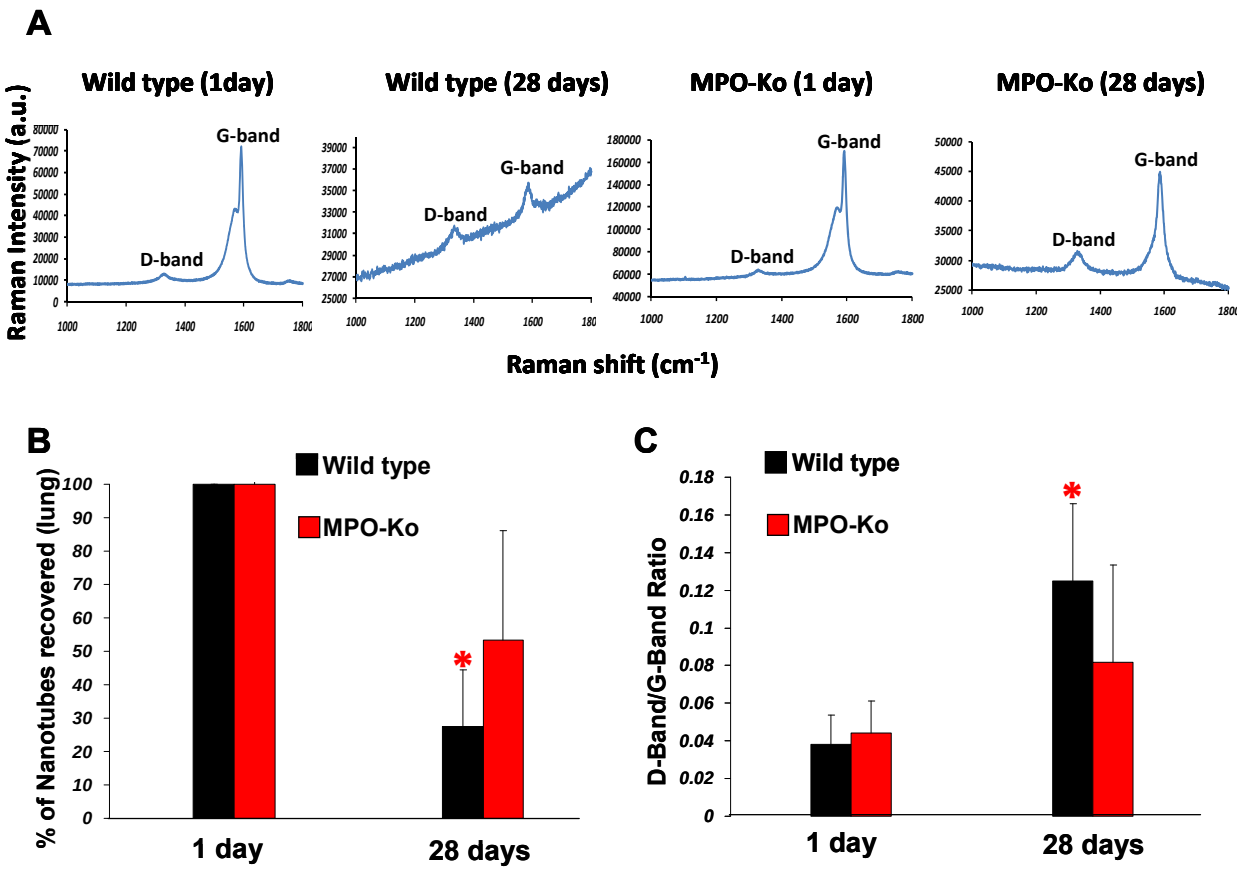


**Figure 30. Raman and Vis-NIR spectroscopic analysis on solubilized lungs of mice.** A, analysis showing characteristic Raman spectra recorded from solubilized lungs of wild type and MPO-Ko mice on day 1 and day 28. Raman spectra showing lowering of G-band and an increase in the D-band. B, Bar graphs representing the level of biodegradation at different time points and is plotted as percentage recovered from mice lungs on day 1 and 28 (n=4) (Note: the estimates of nanotubes on day 1 were normalized to 100 %). The assessments were based on the intensity magnitudes of both the characteristic semi-conducting (S2) and the metallic (M1) peaks of nanotubes present in the recorded Vis-NIR spectra. C, bar graphs representing the D-band to G-band ratios analyzed from recorded Raman spectra as obtained from solubilized lungs of wild type and MPO-Ko mice (n=3). *P < 0.05 vs. wild type 1 day.

## 6.4 CONCLUSIONS

Our studies determined whether nanotube biodegradation by hMPO-dependent oxidative modification would make them inactive in eliciting inflammatory response in vivo. We found that cellular responses (PMN recruitment) and pro-inflammatory cytokine production – highly elevated after nanotubes pharyngeal aspiration, were essentially undistinguishable from control values after exposure of mice to "biodegraded" by hMPO nanotubes. Finally, we were anxious to quantitatively assess the extent to which myeloperoxidase was involved in biodegradation of nanotubes in vivo. Wild type C57BL/6 and MPO-Ko mice were utilized to evaluate the role of the enzyme in neutrophil mediated degradation of nanotubes. We report that MPO-Ko mice showed significantly diminished nanotube biodegradation compared to wild type C57BL6 mice confirmed by both Vis-NIR and Raman spectroscopic studies as indicated by the enhanced D/G –band ratios in the latter mice type.

# 7 CHAPTER 7 - GENERAL CONCLUSIONS AND FUTURE DIRECTIONS

## 7.1 GENERAL CONCLUSIONS

We have shown in this dissertation that activated macrophages produce reactive oxygen and nitrogen species and macrophages can directly participate in apoptotic cell clearance by S-nitrosylation/oxidation and inhibition of APLT causing PS externalization. There were reports previously published reporting s-nitrosylation dependent inhibitions of other proteins/enzymes. However, prior to these studies the role of s-nitrosylation in inhibition of APLT was unknown. PS dependent apoptotic cell clearance by macrophages and its implications in resolution of inflammation have been reported previously. Integrating our results with those published in literature suggests that PS externalization acts as an "eat-me" signal and macrophages effectively can participate in PS externalization on bystander cells upon activation via release of ROS and RNS. In the later dissertation work, we mimicked the phenomenon of PS dependent recognition and clearance of apoptotic cells, by coating carbon nanotubes with PS for effective recognition and phagocytosis. We and others have reported ineffective recognition and clearance of carbon nanotubes contributing for the bio-persistence and toxicity of nanotubes in vivo. By coating nanotubes with PS, we were able to specifically target macrophages and other professional phagocytes, except neutrophils. Later studies following macrophage uptake, led us to think on the directions of biodegradation. As, horse radish peroxidase was reported to biodegrade nanotubes over time, we speculated if animal peroxidases could biodegrade. Of note, none of the studies till date have determined the fate of nanotubes in phagocytes. In this dissertation studies, biodegradation of nanotubes was evaluated targeting two different professional phagocytic cells and we found that isolated neutrophils in vitro biodegrade nanotubes through its MPO/$H_2O_2$ system much more

effectively than macrophages containing low levels of MPO. This suggested that MPO content and activity are important determinants in biodegradation of nanotubes. Finally, we evaluated the degree of biodegradation in vivo and found that biodegradation indeed occurs biologically and MPO plays a very critical role in this process.

Our findings also suggest that pulmonary inflammation following carbon nanotube exposures in mice could be explained by the ineffective internalization of non-functionalized nanotubes by phagocytic cells. Moreover, it is possible that the doses of nanotubes commonly used in toxicological studies may overwhelm the biodegradation capacity of the neutrophil enzymatic system. Nonetheless, the propensity of nanotubes to undergo MPO-mediated biodegradation suggests that these nanomaterials may be considered as tools for delivery of therapeutic agents in biomedical applications when used at appropriate and readily degradable concentrations.

## 7.2 FUTURE DIRECTIONS

The dissertation study is extremely novel and should fundamentally change the perception on toxicity of carbon nanotubes and factors governing it. The study opens up new avenues for nanotechnology. With the need of the hour- are carbon nanotubes biodegradable, the findings of the studies in the dissertation are very critical from the view point of public health concern. With increasing applications of these unique engineered materials, there is an expected exponential increase in the production and hence the potential exposures to these particles both at manufacturing units and consumer end and research units will become inevitable. Our studies for the first time show that the particles are indeed biodegradable in vivo by a neutrophil peroxidase. Future strategies can be developed to target immune cells that in turn can participate in biodegradation of the nanomaterial. We in our studies showed that phosphatidylserine coating of nanotubes targets them specifically to professional phagocytes except the neutrophils. Targeting of nanotubes to macrophages can promote particle clearance and targeting to neutrophils would cause biodegradation. Coating of particles with IgG, enhanced the particle uptake in neutrophils. However, uptake studies on macrophages were not carried out using IgG-coated nanotubes. In this section, I would like to propose studies on recognition and uptake using IgG-coated nanoparticles in macrophages. Arnhold et al (Lessig, Spalteholz et al. 2007) have shown that phosphatidylserine avidly binds to myeloperoxidase. In this context, delivery of PS-myeloperoxidase liposomal complexes would be a logical study as a therapeutic intervention to biodegrade inhaled and biopersistent nanomaterial. In line with the above proposal, in vivo biodegradation studies can also be carried out by over-expressing myeloperoxidase in animals. This would further our understanding on the contribution of myeloperoxidase in determining the degree of biopersistence of nanomaterial. Lastly, because

biodegradation of carbon nanotubes is important to dictate the final toxicity, further studies based on this work may uncover novel therapeutic approaches, increase our understanding of pathophysiology or explain the role of phagocytes (using co-culture studies) in modulating the nanoparticle based toxicity. Many of the above proposed studies could be performed using the experimental techniques established in the dissertation.

# BIBLIOGRAPHY


Alexis, F., E. Pridgen, et al. (2008). "Factors affecting the clearance and biodistribution of polymeric nanoparticles." Mol Pharm 5(4): 505-15.

Allen, B. L., P. D. Kichambare, et al. (2008). "Biodegradation of single-walled carbon nanotubes through enzymatic catalysis." Nano Lett 8(11): 3899-903.

Araujo, J. A. and A. E. Nel (2009). "Particulate matter and atherosclerosis: role of particle size, composition and oxidative stress." Part Fibre Toxicol 6: 24.

Arnhold, J., P. G. Furtmuller, et al. (2003). "Redox properties of myeloperoxidase." Redox Rep 8(4): 179-86.

Arur, S., U. E. Uche, et al. (2003). "Annexin I is an endogenous ligand that mediates apoptotic cell engulfment." Dev Cell 4(4): 587-98.

Auffray, C., M. H. Sieweke, et al. (2009). "Blood monocytes: development, heterogeneity, and relationship with dendritic cells." Annu Rev Immunol 27: 669-92.

Bahr, J. L., J. Yang, et al. (2001). "Functionalization of carbon nanotubes by electrochemical reduction of aryl diazonium salts: a bucky paper electrode." J Am Chem Soc 123(27): 6536-42.

Batrakova, E. V., S. Li, et al. (2007). "A macrophage-nanozyme delivery system for Parkinson's disease." Bioconjug Chem 18(5): 1498-506.

Belin, T. and F. Epron (2005). "Characterization methods of carbon nanotubes: a review" Materials Science and Engineering 119 (2): 105-118.

Bettinger, I., S. Thanos, et al. (2002). "Microglia promote glioma migration." Acta Neuropathol 103(4): 351-5.

Bianco, A. (2004). "Carbon nanotubes for the delivery of therapeutic molecules." Expert Opin Drug Deliv 1(1): 57-65.

Bianco, A., J. Hoebeke, et al. (2005). "Carbon nanotubes: on the road to deliver." Curr Drug Deliv 2(3): 253-9.

Bianco, A., K. Kostarelos, et al. (2005). "Biomedical applications of functionalised carbon nanotubes." Chem Commun (Camb)(5): 571-7.

Bianco, A., K. Kostarelos, et al. (2005). "Applications of carbon nanotubes in drug delivery." Curr Opin Chem Biol 9(6): 674-9.

Bice, D. E., A. J. Harmsen, et al. (1990). "Role of Lung Phagocytes in the Clearance of Particles by the Mucociliary Apparatus" Inhalation Toxicology 2(2): 151-160.

Blanchette, C. D., Y. H. Woo, et al. (2009). "Decoupling internalization, acidification and phagosomal-endosomal/lysosomal fusion during phagocytosis of InlA coated beads in epithelial cells." PLoS One 4(6): e6056.

Borm, P., F. C. Klaessig, et al. (2006). "Research strategies for safety evaluation of nanomaterials, part V: role of dissolution in biological fate and effects of nanoscale particles." Toxicol Sci 90(1): 23-32.

Bottcher, A., U. S. Gaipl, et al. (2006). "Involvement of phosphatidylserine, alphavbeta3, CD14, CD36, and complement C1q in the phagocytosis of primary necrotic lymphocytes by macrophages." Arthritis Rheum 54(3): 927-38.

Boynton, E. L., J. Waddell, et al. (2000). "The effect of polyethylene particle chemistry on human monocyte-macrophage function in vitro." J Biomed Mater Res 52(2): 239-45.

Celli, J. (2006). "Surviving inside a macrophage: the many ways of Brucella." Res Microbiol 157(2): 93-8.

Chen, X., G. S. Lee, et al. (2004). "Biomimetic engineering of carbon nanotubes by using cell surface mucin mimics." Angew Chem Int Ed Engl 43(45): 6111-6.
Chen, X., U. C. Tam, et al. (2006). "Interfacing carbon nanotubes with living cells." J Am Chem Soc 128(19): 6292-3.
Cherukuri, P., C. J. Gannon, et al. (2006). "Mammalian pharmacokinetics of carbon nanotubes using intrinsic near-infrared fluorescence." Proc Natl Acad Sci U S A 103(50): 18882-6.
Clancy, R., A. I. Cederbaum, et al. (2001). "Preparation and properties of S-nitroso-L-cysteine ethyl ester, an intracellular nitrosating agent." J Med Chem 44(12): 2035-8.
Connor, J. and A. J. Schroit (1990). "Aminophospholipid translocation in erythrocytes: evidence for the involvement of a specific transporter and an endofacial protein." Biochemistry 29(1): 37-43.
Costa, S., E. Borowiak-Palen, et al. (2009). "Characterization of carbon nanotubes by Raman spectroscopy." Materials Science-Poland 26(2): 8.
Crow, J. P. and J. S. Beckman (1995). "Reactions between nitric oxide, superoxide, and peroxynitrite: footprints of peroxynitrite in vivo." Adv Pharmacol 34: 17-43.
Dale, D. C., L. Boxer, et al. (2008). "The phagocytes: neutrophils and monocytes." Blood 112(4): 935-45.
Daleke, D. L. (2003). "Regulation of transbilayer plasma membrane phospholipid asymmetry." J Lipid Res 44(2): 233-42.
Daleke, D. L. and J. V. Lyles (2000). "Identification and purification of aminophospholipid flippases." Biochim Biophys Acta 1486(1): 108-27.
Davies, N. M., A. G. Roseth, et al. (1997). "NO-naproxen vs. naproxen: ulcerogenic, analgesic and anti-inflammatory effects." Aliment Pharmacol Ther 11(1): 69-79.
Davoren, M., E. Herzog, et al. (2007). "In vitro toxicity evaluation of single walled carbon nanotubes on human A549 lung cells." Toxicol In Vitro 21(3): 438-48.
de Jong, K., D. Geldwerth, et al. (1997). "Oxidative damage does not alter membrane phospholipid asymmetry in human erythrocytes." Biochemistry 36(22): 6768-76.
DeLano, W. L. (2002). The PyMOL Molecular Graphics System (DeLano Scientific).
Demedts, I. K., T. Demoor, et al. (2006). "Role of apoptosis in the pathogenesis of COPD and pulmonary emphysema." Respir Res 7: 53.
Devaux, P. F., I. Lopez-Montero, et al. (2006). "Proteins involved in lipid translocation in eukaryotic cells." Chem Phys Lipids 141(1-2): 119-32.
Dimmeler, S., J. Haendeler, et al. (1997). "Suppression of apoptosis by nitric oxide via inhibition of interleukin-1beta-converting enzyme (ICE)-like and cysteine protease protein (CPP)-32-like proteases." J Exp Med 185(4): 601-7.
Dobrovolskaia, M. A. and S. E. McNeil (2007). "Immunological properties of engineered nanomaterials." Nat Nanotechnol 2(8): 469-78.
Donaldson, K., V. Stone, et al. (2004). "Nanotoxicology." Occup Environ Med 61(9): 727-8.
Dou, H., C. J. Destache, et al. (2006). "Development of a macrophage-based nanoparticle platform for antiretroviral drug delivery." Blood 108(8): 2827-35.
Dumortier, H., S. Lacotte, et al. (2006). "Functionalized carbon nanotubes are non-cytotoxic and preserve the functionality of primary immune cells." Nano Lett 6(7): 1522-8.
Dutta, D., S. K. Sundaram, et al. (2007). "Adsorbed proteins influence the biological activity and molecular targeting of nanomaterials." Toxicol Sci 100(1): 303-15.
Elder, A. and G. Oberdorster (2006). "Translocation and effects of ultrafine particles outside of the lung." Clin Occup Environ Med 5(4): 785-96.

Ezekowitz, R. A. (2002). "Local opsonization for apoptosis?" Nat Immunol 3(6): 510-2.
Fabisiak, J. P., V. A. Tyurin, et al. (2000). "Nitric oxide dissociates lipid oxidation from apoptosis and phosphatidylserine externalization during oxidative stress." Biochemistry 39(1): 127-38.
Fadeel, B. (2003). "Programmed cell clearance." Cell Mol Life Sci 60(12): 2575-85.
Fadeel, B., A. Ahlin, et al. (1998). "Involvement of caspases in neutrophil apoptosis: regulation by reactive oxygen species." Blood 92(12): 4808-18.
Fadeel, B., B. Gleiss, et al. (1999). "Phosphatidylserine exposure during apoptosis is a cell-type-specific event and does not correlate with plasma membrane phospholipid scramblase expression." Biochem Biophys Res Commun 266(2): 504-11.
Fadok, V. A., D. L. Bratton, et al. (1998). "Macrophages that have ingested apoptotic cells in vitro inhibit proinflammatory cytokine production through autocrine/paracrine mechanisms involving TGF-beta, PGE2, and PAF." J Clin Invest 101(4): 890-8.
Folch, J., M. Lees, et al. (1957). "A simple method for the isolation and purification of total lipides from animal tissues." J Biol Chem 226(1): 497-509.
Forman, H. J. and M. Torres (2001). "Redox signaling in macrophages." Mol Aspects Med 22(4-5): 189-216.
Forsberg, A. J., V. E. Kagan, et al. (2004). "Thiol oxidation enforces phosphatidylserine externalization in apoptosis-sensitive and -resistant cells through a deltapsim/cytochrome C release-dependent mechanism." Antioxid Redox Signal 6(2): 203-8.
Foster, M. W., T. J. McMahon, et al. (2003). "S-nitrosylation in health and disease." Trends Mol Med 9(4): 160-8.
Gaipl, U. S., A. Kuhn, et al. (2006). "Clearance of apoptotic cells in human SLE." Curr Dir Autoimmun 9: 173-87.
Gardai, S. J., D. L. Bratton, et al. (2006). "Recognition ligands on apoptotic cells: a perspective." J Leukoc Biol 79(5): 896-903.
Gleiss, B., V. Gogvadze, et al. (2002). "Fas-triggered phosphatidylserine exposure is modulated by intracellular ATP." FEBS Lett 519(1-3): 153-8.
Gonzalez-Flecha, B. (2004). "Oxidant mechanisms in response to ambient air particles." Mol Aspects Med 25(1-2): 169-82.
Grayson, M. H. (2006). "Lung dendritic cells and the inflammatory response." Ann Allergy Asthma Immunol 96(5): 643-51; quiz 652-3, 678.
Griffin, F. M., Jr., J. A. Griffin, et al. (1975). "Studies on the mechanism of phagocytosis. I. Requirements for circumferential attachment of particle-bound ligands to specific receptors on the macrophage plasma membrane." J Exp Med 142(5): 1263-82.
Hampton, M. B., A. J. Kettle, et al. (1998). "Inside the neutrophil phagosome: oxidants, myeloperoxidase, and bacterial killing." Blood 92(9): 3007-17.
Hanayama, R., K. Miyasaka, et al. (2006). "MFG-E8-dependent clearance of apoptotic cells, and autoimmunity caused by its failure." Curr Dir Autoimmun 9: 162-72.
Hanayama, R., M. Tanaka, et al. (2002). "Identification of a factor that links apoptotic cells to phagocytes." Nature 417(6885): 182-7.
Hanayama, R., M. Tanaka, et al. (2004). "Autoimmune disease and impaired uptake of apoptotic cells in MFG-E8-deficient mice." Science 304(5674): 1147-50.
Hans, M. L. and A. M. Lowman (2002). "Biodegradable nanoparticles for drug delivery and targeting" Curr. Opini. Solid State Mater. Sci. 6: 319-327.

Hart, P. D. and M. R. Young (1975). "Interference with normal phagosome-lysosome fusion in macrophages, using ingested yeast cells and suramin." Nature 256(5512): 47-9.
He, C., Y. Hu, et al. "Effects of particle size and surface charge on cellular uptake and biodistribution of polymeric nanoparticles." Biomaterials 31(13): 3657-66.
Henson, P. M. and D. A. Hume (2006). "Apoptotic cell removal in development and tissue homeostasis." Trends Immunol 27(5): 244-50.
Herzog, E., A. Casey, et al. (2007). "A new approach to the toxicity testing of carbon-based nanomaterials--the clonogenic assay." Toxicol Lett 174(1-3): 49-60.
Hess, D. T., A. Matsumoto, et al. (2005). "Protein S-nitrosylation: purview and parameters." Nat Rev Mol Cell Biol 6(2): 150-66.
Hoffman, A. S., F. J. Schoen, et al. (2004). Biomaterials Science: An Introduction to Materials in Medicine. The Complement System. R. J. Johnson, Elsevier Academic Press: 318-328.
Hoffmann, P. R., J. A. Kench, et al. (2005). "Interaction between phosphatidylserine and the phosphatidylserine receptor inhibits immune responses in vivo." J Immunol 174(3): 1393-404.
Houben, E. N., L. Nguyen, et al. (2006). "Interaction of pathogenic mycobacteria with the host immune system." Curr Opin Microbiol 9(1): 76-85.
Hubeau, C., M. Lorenzato, et al. (2001). "Quantitative analysis of inflammatory cells infiltrating the cystic fibrosis airway mucosa." Clin Exp Immunol 124(1): 69-76.
Huynh, M. L., V. A. Fadok, et al. (2002). "Phosphatidylserine-dependent ingestion of apoptotic cells promotes TGF-beta1 secretion and the resolution of inflammation." J Clin Invest 109(1): 41-50.
Iijima, S., P. M. Ajayan, et al. (1992). "Growth model for carbon nanotubes." Phys Rev Lett 69(21): 3100-3103.
Jia, G., H. Wang, et al. (2005). "Cytotoxicity of carbon nanomaterials: single-wall nanotube, multi-wall nanotube, and fullerene." Environ Sci Technol 39(5): 1378-83.
Jiang, J., V. Kini, et al. (2004). "Cytochrome c release is required for phosphatidylserine peroxidation during Fas-triggered apoptosis in lung epithelial A549 cells." Lipids 39(11): 1133-42.
Jones, F. S. and P. Rous (1917). "The Phagocytic Power of Connective Tissue Cells." J Exp Med 25(1): 189-93.
Jourd'heuil, D. (2002). "Increased nitric oxide-dependent nitrosylation of 4,5-diaminofluorescein by oxidants: implications for the measurement of intracellular nitric oxide." Free Radic Biol Med 33(5): 676-84.
Kagan, V. E., N. V. Konduru, et al. (2010). "Carbon nanotubes degraded by neutrophil myeloperoxidase induce less pulmonary inflammation." Nat Nanotechnol 5(5):354-9.
Kagan, V. E., V. A. Tyurin, et al. (2005). "Cytochrome c acts as a cardiolipin oxygenase required for release of proapoptotic factors." Nat Chem Biol 1(4): 223-32.
Kagan, V. E., Y. Y. Tyurina, et al. (2006). "Direct and indirect effects of single walled carbon nanotubes on RAW 264.7 macrophages: role of iron." Toxicol Lett 165(1): 88-100.
Kam, N. W. and H. Dai (2005). "Carbon nanotubes as intracellular protein transporters: generality and biological functionality." J Am Chem Soc 127(16): 6021-6.
Kam, N. W., M. O'Connell, et al. (2005). "Carbon nanotubes as multifunctional biological transporters and near-infrared agents for selective cancer cell destruction." Proc Natl Acad Sci U S A 102(33): 11600-5.

Kam, N. W. S. and H. Dai (2006). "Single walled carbon nanotubes for transport and delivery of biological cargos." phys. stat. sol. 243(13): 3561–3566.
Kanno, S., A. Furuyama, et al. (2007). "A murine scavenger receptor MARCO recognizes polystyrene nanoparticles." Toxicol Sci 97(2): 398-406.
Kearns, S. and R. Dawson, Jr. (2000). "Cytoprotective effect of taurine against hypochlorous acid toxicity to PC12 cells." Adv Exp Med Biol 483: 563-70.
Kettle, A. J., C. A. Gedye, et al. (1997). "Mechanism of inactivation of myeloperoxidase by 4-aminobenzoic acid hydrazide." Biochem J 321 ( Pt 2): 503-8.
Kisin, E., A. R. Jurray, et al. (2005). "Pulmonary toxicity of carbon nanotubes." Toxicologist 84 212.
Klebanoff, S. J. (1999). "Myeloperoxidase." Proc Assoc Am Physicians 111(5): 383-9.
Klumpp, C., K. Kostarelos, et al. (2006). "Functionalized carbon nanotubes as emerging nanovectors for the delivery of therapeutics." Biochim Biophys Acta 1758(3): 404-12.
Knapp, P. E. and J. A. Swanson (1990). "Plasticity of the tubular lysosomal compartment in macrophages." J Cell Sci 95 ( Pt 3): 433-9.
Kojima, H., N. Nakatsubo, et al. (1998). "Detection and imaging of nitric oxide with novel fluorescent indicators: diaminofluoresceins." Anal Chem 70(13): 2446-53.
Konduru, N. V., Y. Y. Tyurina, et al. (2009). "Phosphatidylserine targets single-walled carbon nanotubes to professional phagocytes in vitro and in vivo." PLoS One 4(2):e4398.
Kostarelos, K., L. Lacerda, et al. (2007). "Cellular uptake of functionalized carbon nanotubes is independent of functional group and cell type." Nat Nanotechnol 2(2): 108-13.
Kuznetsova, A., I. Popova, et al. (2001). "Oxygen-containing functional groups on single-wall carbon nanotubes: NEXAFS and vibrational spectroscopic studies." J Am Chem Soc 123(43): 10699-704.
Lam, C. W., J. T. James, et al. (2004). "Pulmonary toxicity of single-wall carbon nanotubes in mice 7 and 90 days after intratracheal instillation." Toxicol Sci 77(1): 126-34.
Lauber, K., E. Bohn, et al. (2003). "Apoptotic cells induce migration of phagocytes via caspase-3-mediated release of a lipid attraction signal." Cell 113(6): 717-30.
Lecaroz, C., C. Gamazo, et al. (2006). "Nanocarriers with gentamicin to treat intracellular pathogens." J Nanosci Nanotechnol 6(9-10): 3296-302.
Lekstrom-Himes, J. A., D. B. Kuhns, et al. (2005). "Inhibition of human neutrophil IL-8 production by hydrogen peroxide and dysregulation in chronic granulomatous disease." J Immunol 174(1): 411-7.
Lessig, J., H. Spalteholz, et al. (2007). "Myeloperoxidase binds to non-vital spermatozoa on phosphatidylserine epitopes." Apoptosis 12(10): 1803-12.
Li, N., T. Xia, et al. (2008). "The role of oxidative stress in ambient particulate matter-induced lung diseases and its implications in the toxicity of engineered nanoparticles." Free Radic Biol Med 44(9): 1689-99.
Liu, J., A. G. Rinzler, et al. (1998). "Fullerene pipes." Science 280(5367): 1253-6.
Liu, X., R. H. Hurt, et al. "Biodurability of Single-Walled Carbon Nanotubes Depends on Surface Functionalization." Carbon N Y 48(7): 1961-1969.
Lu, X., F. Tian, et al. (2002). "Organic functionalization of the sidewalls of carbon nanotubes by diels-alder reactions: a theoretical prediction." Org Lett 4(24): 4313-5.
Mannick, J. B., C. Schonhoff, et al. (2001). "S-Nitrosylation of mitochondrial caspases." J Cell Biol 154(6): 1111-6.

Martin, S. J., C. P. Reutelingsperger, et al. (1995). "Early redistribution of plasma membrane phosphatidylserine is a general feature of apoptosis regardless of the initiating stimulus: inhibition by overexpression of Bcl-2 and Abl." J Exp Med 182(5): 1545-56.

Maugeri, N., P. Rovere-Querini, et al. (2009). "Neutrophils phagocytose activated platelets in vivo: a phosphatidylserine, P-selectin, and {beta}2 integrin-dependent cell clearance program." Blood 113(21): 5254-65.

Maynard, A. D., P. A. Baron, et al. (2004). "Exposure to carbon nanotube material: aerosol release during the handling of unrefined single-walled carbon nanotube material." J Toxicol Environ Health A 67(1): 87-107.

McKenzie, S. E. and A. D. Schreiber (1998). "Fc gamma receptors in phagocytes." Curr Opin Hematol 5(1): 16-21.

Meagher, L. C., J. S. Savill, et al. (1992). "Phagocytosis of apoptotic neutrophils does not induce macrophage release of thromboxane B2." J Leukoc Biol 52(3): 269-73.

Meckenstock, R. U., E. Annweiler, et al. (2000). "Anaerobic naphthalene degradation by a sulfate-reducing enrichment culture." Appl Environ Microbiol 66(7): 2743-7.

Melino, G., F. Bernassola, et al. (1997). "S-nitrosylation regulates apoptosis." Nature 388(6641): 432-3.

Mercer, R. R., J. Scabilloni, et al. (2008). "Alteration of deposition pattern and pulmonary response as a result of improved dispersion of aspirated single-walled carbon nanotubes in a mouse model." Am J Physiol Lung Cell Mol Physiol 294(1): L87-97.

Miyanishi, M., K. Tada, et al. (2007). "Identification of Tim4 as a phosphatidylserine receptor." Nature 450(7168): 435-9.

Moghimi, S. M., I. S. Muir, et al. (1993). "Coating particles with a block co-polymer (poloxamine-908) suppresses opsonization but permits the activity of dysopsonins in the serum." Biochim Biophys Acta 1179(2): 157-65.

Mollinedo, F., N. Borregaard, et al. (1999). "Novel trends in neutrophil structure, function and development." Immunol Today 20(12): 535-7.

Moore, A., R. Weissleder, et al. (1997). "Uptake of dextran-coated monocrystalline iron oxides in tumor cells and macrophages." J Magn Reson Imaging 7(6): 1140-5.

Muradyan, V. E., B. P. Tarasov, et al. (2008). "Optimization of Synthesis Methods of Single-Walled Carbon Nanotubes Using 3 d Transition Metals", Carbon Nanomaterials in Clean Energy Hydrogen Systems 317-320

Napirei, M. and H. G. Mannherz (2009). Molecules Involved in Recognition and Clearance of Apoptotic/Necrotic Cells and Cell Debris Phagocytosis of Dying Cells: From Molecular Mechanisms to Human Diseases. D. V. Krysko and P. Vandenabeele, Springer Netherlands 103-145.

Nimmagadda, A., K. Thurston, et al. (2006). "Chemical modification of SWNT alters in vitro cell-SWNT interactions." J Biomed Mater Res A 76(3): 614-25.

Obeid, M., A. Tesniere, et al. (2007). "Calreticulin exposure dictates the immunogenicity of cancer cell death." Nat Med 13(1): 54-61.

Oberdorster, G., E. Oberdorster, et al. (2005). "Nanotoxicology: an emerging discipline evolving from studies of ultrafine particles." Environ Health Perspect 113(7): 823-39.

Oberdorster, G., Z. Sharp, et al. (2004). "Translocation of inhaled ultrafine particles to the brain." Inhal Toxicol 16(6-7): 437-45.

Olivier, M. L. and R. O. Paul (2000). "EPR spin-trapping of a myeloperoxidase protein radical. ." Biochem. Biophys. Res. Commun 1: 199-202.

Panasenko, O. M., A. V. Chekanov, et al. (2005). "Generation of free radicals during decomposition of hydroperoxide in the presence of myeloperoxidase or activated neutrophils." Biochemistry (Mosc) 70(9): 998-1004.
Panyam, J. and V. Labhasetwar (2003). "Biodegradable nanoparticles for drug and gene delivery to cells and tissue." Adv Drug Deliv Rev 55(3): 329-47.
Park, D., A. C. Tosello-Trampont, et al. (2007). "BAI1 is an engulfment receptor for apoptotic cells upstream of the ELMO/Dock180/Rac module." Nature 450(7168): 430-4.
Park, J., P. M. Fong, et al. (2009). "PEGylated PLGA nanoparticles for the improved delivery of doxorubicin." Nanomedicine 5(4): 410-8.
Parnaik, R., M. C. Raff, et al. (2000). "Differences between the clearance of apoptotic cells by professional and non-professional phagocytes." Curr Biol 10(14): 857-60.
Pick, E. and D. Mizel (1981). "Rapid microassays for the measurement of superoxide and hydrogen peroxide production by macrophages in culture using an automatic enzyme immunoassay reader." J Immunol Methods 46(2): 211-26.
Plowden, J., M. Renshaw-Hoelscher, et al. (2004). "Innate immunity in aging: impact on macrophage function." Aging Cell 3(4): 161-7.
Poland, C. A., R. Duffin, et al. (2008). "Carbon nanotubes introduced into the abdominal cavity of mice show asbestos-like pathogenicity in a pilot study." Nat Nanotechnol 3(7): 423-8.
Porter, A. E., M. Gass, et al. (2007). "Direct imaging of single-walled carbon nanotubes in cells." Nat Nanotechnol 2(11): 713-7.
Porter, D. W., K. Sriram, et al. (2008). "A biocompatible medium for nanoparticle dispersion." Nanotoxicology 2: 144−154.
Pulskamp, K., S. Diabate, et al. (2007). "Carbon nanotubes show no sign of acute toxicity but induce intracellular reactive oxygen species in dependence on contaminants." Toxicol Lett 168(1): 58-74.
Rao, G. V., S. Tinkle, et al. (2003). "Efficacy of a technique for exposing the mouse lung to particles aspirated from the pharynx." J Toxicol Environ Health A 66(15): 1441-52.
Ravetch, J. V. and J. P. Kinet (1991). "Fc receptors." Annu Rev Immunol 9: 457-92.
Raynal, I., P. Prigent, et al. (2004). "Macrophage endocytosis of superparamagnetic iron oxide nanoparticles: mechanisms and comparison of ferumoxides and ferumoxtran-10." Invest Radiol 39(1): 56-63.
Rosales, C. and E. J. Brown (1991). "Two mechanisms for IgG Fc-receptor-mediated phagocytosis by human neutrophils." J Immunol 146(11): 3937-44.
Rubbo, H., C. Batthyany, et al. (2000). "Nitric oxide-oxygen radicals interactions in atherosclerosis." Biol Res 33(2): 167-75.
Savill, J. and V. Fadok (2000). "Corpse clearance defines the meaning of cell death." Nature 407(6805): 784-8.
Sayes, C. M., F. Liang, et al. (2006). "Functionalization density dependence of single-walled carbon nanotubes cytotoxicity in vitro." Toxicol Lett 161(2): 135-42.
Schipper, M. L., N. Nakayama-Ratchford, et al. (2008). "A pilot toxicology study of single-walled carbon nanotubes in a small sample of mice." Nat Nanotechnol 3(4): 216-21.
Schwarzer, E., F. De Matteis, et al. (1999). "Hemozoin stability and dormant induction of heme oxygenase in hemozoin-fed human monocytes." Mol Biochem Parasitol 100(1): 61-72.
Serhan, C. N. and J. Savill (2005). "Resolution of inflammation: the beginning programs the end." Nat Immunol 6(12): 1191-7.

Serinkan, B. F., F. Gambelli, et al. (2005). "Apoptotic cells quench reactive oxygen and nitrogen species and modulate TNF-alpha/TGF-beta1 balance in activated macrophages: involvement of phosphatidylserine-dependent and -independent pathways." Cell Death Differ 12(8): 1141-4.

Service, R. F. (2004). "Nanotoxicology. Nanotechnology grows up." Science 304(5678): 1732-4.

Sharma, C. S., S. Sarkar, et al. (2007). "Single-walled carbon nanotubes induces oxidative stress in rat lung epithelial cells." J Nanosci Nanotechnol 7(7): 2466-72.

Shvedova, A. A., V. Castranova, et al. (2003). "Exposure to carbon nanotube material: assessment of nanotube cytotoxicity using human keratinocyte cells." J Toxicol Environ Health A 66(20): 1909-26.

Shvedova, A. A., V. E. Kagan, et al. "Close encounters of the small kind: adverse effects of man-made materials interfacing with the nano-cosmos of biological systems." Annu Rev Pharmacol Toxicol 50: 63-88.

Shvedova, A. A., E. Kisin, et al. (2008). "Inhalation vs. aspiration of single-walled carbon nanotubes in C57BL/6 mice: inflammation, fibrosis, oxidative stress, and mutagenesis." Am J Physiol Lung Cell Mol Physiol 295(4): L552-65.

Shvedova, A. A., E. R. Kisin, et al. (2005). "Unusual inflammatory and fibrogenic pulmonary responses to single-walled carbon nanotubes in mice." Am J Physiol Lung Cell Mol Physiol 289(5): L698-708.

Shvedova, A. A., E. R. Kisin, et al. (2008). "Increased accumulation of neutrophils and decreased fibrosis in the lung of NADPH oxidase-deficient C57BL/6 mice exposed to carbon nanotubes." Toxicol Appl Pharmacol 231(2): 235-40.

Shvedova, A. A., E. R. Kisin, et al. (2009). "Mechanisms of pulmonary toxicity and medical applications of carbon nanotubes: Two faces of Janus?" Pharmacol Ther 121(2): 192-204.

Simmons, J. M., B. M. Nichols, et al. (2006). "Effect of ozone oxidation on single-walled carbon nanotubes." J Phys Chem B 110(14): 7113-8.

Smart, S. K., A. I. Cassady, et al. (2006). "The biocompatibility of carbon nanotubes." Carbon 44(6): 1034-1047.

Soto, K., K. M. Garza, et al. (2007). "Cytotoxic effects of aggregated nanomaterials." Acta Biomater 3(3): 351-8.

Spitznagel, J. K., F. G. Dalldorf, et al. (1974). "Character of azurophil and specific granules purified from human polymorphonuclear leukocytes." Lab Invest 30(6): 774-85.

Stoyanovsky, D. A., Y. Y. Tyurina, et al. (2005). "Thioredoxin and lipoic acid catalyze the denitrosation of low molecular weight and protein S-nitrosothiols." J Am Chem Soc 127(45): 15815-23.

Sutherland, K., J. R. Mahoney, 2nd, et al. (1993). "Degradation of biomaterials by phagocyte-derived oxidants." J Clin Invest 92(5): 2360-7.

Thery, C., L. Zitvogel, et al. (2002). "Exosomes: composition, biogenesis and function." Nat Rev Immunol 2(8): 569-79.

Torok, N. J., H. Higuchi, et al. (2002). "Nitric oxide inhibits apoptosis downstream of cytochrome C release by nitrosylating caspase 9." Cancer Res 62(6): 1648-53.

Touyz, R. M. (2008). "Apocynin, NADPH oxidase, and vascular cells: a complex matter." Hypertension 51(2): 172-4.

Trivedi, V., S. C. Zhang, et al. (2006). "Immunoglobulin G signaling activates lysosome/phagosome docking." Proc Natl Acad Sci U S A 103(48): 18226-31.

Twigg, H. L., 3rd (2004). "Macrophages in innate and acquired immunity." Semin Respir Crit Care Med 25(1): 21-31.

Tyurin, V. A., Y. Y. Tyurina, et al. (2002). "Quantitation of S-nitrosothiols in cells and biological fluids." Methods Enzymol 352: 347-60.

Tyurina, Y. Y., F. B. Serinkan, et al. (2004). "Lipid antioxidant, etoposide, inhibits phosphatidylserine externalization and macrophage clearance of apoptotic cells by preventing phosphatidylserine oxidation." J Biol Chem 279(7): 6056-64.

Tyurina, Y. Y., L. V. Basova, et al. (2007). "Nitrosative stress inhibits the aminophospholipid translocase resulting in phosphatidylserine externalization and macrophage engulfment-Implications for the resolution of inflammation." J Biol Chem 282(11):8498-509.

Underhill, D. M. (2003). "Macrophage recognition of zymosan particles." J Endotoxin Res 9(3): 176-80.

Uthaisang, W., L. K. Nutt, et al. (2003). "Phosphatidylserine exposure in Fas type I cells is mitochondria-dependent." FEBS Lett 545(2-3): 110-4.

Vadiveloo, P. K. (1999). "Macrophages--proliferation, activation, and cell cycle proteins." J Leukoc Biol 66(4): 579-82.

van der Vliet, A., P. A. Hoen, et al. (1998). "Formation of S-nitrosothiols via direct nucleophilic nitrosation of thiols by peroxynitrite with elimination of hydrogen peroxide." J Biol Chem 273(46): 30255-62.

van Engeland, M., L. J. Nieland, et al. (1998). "Annexin V-affinity assay: a review on an apoptosis detection system based on phosphatidylserine exposure." Cytometry 31(1): 1-9.

van Ravenzwaay, B., R. Landsiedel, et al. (2009). "Comparing fate and effects of three particles of different surface properties: nano-TiO(2), pigmentary TiO(2) and quartz." Toxicol Lett 186(3): 152-9.

Vanags, D. M., M. I. Porn-Ares, et al. (1996). "Protease involvement in fodrin cleavage and phosphatidylserine exposure in apoptosis." J Biol Chem 271(49): 31075-85.

Vandivier, R. W., P. M. Henson, et al. (2006). "Burying the dead: the impact of failed apoptotic cell removal (efferocytosis) on chronic inflammatory lung disease." Chest 129(6): 1673-82.

Verhoven, B., S. Krahling, et al. (1999). "Regulation of phosphatidylserine exposure and phagocytosis of apoptotic T lymphocytes." Cell Death Differ 6(3): 262-70.

Vermes, I., C. Haanen, et al. (1995). "A novel assay for apoptosis. Flow cytometric detection of phosphatidylserine expression on early apoptotic cells using fluorescein labelled Annexin V." J Immunol Methods 184(1): 39-51.

Villanueva, A., M. Canete, et al. (2009). "The influence of surface functionalization on the enhanced internalization of magnetic nanoparticles in cancer cells." Nanotechnology 20(11): 115103.

Wallace, J. L. (2006). "Nitric oxide, aspirin-triggered lipoxins and NO-aspirin in gastric protection." Inflamm Allergy Drug Targets 5(2): 133-7.

Wang, S. F., L. Shen, et al. (2005). "Preparation and mechanical properties of chitosan/carbon nanotubes composites." Biomacromolecules 6(6): 3067-72.

Wang, S. G., R. Wang, et al. (2004). "DNA biosensors based on self-assembled carbon nanotubes." Biochem Biophys Res Commun 325(4): 1433-7.

Warheit, D. B., B. R. Laurence, et al. (2004). "Comparative pulmonary toxicity assessment of single-wall carbon nanotubes in rats." Toxicol Sci 77(1): 117-25.

Wei, Z., M. Kondratenko, et al. (2006). "Rectifying diodes from asymmetrically functionalized single-wall carbon nanotubes." J Am Chem Soc 128(10): 3134-5.
Weiss, J., P. Elsbach, et al. (1992). "Human bactericidal/permeability-increasing protein and a recombinant NH2-terminal fragment cause killing of serum-resistant gram-negative bacteria in whole blood and inhibit tumor necrosis factor release induced by the bacteria." J Clin Invest 90(3): 1122-30.
Wick, P., P. Manser, et al. (2007). "The degree and kind of agglomeration affect carbon nanotube cytotoxicity." Toxicol Lett 168(2): 121-31.
Winterbourn, C. C. and A. J. Kettle (2000). "Biomarkers of myeloperoxidase-derived hypochlorous acid." Free Radic Biol Med 29(5): 403-9.
Winterbourn, C. C., M. C. Vissers, et al. (2000). "Myeloperoxidase." Curr Opin Hematol 7(1): 53-8.
Worle-Knirsch, J. M., K. Pulskamp, et al. (2006). "Oops they did it again! Carbon nanotubes hoax scientists in viability assays." Nano Lett 6(6): 1261-8.
Wu, C. H. (2007). "Studies of the equilibrium and thermodynamics of the adsorption of Cu(2+) onto as-produced and modified carbon nanotubes." J Colloid Interface Sci 311(2): 338-46.
Yanamala, N., K. C. Tirupula, et al. (2008). "Preferential binding of allosteric modulators to active and inactive conformational states of metabotropic glutamate receptors." BMC Bioinformatics 9 Suppl 1: S16.
Yoon, S. M., S. J. Kim, et al. (2008). "Selective oxidation on metallic carbon nanotubes by halogen oxoanions." J Am Chem Soc 130(8): 2610-6.
Yoshida, H., K. Kawane, et al. (2005). "Phosphatidylserine-dependent engulfment by macrophages of nuclei from erythroid precursor cells." Nature 437(7059): 754-8.
Zeinali, M., M. Vossoughi, et al. (2008). "Degradation of phenanthrene and anthracene by Nocardia otitidiscaviarum strain TSH1, a moderately thermophilic bacterium." J Appl Microbiol 105(2): 398-406.
Zhang, Y. and N. Hogg (2004). "The mechanism of transmembrane S-nitrosothiol transport." Proc Natl Acad Sci U S A 101(21): 7891-6.
Zhao, H., S. Kalivendi, et al. (2003). "Superoxide reacts with hydroethidine but forms a fluorescent product that is distinctly different from ethidium: potential implications in intracellular fluorescence detection of superoxide." Free Radic Biol Med 34(11): 1359-68.
Zhuang, J., Y. Ren, et al. (1998). "Dissociation of phagocyte recognition of cells undergoing apoptosis from other features of the apoptotic program." J Biol Chem 273(25): 15628-32.
Zipfel, M., T. C. Carmine, et al. (1997). "Evidence for the activation of myeloperoxidase by f-Meth-Leu-Phe prior to its release from neutrophil granulocytes." Biochem Biophys Res Commun 232(1): 209-12.